AN ABSTRACT OF THE THESIS OF

Thilo Stefan Heiberger for the degree of Master of Science in Civil Engineering presented on May 20, 1996. Title: Simulating the Effects of a Capillary Barrier using the Two-Dimensional Variably Saturated Flow Model SWMS-2D / HYDRUS-2D.

Abstract approved: _____

John S. Selker

Engineering applications of a capillary barrier system - an arrangement of fine material overlaying a coarser material at a sloping interface to protect e.g. waste or low radioactive deposits - are considered to be an alternative to the typically used low permeability layer as a protector against water percolation into deposits.

Ross (1990) developed equations that used material and site-geometric properties as well as infiltration rate to calculate the diversion capacity, Q_{max}, total amount of water diverted along the sloping interface, and the diversion length, L, length along the interface before water is percolating into the coarse layer. While Ross' equation strongly depends upon the value of α (exponent in Gardner's conductivity function), Steenhuis et al. (1990) developed a similar equation with water (h_w) and air entry pressure (h_a) as most critical parameters. Steenhuis et al. (1991) combined Ross' and Steenhuis' solution to obtain a more accurate prediction of the diversion length. Stormont (1995) modified Ross' solution to account for constant anisotropy within the fine layer.

Billiotte et al. (1988), Fayer et al. (1992), and Oldenburg and Pruess (1993) performed numerical simulation to test the effect of a capillary barrier. However, none of these articles provided comprehensive tests of the validity of above mentioned equations.

In this project the SWMS-2D/HYDRUS-2D code of the U.S. Salinity Laboratory, Riverside, California was used to simulate the water flow in a two-dimensional variably saturated capillary barrier system. The program allowed to incorporate changes in dip angle, infiltration rate, material properties, anisotropy, defects along the interface as well as to show the effects of single-layered and double-layered straight and curved interfaces. A sensitivity and plausibility analysis was performed to test the outputs of the simulation and a comparison with a finite difference method are outlined in this paper.

The results of the simulation showed a much more complicated flow pattern in the vicinity of a capillary barrier than predicted by the simple analytical approaches. While the analytical solutions predict limited leakage into the coarse material for a down-dip distance smaller than L, the simulation outputs showed insignificant percolation in that region. A parabolic curved interface, compared to a straight interface of same drop height between up-dip and down-dip end, was shown to provide a smaller breakthrough. Defects, both protending upward and downward, at the interface lead to a penetration of the barrier far before that predicted by the analytical solution.

Simulating the Effects of a Capillary Barrier using the Two - Dimensional Variably Saturated Flow Model SWMS-2D / HYDRUS-2D

by

Thilo Stefan Heiberger

A THESIS

submitted to

Oregon State University

in partial fulfillment of
the requirements for the
degree of

Master of Science

Presented May 20, 1996
Commencement June 1997

Master of Sciences thesis of Thilo Stefan Heiberger presented on May 7, 1996

APPROVED:

Redacted for Privacy

Major Professor, representing Civil Engineering

Redacted for Privacy

Chair of Department of Civil Engineering

Redacted for Privacy

Dean of Graduate School

I understand that my thesis will become part of the permanent collection of Oregon State University libraries. My signature below authorizes release of my thesis to any reader upon request.

Redacted for Privacy

Thilo Stefan Heiberger, Author

ACKNOWLEDGMENT

This paper about the effects of capillary barriers on the water movement is not only a fingerprint of one person. Many people were involved helping to overcome some "barriers" during research and write up, and their ideas "percolated" into this work.

In that sense a very special thanks to my major Professor, Dr. John Selker, whose ideas and suggestions were always a driving force in improving this research. His outstanding ability to explain processes in an understandable, pictorial way and to interpret difficult results and put those in a bigger context guided me through some dark moments. Dr. Selker supported me not only subject-specifically but also helped me financially with his funding in my second year at Oregon State University.

A special thanks to Dr. P. Klingeman who was my advisor in the first year at Oregon State University and who helped me to put together my program and get started in the new study environment; he also assisted me to get around some language barriers in the beginning of my study at Oregon State University.

A special thanks also to the members of my defense committee to Dr. R. Beschta representing my minor professor, whose teaching widened my scope of knowledge in hydrology; to Dr. J. Istok whose knowledge in computer modeling and capability to transmit this wisdom improved this research substantially and to my graduate representative Dr. C. Smith.

This research would not have come that far if not another person, Dr. J. Šimunek (from the U.S. Salinity Laboratory, Riverside/California) who wrote the HYDRUS-2D code, answered all the questions about the model that came up and whose explanations and suggestions helped to understand and improve the results.

A special thanks also to Martin Schroth who answered many of the question that came up and the discussion with him made me understand more about capillary barriers; Martin Schroth also performed the simulations with the finite difference method.

A very special thanks to my parents who spiritually and financially supported and sustained my studies at Oregon State University and gave me the opportunity to realize some of my dreams; without their way of education I would have never had the chance to accomplish the studies at Oregon State University.

A very special thanks also to Lisa Jones who helped me to realize that there is more to be concerned about beyond this research work.

At the end, I do not want to forget to give thanks to all the members of the Department of Bioresources Engineering at Oregon State University, whose contributions and patience guided this research.

TABLE OF CONTENTS

TABLE OF CONTENTS (Continued)

LIST OF FIGURES

LIST OF FIGURES (Continued)

LIST OF FIGURES (Continued)

LIST OF FIGURES (Continued)

LIST OF TABLES

LIST OF APPENDICES

LIST OF APPENDIX FIGURES

LIST OF VARIABLES

Symbol	Description	Dimensions
1	notation for fine soil	
2	notation for coarse soil	
α	exponent in Gardner's conductivity function; sorptive number	[ ]
α^*	sorptive number of the coarse material in Fig.7. Equivalent to α_2	[ ]
α_f	coefficient in the soil water retention function	[ ]
β	contact angles between water and a tube	[ ]
δ	angle between x' and z'	[ ]
ϕ	angle of sloping interface	[ ]
γ	unit weight of water	$[FT^{-3}]$
λ	pore size distribution parameter	[ ]
θ	volumetric water content	$[L^3L^{-3}]$
θ_a	fictitious extrapolated parameter of the volumetric water content in the soil water retention function used in HYDRUS-2D	$[L^3L^{-3}]$
θ_k	fictitious extrapolated parameter of the volumetric water content in the soil water retention function used in HYDRUS-2D	$[L^3L^{-3}]$
θ_m	fictitious extrapolated parameter of the volumetric water content in the soil water retention function used in HYDRUS-2D	$[L^3L^{-3}]$
θ_r	residual water content	$[L^3L^{-3}]$
θ_s	saturated water content	$[L^3L^{-3}]$
σ	interfacial tension between water and tube wall	$[FL^{-1}]$
ξ	angle between the vector z and the anisotropic flux vector	[ ]
ψ	pressure potential	[L]
b	thickness of fine layer	[L]
C_a	unknown constant in general solution equation (8)	[ ]
C_b	unknown constant in general solution equation (8)	[ ]
d	diameter of a tube	[L]
d_1, d_2	diameter of a tube (notation 1 for fine and 2 for coarse material)	[L]
e_r	relative error in water balance per time step over the entire domain	[%]
F_G	gravity force of water	[F]
F_R	capillary force of water	[F]
h	pressure head	[L]
h_1, h_2	water height in tube (notation 1 for fine and 2 for coarse material)	[L]
h_a	air entry pressure	[L]
h_c	critical height ($h_c = h_1 - h_2$)	[L]
h_d	empirical parameter in the Brooks-Corey equation	$[L^{-1}]$
h_{il}	height of intermediate layer	[L]
h_k	fictitious, extrapolated parameter in the hydraulic conductivity function used in HYDRUS-2D	[L]

LIST OF VARIABLES (Continued)

Symbol	Description	Dimension
h_w	water entry pressure	[L]
H	total potential	[L]
K	unsaturated hydraulic conductivity function; hydraulic conductivity	$[LT^{-1}]$
K^A	dimensionless anisotropy tensor	[ ]
K_k	fictitious, extrapolated parameter in the hydraulic conductivity function used in HYDRUS-2D	$[LT^{-1}]$
K_r	relative hydraulic conductivity	[ ]
K_s	saturated hydraulic conductivity	$[LT^{-1}]$
K_{xx}	component of hydraulic conductivity function in x-direction	[ ]
K_{zz}	component of hydraulic conductivity function in z-direction	[ ]
K^A_{ij}	first component of the dimensionless anisotropy tensor K^A	[ ]
K^A_{iz}	second component of the dimensionless anisotropy tensor K^A	[ ]
L	upper limit of the diversion length	[L]
l_p	model parameter	[ ]
m	fitting parameter in Van Genuchten equation	[ ]
n	fitting parameter in Van Genuchten equation	[ ]
p	fitting parameter in equation (3a)	[ ]
Q	water flux	$[L^3T^{-1}]$
Q_{max}	upper limit of the diversion capacity	$[L^3T^{-1}]$
q	infiltration rate	$[LT^{-1}]$
q_a	maximum acceptable leakage	$[LT^{-1}]$
q_{an}	resultant flux due to anisotropy	$[LT^{-1}]$
q_t	water velocity	$[LT^{-1}]$
q_w	flux parallel to the inclined interface	$[LT^{-1}]$
S	sink term	[L]
t	time	[T]
∇	Laplacian operator	[ ]
x	horizontal coordinates rotated by the angle ϕ	[L]
x'	horizontal coordinates	[L]
x_i	spatial coordinates	[L]
$\hat{x}$	unit vector in x direction	[ ]
z	vertical coordinates rotated by the angle ϕ	[L]
z'	vertical coordinates	[L]
z_i	spatial coordinates	[L]
$\hat{z}$	unit vector in z direction	[ ]
z''	depth at the water table	[L]

SIMULATING THE EFFECTS OF A CAPILLARY BARRIER USING THE TWO - DIMENSIONAL VARIABLY SATURATED FLOW MODEL SWMS-2D/HYDRUS-2D

1. INTRODUCTION

In the last decades, the influence and importance of the vadose zone as the media transporting atmospheric water towards aquifers has been increasingly reflected in the hydrologic literature. In many regions water supply is strongly dependent upon groundwater as a source; contamination of this water can have tremendous effects on the development of these regions.

Deposition of municipal wastes and hazardous materials can have adverse effects on the subsurface environment due to water percolating through this matter and being contaminated. Covering the wastes with a media of low permeability such as clay or plastic liners is a commonly used engineering method to diminish the amount of water percolating through wastes (Ross, 1990: p. 2625).

Another method of reducing the amount of water percolating into waste deposits is to engineer a capillary barrier above the waste deposits; an arrangement of fine material overlaying coarse material. Due to the higher capillarity in the overlaying fine material, this system can, when constructed with a sloped interface between fine and coarse material, lead to lateral diversion of infiltrating water along the interface. However, at a certain down-dip distance infiltrating water plus lateral flowing water will lead to higher

water pressure above the interface and water will (increasingly in down-dip direction) percolate into the coarse layer, potentially into the waste material deposited.

The knowledge about the so called diversion capacity, Q_{max}, total amount of water diverted laterally, and the diversion length, L, length along the interface before water is infiltrating into the coarse material, is essential for an engineering application of a capillary barrier system. Capillary barriers are also seen in natural features, which might be able to partly explain the relatively quick responses of watersheds (despite lacking surface runoff) upon atmospheric water input.

Ross (1990) developed predictive relationships for Q_{max} and L in terms of material and site-geometric properties and infiltration rate. While Ross considers the α-value (exponent in Gardner's conductivity function) as an important factor in his equation, Steenhuis et al. (1990) used the fine soil air entry pressure, h_a, and the water entry pressure of the coarse soil, h_w, as parameters to obtain the diversion length. Steenhuis et al. (1991) stated that both Ross' equation and Steenhuis' equation have to be combined to calculate the actual ability of a capillary barrier to divert water. Stormont (1995) extended these solutions to incorporate effects of anisotropy in the fine layer.

Billiotte et al. (1988), Fayer et al. (1992), and Oldenburg, Kung and Pruess (1993) performed numerical simulation to test the effect of a capillary barrier. However, none of these authors carried out comprehensive evaluations of the validity of above equations by

changing all involved parameters such as dip angle or infiltration rate as well as the properties of the material used.

In this project the SWMS-2D/HYDRUS-2D[1] code of the U.S. Salinity Laboratory, Riverside, California was used to simulate the water flow in a two-dimensional variably saturated capillary barrier system. The program can incorporate changes in dip angle, infiltration rate, material properties, anisotropy, defects along the interface and can implement single-layered and double-layered straight and curved interfaces. A sensitivity and plausibility analysis was performed in this study to test the outputs of the simulation.

In this report the most important physical features of a capillary barrier are outlined in chapter 2. Chapter 3 then emphasizes on the analytical approaches established by different authors to calculate diversion length and capacity. The HYDRUS-2D - model is briefly described in chapter 4; some aspects of the simulations performed such as material, domain, and mesh properties, as well as a sensitivity/plausibility analysis are outlined in chapter 5. Finally, the results of the simulation in relation to the predicted results given by the analytical approaches from chapter 3 are presented in chapter 6 and chapter 7.

[1] Both codes SWMS-2D and HYDRUS-2D were used in this work to simulate the effects of a capillary barrier. SWMS-2D is the former version of the commercially available HYDRUS-2D version. For convenience, in this report the name HYDRUS-2D will be used, only.

The purpose of this research is to

1. evaluate the general effects of a capillary barrier system upon the movement of infiltrating water using a numerical model,
2. illustrate the expected results of an engineered capillary barrier system with well known and commercially available material,
3. test the published analytical approaches from which the diversion capacity and diversion length can be calculated.

2. CONCEPT OF A CAPILLARY BARRIER

2.1 Definition of a capillary barrier

Ross (1990: p.2625) defined a capillary barrier as an arrangement of unsaturated fine-grained soil overlaying unsaturated coarse-grained soil along a sloping contact which can lead to the diversion of infiltrating water away from the coarser material. A similar definition is given by Stormont (1995: p.783); he also stated that a capillary barrier is effective if the combined effect of evaporation, transpiration and lateral divergence exceeds infiltration from precipitation, thereby retaining a sufficiently negative pressure potential so that breakthrough into the coarse layer does not occur.

2.2 Physical background of a capillary barrier

To predict or simulate the behavior of water flowing in a capillary barrier system one has to have some understanding of (a) the variably saturated flow in porous media and some knowledge of (b) the material's properties that comprise the system. Therefore these two issues will discussed in this chapter.

Let us first have a close look to the interface of two materials of different grain sizes and idealize the pores between the particles as equal-shaped tubes of diameter d (notation 1 will be used for the fine and 2 for the coarse material throughout this report). Such a system is shown in Fig.1. Theoretically, water can not flow from the smaller tube

to the larger tube until the height of the water column h_1 exceeds the critical height h_c, which is equivalent to the difference in the capillary rise of both tubes (Montazer and Wilson, 1984; p.28). Montazer and Wilson stated furthermore that h_c is given by:

$$h_c = h_1 - h_2 = \frac{2\sigma}{\gamma}\left(\frac{\cos(\beta_1)}{d_1} - \frac{\cos(\beta_2)}{d_2}\right) \quad (1)$$

where β_1 and β_2 are the contact angles between water and the tubes, σ is the interfacial tension between water and the tube wall [FL^{-1}] and γ is the unit weight of water [FT^{-3}]. This equation indicates that for increasing differences in pore size or tube diameter, respectively, the value of h_c will increase and therefore the capillary barrier will be more effective.

Montazer and Wilson (1984: p.29) noted three factors affecting the effectiveness of natural capillary barriers: (a) the contrast in pore sizes, (b) the state of flux and (c) the moisture-content distribution of the adjoining units. Clearly the contrast between the material used in an engineered capillary barrier system ought to be as big as possible. Fig.2 shows a sketch of such a system with high contrasting materials, where a nearly-saturated, fine soil overlays a nearly-unsaturated, coarse soil.

With sufficient infiltration, water will accumulate above the interface such that the negative pressure potential in the upper fine soil, h_1, will be bigger than h_c. The pressure potential in the lower coarser material will adjust its magnitude to the changing pressure

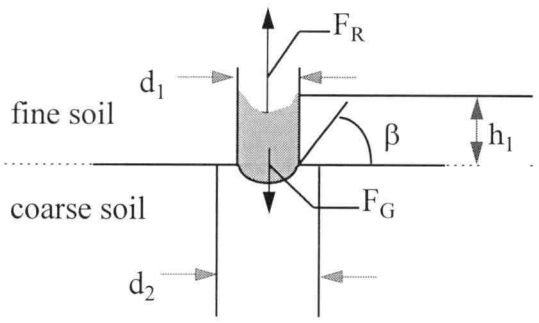

Fig.1 Idealized capillary barrier system of two different materials with pore sizes d_1 and d_2. (F_G: gravity force; F_R: capillary force). (from Montazer 1984; p.27, modified)

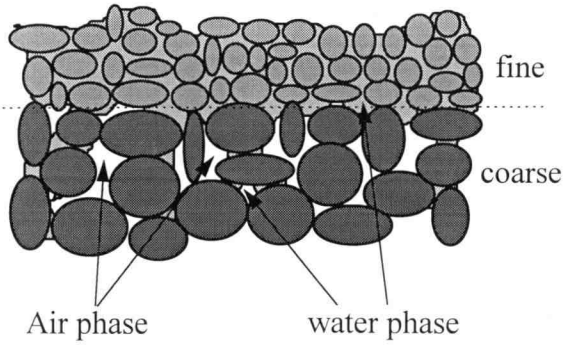

Fig.2 Sketch of a fine-grained layer overlaying a coarse-grained layer. (from Montazer 1984; p.29, modified)

potential above. Since the hydraulic conductivity is a function of pressure potential, as mentioned by Ross (1990; p.2625), the hydraulic conductivity and thus the water content in the coarse material will increase and both will approach a certain value that is dependent upon the infiltration rate q. But if we can modify this system in a way that the upper fine layer is drained laterally, by means of a sloping interface, the capillary barrier might be still effective for a high infiltration rate.

However, before we consider this sloping system we should be able to understand the expected effects of different soils in a capillary system. Therefore, the properties and characteristics of the sands used in the simulation are discussed below.[2]

[2] To emphasize on the engineering application of these simulations commercially-available silica sands (available from Unimin Corporation, Le Sueur, MN; trade name: Accusand) with four different grain sizes were used (12-20, 20-30, 30-40, 40-50). For more details about the characteristics of the sands used in the simulation refer to Schroth et al. (1996 in press) and chapter 3.1.

We know at this point that the contrast of the fine and coarse material should be large and that the hydraulic conductivity is a function of pressure potential. In Fig. 3 the water characteristic curves of three different sands (12-20, 30-40 and 40-50)[3] are graphed

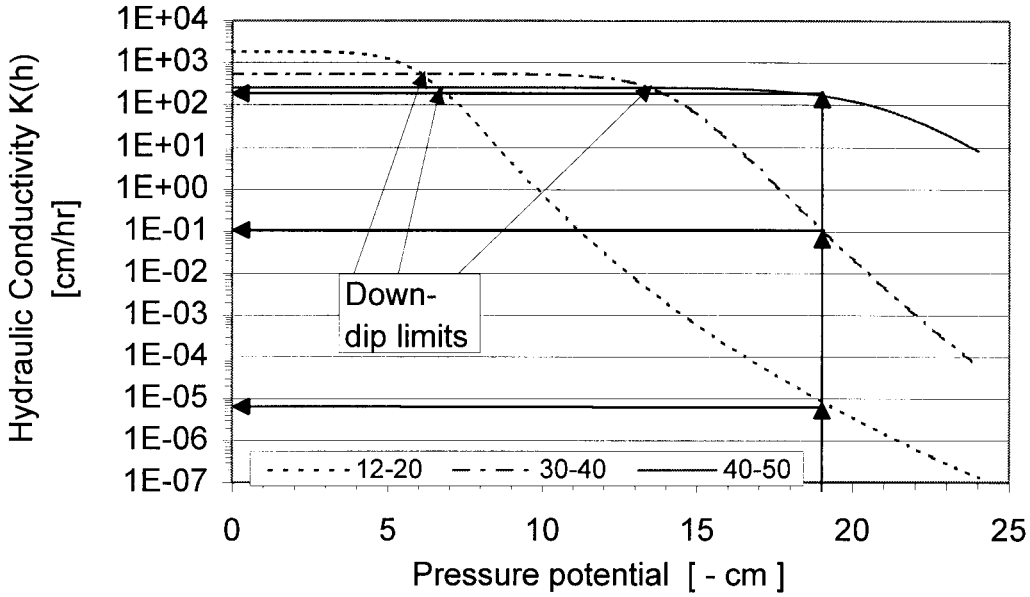

Fig.3 Hydraulic conductivity, K, as a function of pressure potential for the sands used in the simulations (calculated with the Van Genuchten (-Mualem) equation).

on a log-linear scale. If we pick, for example, a pressure potential of ψ = - 19 cm we obtain for the hydraulic conductivity a value of $8.5*10^{-6}$ cm/hr for the 12-20 sand, 0.105 cm/hr for the 30-40 sand, and 166.77 cm/hr for the 40-50 sand. These vast differences (up to 8 orders of magnitude) indicate the usefulness of these sands in a capillary barrier.

[3] The numbers give the range of particles that fall, e.g. for a 12/20 sand, through sieve number 12 but are retained in sieve number 20. Sieve number 12 corresponds to a particle diameter of 1.678 mm, sieve number 20 to 0.841 mm, number 30 to 0.589 mm, number 40 to 0.419 mm and number 50 to 0.297 mm.

As mentioned above, the lateral drainage of the fine soil increases the efficacy of a capillary barrier by increasing the negative pressure potential above the sloped interface. A cartoon of such a system is provided in Fig.4, where q is the infiltration rate at the upper constant flow boundary, ϕ is the slope angle of the interface and the arrows are representing the direction and magnitude of the water flux q_t (the magnitude is outlined by the number of parallel arrows for $q_t > q$ and for $q_t < q$ by means of shifting from dotted to solid lines for increasing flow. The lower boundary condition is considered to be determined by a water table far enough below the system to have no influence on it.

Let us now discuss the movement of water in this system of a sloped interface with a constant infiltration rate and under steady state condition with 12-20 sand as coarse and 40-50 sand as fine material. Infiltrating water at the up-dip position 1 in Fig. 4 will be diverted laterally along the interface. Farther down-dip (Position 2) lateral flowing water plus the infiltrating water will aggregate and lead to a higher water content and the hydraulic conductivity and thickness of the lateral flow region must increase to account for the increased lateral flow. This means, as we can see in Fig.3, that the pressure potential in the upper soil must become less negative. Thus farther down-dip, the system moves more and more towards the left boundary of the graph (in Fig.3) and water starts to infiltrate into the coarse material at Position 3 (of Fig.4). The horizontal length from the up-dip limit to the position 3 is called the diversion length.

At position 4, we reach the point where the pressure at the interface is at that which renders the hydraulic conductivities of both the fine and coarse sand equal. This

point, where the flow into the coarse sand is equal to the infiltration rate q, is called the asymptotic down-dip limit of the capillary barrier (see also Fig.3).

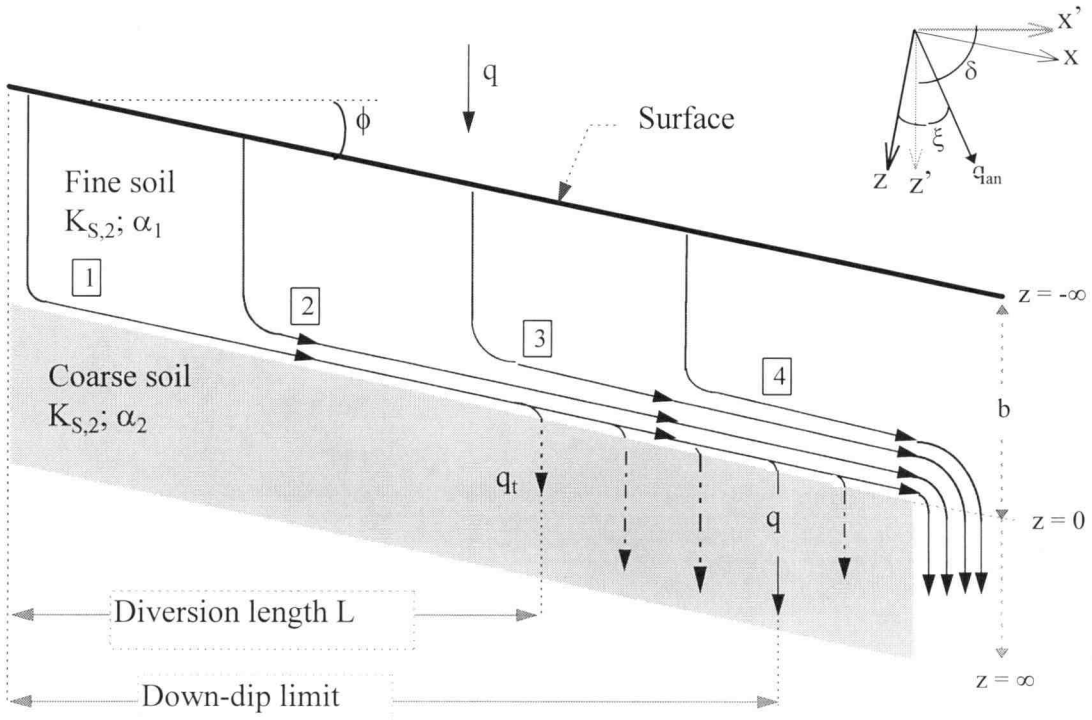

Fig. 4 Flow pattern in an idealized capillary barrier system with an inclined interface between fine and coarse material. (Ross 1990, modified). q: infiltration rate; ϕ: slope angle; x', z': horizontal and vertical coordinates; x, z: coordinates rotated by the angle ϕ, ξ is the angle between the vector of z and the anisotropic flux vector; dark arrows: direction and magnitude of the water flow q_t (the latter is outlined by the number of parallel arrows for $q_t > q$ and for $q_t < q$ by means of shifting from dotted to solid lines for increasing flow).

Besides these definitions Ross (1990; p.2625) introduced another expression: the diversion capacity, which is the flow a capillary barrier can divert before water infiltrates

into the coarse soil. Concluding from above, for an engineering application of a capillary barrier system, we are, of course, interested to calculate diversion length, diversion capacity, and depending upon the application, we may also want to know how much water is infiltrating into the coarse layer at a certain down-dip distance for a given infiltration rate.

3. LITERATURE REVIEW

In this chapter some of the main and most important publications will be reviewed and analytical solutions will be calculated with the equations given in these publications to have a comparison to the numerical solutions presented in chapter 6.

3.1 Properties of the sands used in the simulation - Schroth et al., 1996

An engineering application of a capillary barrier system with well-characterized materials, will reduce the probability of failure due to uncertainties in material parameter range. Schroth et al. (1996) investigated four different sand grades (12-20, 20-30, 30-40 and 40-50 sand) that are commercially-available (Tradename: Accusand®) and determined hydrologically relevant parameters of these sands[4] .

Schroth et al. (1996) obtained values of hydraulic conductivity, K, and water content, θ, as a function of pressure potential, h, using Brooks-Corey-Burdine equation[5]:

$$K(h) = \frac{K_s}{(h_d h)^{\lambda(l_p+1)+2}} \tag{2a}$$

$$\theta(h) = \begin{cases} \theta_r + (\theta_s - \theta_r)(h_d h)^{-n} & (h_d h) > 1 \\ \theta_s & (h_d h) \le 1 \end{cases} \tag{2b}$$

[4] For modeling purposes Schroth et al. (1996) recommended to use the corrected parameters, which will be done throughout the report.

[5] This form of Brooks and Corey's equation was taken out of Van Genuchten et al. (1991; p. 32). More details about this equation are given in Brooks and Corey (1966)

where K_s is the saturated hydraulic conductivity, h_d is an empirical parameter (similar, but not equal to, the inverse of the air entry value h_a), λ is the pore size distribution parameter, l_p is a model parameter (in Mualem's model $l_p = 1.5$; in Burdine's model $l_p = 2$), and θ_s and θ_r are the saturated and residual water contents. The Van Genuchten equation[6] is also widely used:

$$K = K_s \left\{ \frac{\left\{ 1 - (\alpha h)^{n-p} \left[1 = (\alpha h)^n \right]^{-m} \right\}^{3-p}}{\left[1 + (\alpha h)^n \right]^{p^3 m/2p}} \right\} \qquad (3a)$$

$$\theta(h) = \begin{cases} \theta_r + \dfrac{\theta_s - \theta_r}{\left[1 + |\alpha h|^n \right]^m} & h < 0 \\ \theta_s & h \geq 0 \end{cases} \qquad (3b)$$

where α is the sorptive number (or the inverse of the air entry pressure h_a), p is a fitting parameter (p = 1 for Mualem's model and p = 2 for Burdine's model), and m and n are related retention parameters given in Mualem's model as m = 1-1/n and in Burdine's model as m = 1 - 2/n .

With these equations the water retention curves for all four different sand grades were calculated and graphed in Fig.5. From this figure, using the Van Genuchten equation, for a given value of pressure potential, e.g. -19 cm, a hydraulic conductivity of $8.5*10^{-6}$ cm/hr for the 12-20 sand cm and 166.77 cm/hr for the 40-50 sand can be found.

[6] This equation is taken out of Van Genuchten (1980) and modified by the fitting parameter p; p is used to be able to adjust both Mualem's (Mualem, 1976) and Burdine's model into one equation.

For the same value of pressure potential, Fig.6, in which the water characteristic curve of the sands are shown, leads to a water content of about 0.015 cm^3/cm^3 for the 12-20 and 0.3 cm^3/cm^3 for the 40-50 sand.

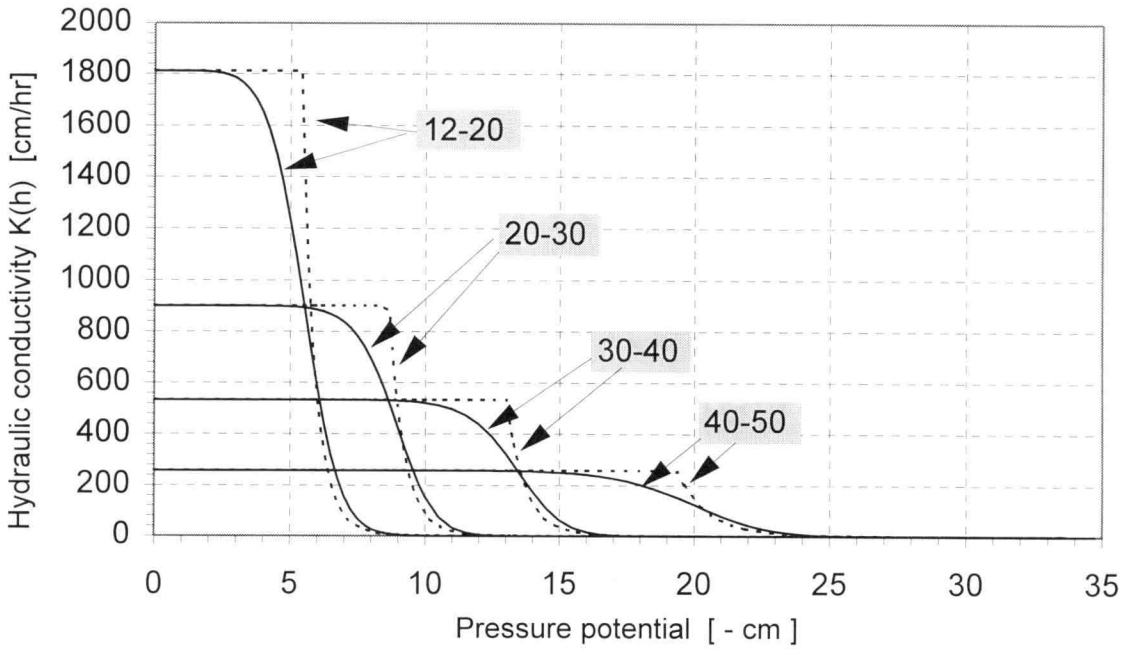

Fig.5 Hydraulic conductivity, K, as a function of pressure potential for the sands used in the simulations. Comparison of Brooks/Corey's equation (dashed line) and Van Genuchten's equation (solid line).

Both the water retention and characteristic curves show highly contrasting properties of the materials. In Fig.6, the air entry pressure h_a for the 40 - 50 sand and water entry pressure h_w for the 12 - 20 sand are also depicted; the contrast between these two values is stated by Steenhuis et al. (1990) to be of importance. Fig.6 also indicates

that there is no preference to use Van Genuchten's equation or Brooks-Corey equation as long as the values of volumetric water content are in the range of 0.05 - 0.3 cm^3/cm^3. Since HYDRUS-2D uses Mualem's model in the Van Genuchten equation, Fig. 5 and Fig. 6 are also based upon this selection[7]. The methods of both Brooks-Corey and Van Genuchten will later be used to simulate the effects of a capillary barrier.

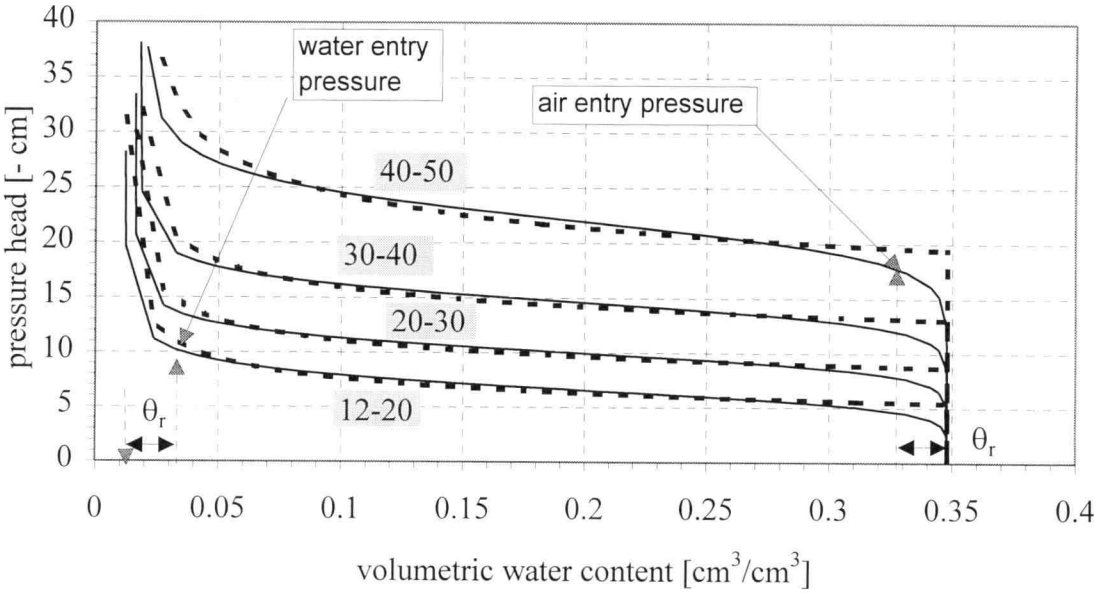

Fig. 6 Water retention curves for the sands used in the simulations calculated with the Van Genuchten-(Mualem) equation (solid line) and Brooks-Corey-(Burdine) equation (dashed line).

The most hydrologically relevant parameters for the sands are outlined in Tab.1; where θ_s and θ_r are the saturated and residual water content, K_s is the saturated hydraulic conductivity, n is the Van Genuchten retention parameter, α is the exponent in Gardner's

[7] Van Genuchten found that calculated values from his equation in combination with Mualem's model fit better to his field data. In literature, there is a preference to use the Brooks-Corey equation associated with Burdine's model and Van Genuchten's equation with Mualem's model.

Tab.1 Corrected values of some of the hydrologically relevant parameters of the sands used in the simulation. (from Schroth et al. 1996).

sand grades	θ_s **[cm^3/cm^3]**	θ_r **[cm^3/cm^3]**	α **[cm^{-1}]**	**n [ ]**	K_s **[cm/hr]**	h_d	h_a **[-cm]**	h_w **[-cm]**	λ
12 - 20	0.348	0.012	0.151	7.35	1800	5.42	4.5	11.2	3.94
20 - 30	0.348	0.016	0.0995	10.57	900	8.66	7.6	13.4	5.57
30 - 40	0.348	0.018	0.0679	13.10	534	13.03	11.8	18.6	6.91
40 - 50	0.348	0.020	0.0453	12.18	258	19.37	17.6	28.2	6.17

conductivity function (or air entry value $h_a = \alpha^{-1}$), λ is the pore size distribution parameter, h_a and h_w are air and water entry pressure, and h_d is an empirical parameter Those parameters will be used later in this report to obtain analytical solutions and were also used in the simulation.

The values of h_a and h_w are obtained as follows: For h_w, by setting the volumetric water content equal to two times the residual water content, θ_r, and for h_a, by setting the volumetric water content equal to the saturated water content, θ_s, minus θ_r and calculating the appropriate value of pressure head h with the Van Genuchten equation (see also Fig.6). Since the diversion length depends on the difference between h_a and h_w in the Steenhuis (28) and Ross - Steenhuis (31a, 31b) equation given in a paragraph 3.6, with above described procedure, the calculated values for the diversion length L are relatively conservative.

3.2 Diversion length and capacity - Ross (1990)

"The diversion capacity of capillary barriers", published in 1990 by Benjamin Ross, emphasized the development of an equation to calculate diversion capacity, Q_{max}, and diversion length, L, of a capillary barrier. In this chapter and in appendix A the mathematical derivation obtained by Ross will be summarized and Ross' solution will be applied to a capillary barrier system with the same properties and features as like as the one numerically solved and presented in a later chapter.

Ross derived the following equation for steady unsaturated water flow[8] from Richard's equation

$$\nabla^2 K_r = \frac{\partial K_r}{\partial x}\alpha \sin\phi + \frac{\partial K_r}{\partial z}\alpha \cos\phi \qquad (4)$$

whereas ∇^2 is the Laplacian operator, x and z are the horizontal and vertical coordinates rotated by the angle ϕ (as depicted in Fig.4 in chapter 2.2), K_r is the relative hydraulic conductivity, and α is the exponent in Gardner's conductivity function. Referring to Fig. 4, setting $z = 0$ at the contact of fine and coarse material and using the conservation laws, the potentials and the fluxes have to be equal across the interface; this means that $\psi_1(0) = \psi_2(0)$ [9] or using Gardner's relationship $K_r(0) = K_s e^{\alpha\psi(0)}$ with $K_r = K/K_s$ that

$$\frac{1}{\alpha_2}\ln K_{r,2}(0) = \frac{1}{\alpha_1}\ln K_{r,1}(0) \qquad (5)$$

---

[8] The derivation is outlined in Appendix A (A.1.1)

[9] Notation 1 for the fine and 2 for the coarse material will be used throughout this report.

For steady state condition, the infiltration rate q equals the hydraulic conductivity K_1 at the upper boundary and therefore

$$K_{r1} = q / K_{s1}. \tag{6}$$

Ross (1990) stated that a regime as shown in Fig.4 has no gradient in x direction; thus (4) can be written as

$$\frac{\partial^2 K_r}{\partial z^2} - \alpha \cos\phi \frac{\partial K_r}{\partial z} = 0 \tag{7}$$

A general solution[10] of (7) with two unknown constants C_a and C_b is given by

$$K_r = C_a^{\,\alpha \cos\phi\, z} + C_b \tag{8}$$

Since (7) has to be solved for the upper and the lower material, the constants C_a and C_b have to be calculated for the fine ($z < 0$) and the coarse ($z > 0$) sand; therefore notation C_{a1} and C_{b1} is used for the fine and C_{a2} and C_{b2} for the coarse material.

For the coarse material (8) can be written as

$$K_{r1}(z) = C_{a2}^{\,\alpha_2 z \cos\phi} + C_{b2} \qquad (z > 0) \tag{9}$$

Assuming that the water table is far below the interface ($z >> 0$, with z" the depth at the water table) and K_{r2} equals 1 near the water table, (9) can be solved for C_{a2}, which gives

[10] The derivation of the general solution for (6) is performed in Appendix A (A.1.2)

$$C_{a2} = e^{-\alpha_2 z'' \cos\phi}(1 - C_{b2}) \tag{10}$$

Substituting (10) into (9) and considering that $e^{-\alpha_2 \cos\phi z}$ is very small for $z >> 0$ leads to

$$K_{r2}(0) = C_{b2} \tag{11}$$

Ross (1990; p.2627) showed that k_{r2} declines from 1 at the water table toward an asymptotic value C_{b2} at the interface. The assumption that the water table is far below the interface leads to the fact that k_{r2} is dependent on the downward flux into the lower layer only, and thus (6) can be written for the coarse material as

$$K_{r2} = C_{b2} = q / K_{s2} \tag{12}$$

Similar to that, for the upper boundary (the fine material) the value of K_{r1} is given from (6) as $K_{r1} = q / K_{s1}$, thus the value of C_{b1} is equal to q / K_{s1}.

Solving (5) for K_{r1} gives

$$K_{r1}(0) = [K_{r2}(0)]^{\frac{\alpha_1}{\alpha_2}} \tag{13}$$

writing (8) in terms of the fine material,

$$K_{r1} = C_{a1}{}^{\alpha_1 \cos\phi z} + C_{b1} \tag{14}$$

substituting (12) and (14) with $z = 0$ and $C_{b1} = q/K_{s1}$ into (13), to obtain

$$C_{a1} + \frac{q}{K_{s1}} = \left(\frac{q}{K_{s2}}\right)^{\frac{\alpha_1}{\alpha_2}} \tag{15}$$

putting (15) into (14) and considering that $C_{b1} = q/K_{s1}$ gives

$$K_{r1}(0) = \left[\left(\frac{q}{K_{s2}}\right)^{\frac{\alpha_1}{\alpha_2}} - \frac{q}{K_{s1}}\right] e^{\alpha_1 \cos\phi z} + \frac{q}{K_{s1}} \tag{16}$$

which is the exact solution for conductivity and pressure for the sloping interface in the fine soil at the down-dip limit.

To get the horizontal flux along the capillary barrier we use Darcy's law, stated as

$$q = -K\vec{v}\left[\psi\left(\hat{x}\cos\phi - \hat{z}\sin\phi\right)\right] \tag{17}$$

with $\hat{z}$ and $\hat{x}$ as the unit vectors; or (since there are no gradients in x direction and $K_1 = K_{r1} K_{s1}$ for the fine material)

$$q = K_{s1} K_{r1}(z)\left[\frac{\partial\psi}{\partial z}\sin\phi\right] \tag{18}$$

Integrating (18) from z = 0 to z = -∞, with vertical length given by dz/dcosϕ leads to

$$Q = \int_{z=0}^{-\infty} K_{s1} K_{r1}(z)\left[\frac{\partial\psi}{\partial z}\sin\phi\frac{dz}{\cos\phi}\right] \tag{19}$$

then integrating over pressure gives

$$Q = \int_{\psi(-\infty)}^{\psi(0)} K_{s1} K_{r1}(z) \tan\phi \, d\psi \tag{20}$$

Now using $K_{r1} = K_s e^{\alpha_1 \psi}$ and (20) can be written as

$$Q = \frac{K_{s1} \tan\phi}{\alpha_1} [K_s e^{\alpha_1 \psi(0)} - K_s e^{\alpha_1 \psi(-\infty)}] \tag{21}$$

or since $K_s e^{\alpha_1 \psi(0)} = K_{r1}(0) = (q / K_{s2})^{(\alpha_1/\alpha_2)}$ and $K_s e^{\alpha_1 \psi(-\infty)} = K_{r1}(-\infty) = q/K_{s1}$, the down-dip diversion capacity Q_{max} is found to be

$$Q_{max} = \frac{K_{s1} \tan\phi}{\alpha_1} \left[\left(\frac{q}{K_{s2}} \right)^{\frac{\alpha_1}{\alpha_2}} - \left(\frac{q}{K_{s1}} \right) \right] \tag{22}$$

Ross reported that a reasonable assumption is to say $q << K_{s1}$ and that $K_{r1}(0) \approx 1$ (the fine soil is essentially saturated at the point where breakthrough occurs) and so

$$Q_{max} = \frac{K_{s1} \tan\phi}{\alpha_1} \tag{23}$$

To get the diversion length L, defined as the horizontal length for which water is fully diverted by the capillary barrier, the total flux over distance L is equal to the vertical flux q times L ($Q_{max} = q\ L$); using this relationship (22) and (23) are found to be

$$L = \frac{K_{s1} \tan\phi}{q\alpha_1}\left[\left(\frac{q}{K_{s2}}\right)^{\frac{\alpha_1}{\alpha_2}} - \left(\frac{q}{K_{s1}}\right)\right] \tag{24}$$

and

$$L = \frac{K_{s1} \tan\phi}{q\alpha_1} \tag{25}$$

Both Q_{max} and L in equations (22), (23), (24) and (25) must be seen as upper bounds on diversion capacity and length. Ross (1990; p.2628) mentioned that the down-dip limit, the horizontal length for which the leakage into the underlying coarse material equals the infiltration rate q (see Fig.4), will be achieved soon after the initial breakthrough occurred; for strongly contrasting materials, there will be a rather short transition zone. Ross (1990; p.2628) also stated that equation (22), (23), (24) and (25) are valid only, if the thickness of the overlaying layer is at least a few times α^{-1}.

3.3 Diversion length and capacity - Steenhuis et al. (1990), Steenhuis et al. (1991)

In 1990, Steenhuis et al. presented a paper ("Flow regimes in sandy soils with inclined layers") in which, among others, the flow pattern in the vicinity of a capillary barrier was investigated and a mathematical expression to calculate the diversion length was derived. Laboratory experiments were also conducted to test the validity of this equation.

Referring to Fig.1 in chapter 2.2, Montazer and Wilson stated that water can flow from the upper smaller pore (diameter d_1) into the lower larger pore (d_2) only, if the water height h_1 in the upper pore exceeds the critical height h_c (with h_c defined as the difference in capillary rise of both tubes). Steenhuis et al. (1990), employ the same conceptual model, where they posit that water will flow from the smaller tubes of the fine soil into the larger tube of the coarse soil as soon as the water height h_1 exceeds the difference between the water entry pressure of the coarse soil, h_{w2}, and the air entry pressure of the fine soil, h_{a1}. Or mathematically stated:

$$h_{a1} + h_1 = h_{w2} \tag{26}$$

Again, solving for h_1 ($h_1 = h_{w2} - h_{a1}$) shows that high contrasting materials for the fine and coarse layer will increase the efficacy of a capillary barrier; however, water moves immediately into the coarse layer if h_{a1} is larger than h_{w2}. Montazer and Wilson's approach does, in contrast to Steenhuis et al. (1990), not consider any hysteresis effects.

Steenhuis et al. (1990) found that the flux per unit width, q_w, defined as the flux parallel to the inclined interface at a down-dip distance equal to the diversion length, is

$$q_w = \sin\phi \int_{h_{w2}}^{h_{a1}} K_1(\psi)\,d\psi \tag{27}$$

since at this point (point 3 in Fig.4 of chapter 2) the pressure potential, ψ, in the capillary fringe at the interface is equal to $-h_{w2}$.

Assuming that at steady state K is independent of ψ (being essentially saturated) and since the infiltration rate q is related to the diversion length L as ($L = q_w/q$), (27) can also be written as

$$L = \frac{K_{s1} \sin\phi}{q}\left(h_{a1} - h_{w2}\right) \qquad (28)$$

Steenhuis et al. (1990, p.12) analyzed experimental data conducted in a flow apparatus in comparison to the results given by (28), which showed an underestimation of the diversion length L when calculated with (28). A sketch of a typical flow pattern (fingered flow) observed by Steenhuis et al.(1990; p. 11) in the experiments is presented in App.B-Fig.1. Chapter 6 will show if this flow pattern can also be found with the HYDRUS-2D model.

A second paper presented in this chapter, published in 1991 by Steenhuis et al. (Comment on "The diversion capacity of Capillary barriers" by Benjamin Ross), combined Ross' (24) and Steenhuis' (28) equation, since in both equation some assumptions restricted their applicability.

Steenhuis et al. (1991; p.2155) criticized Ross' assumptions that he pre-requested (a) "a stable wetting front produced by the interface of two layers", despite the fact that unstable flow regimes (finger flows) were found by many authors, and that (b) the α - value is a constant in Gardner's conductivity function; Steenhuis et al. (1991; p.2155) stated that the α - value might be not constant near saturation and suggested, instead of

using Gardner's relationship $K = K_s e^{\alpha\psi}$, to calculate K with Rijtema's relationship, which is especially valuable near saturation, given as

$$K = K_s \qquad \text{for } |\psi| < h_a \quad \text{and} \tag{29a}$$

$$K = K_s e^{[\alpha(\psi + h_a)]} \qquad \text{for } |\psi| \geq h_a \tag{29b}$$

Thus using (29b) and combining Steenhuis' (28) and Ross' (24) solution, gives

$$L = \frac{K_{s1} \sin\phi}{q}\left(h_{a1} - h_{w2}\right) + \frac{K_{s1} \tan\phi}{q}\alpha_1^{-1} \tag{30}$$

if q is much smaller than K_{s1}; or more accurately and assuming that $\tan\phi = \sin\phi$ for small interface angles[11]

$$L = \frac{K_{s1} \tan\phi}{q}\left[\alpha^{-1}\left(1 - \frac{q}{K_{s1}}\right) + \left(h_{a1} - h_{w2}\right)\right] \qquad \text{for } h_{a1} > h_{w2} \tag{31a}$$

and

$$L = \frac{K_{s1} \tan\phi}{q}\left[e^{\alpha_1(h_{a1} - h_{w2})} - \frac{q}{K_{s1}}\right] \qquad \text{for } h_{a1} \leq h_{w2} \tag{31b}$$

As shown above, where (22) is diminished to (23), then (31a) reduces to (30) when $q << K_{s1}$. Steenhuis et al. (1991; p.2155) stated that α_1^{-1} and h_{a1} are very often of the same

[11] Ross (1991) also derived both equations (31a, 31b) from his solution scheme on a reply to Steenhuis et al. (1991). The derivation of (31b) is shown in App. A. (A.2.)

magnitude and therefore both Steenhuis and Ross do underestimate the ability of a capillary barrier to divert water laterally, but using (30), (31a, 31b) will give more accurate results.

3.4 Anisotropy in a capillary barrier system - Stormont (1995)

In 1995, Stormont presented a paper ("The effects of constant anisotropy on capillary barrier performance") in which he modified Ross' solution (24) and Ross - Steenhuis' solution (31a, 31b) to incorporate constant hydraulic conductivity anisotropy of the fine layer.

Stormont (1995; p.783) stated that in a homogenous layer, anisotropy is due to particle orientation which could be engineered purposefully by inducing a preferential particle orientation or constructing a layered profile; he cited Chapius and Gill (1989) who found the limit of anisotropy[12] for a homogenous material to be 4. Thus an engineered capillary barrier with an anisotropic upper layer by means of higher conductivity in lateral direction can increase the effect of capping.

To include anisotropy into Ross' solution, the same problem domain as shown in Fig.4 of chapter 2.2 is used. Referring to Ross' definition (1990: p. 2626) of hydraulic conductivity (Gardner's quasi-linear approximation of K), $K_{l,ij}$ for the fine material in this problem is given as

[12] This ratio will be used later in the simulation.

$$K_{1,ij} = K_{s1,ij} e^{\alpha_1 \psi} \tag{32}$$

where $K_{s1,ij}$ is the saturated hydraulic conductivity in a two-dimensional system with its coordinates parallel and perpendicular to the interface.

Stormont makes the assumptions that (a) the media is homogenous and α is constant and therefore independent of moisture content or direction; and, (b) that the fine layer is relatively thick so that the thickness, b, has no influence on the capillary barrier. Referring to Ross' solution of relative conductivity (16) and incorporating (32) into (16) gives

$$K_{r1}(z) = \left[\left(\frac{q}{K_{s2}} \right)^{\frac{\alpha_1}{\alpha_2}} - \frac{q \cos\xi}{K_{s1,zz} \cos\phi} \right] e^{\alpha \cos\phi z} + \frac{q \cos\xi}{K_{s1,zz} \cos\phi} \tag{33}$$

where the term $\cos\xi/\cos\phi$ reflects the deviation of K_1 from vertical with $q \cos\xi$ representing the z - vector and $K_{s1,zz} \cos\phi$ representing the x - vector.
The horizontal flux is found similar to Ross' solution scheme as

$$Q_{max} = \frac{K_{s1,xx} \tan\phi}{\alpha_1} \left[\left(\frac{q}{K_{s2}} \right)^{\frac{\alpha_1}{\alpha_2}} - \frac{q \cos\xi}{K_{s1,zz} \cos\phi} \right] + \left(\frac{K_{s1,xx} - K_{s1,zz}}{K_{s1,zz}} \right) bq \tan\phi \cos\xi \tag{34}$$

where the first term will reduce to Ross' solution (24) for an isotropic material, while the second term goes to zero. Using the relationship $L = q/Q_{max}$ leads to

$$L = \frac{K_{s1,xx}\tan\phi}{q\alpha_1}\left[\left(\frac{q}{K_{s2}}\right)^{\frac{\alpha_1}{\alpha_2}} - \frac{q\cos\xi}{K_{s1,zz}\cos\phi}\right] + \left(\frac{K_{s1,xx} - K_{s1,zz}}{K_{s1,zz}}\right) bq\tan\phi\cos\xi \qquad (35)$$

A second way to determine the effects of anisotropy is to use Ross - Steenhuis equation (31a, 31b) as a basic equation. Again, the term $\cos\xi/\cos\phi$ accounts for the deviation of K_1 from vertical. Thus, taking

$$K_{r1} = 1 \qquad |\psi| \le h_{a1} \qquad (36a)$$

and

$$K_{r1} = e^{\alpha(\psi + h_{a1})} \qquad |\psi| > h_{a1} \qquad (36b)$$

and including h_{w2} into Ross' derivation scheme, gives

$$K_{r1}(z) = \left[e^{\alpha(h_{a1} - h_{w2})} - \frac{q\cos\xi}{K_{s1,zz}\cos\phi}\right] e^{\alpha\cos\phi z} + \frac{q\cos\xi}{K_{s1,zz}\cos\phi} \qquad (37)$$

Similar to the Ross - Steenhuis equation, we have to consider two cases, since the divergence capacity is dependent on the values of h_{a1} and h_{w2}; the first case is when $h_{a1} \le h_{w2}$, and water infiltrates into the coarse layer before the fine material exhibits the saturated hydraulic conductivity. The second case, when $h_{a1} \ge h_{w2}$, water will not move into the coarse layer before the air entry pressure in the fine soil, h_{a1}, is reached. For the first case ($h_{a1} \le h_{w2}$), we find the diversion length to be

$$L = \frac{K_{s1,xx}\tan\phi}{q\alpha_1}\left[e^{\alpha(h_{a1} - h_{w2})} - \frac{q\cos\xi}{K_{s1,zz}\cos\phi}\right] + \left(\frac{K_{s1,xx} - K_{s1,zz}}{K_{s1,zz}}\right) bq\tan\phi\cos\xi \qquad (38a)$$

and for $h_{a1} \geq h_{w2}$

$$L = \frac{K_{s1,xx} \tan\phi}{q\alpha_1}\left[\left(1 - \frac{q\cos\xi}{K_{s1,zz}\cos\phi}\right) + \alpha\left(h_{a1} - h_{w2}\right)\right] + \left(\frac{K_{s1,xx} - K_{s1,zz}}{K_{s1,zz}}\right) bq \tan\phi \cos\xi \quad (38b)$$

(38a, 38b) can also be expressed in form of the diversion capacity using $Q_{max} = q / L$.

Stormont (1995; p.785) wrote that an anisotropy ratio of 4 ($K_{1,xx} = 4\ K_{1,zz}$) will increase the diversion length by a factor of 4. The analytical results (shown in chapter 3.6) will be compared with the numerical solutions in chapter 6.2.4 and 7.

3.5 Simulation of a capillary barrier - Oldenburg and Pruess (1993)

Oldenburg and Pruess (1993; p.1045) reported that simulations of a capillary barrier system using a numerical model can help to "bridge the gap between the simple theoretical approaches and the field observations."[13] In their paper ("On numerical modeling of capillary barrier") a finite difference method was used to (a) determine the leakage pattern into the coarse underlying soil, to (b) test the ability of the model to represent flow exclusion and leakage effects as well as to (c) compare the numerical with the analytical results.

Considering some of the laboratory experiments performed by Steenhuis et al. (1990), in which finger instabilities and channeling in capillary barrier systems were

[13] Simulation of water movement in the vicinity of a capillary barrier were also performed by other authors (Frind et al. 1977, Johnson T. et al 1983 and Billiotte et al. 1988); their papers will not specifically being reviewed.

found, the analytical approaches by Ross (1990), Steenhuis et al. (1990, 1991) and Stormont (1995) seem to be strongly simplified and idealized. Prediction of the leakage pattern using a numerical model can, quoting Oldenburg and Pruess (1993; p.1046), give "a further understanding of the behavior of a capillary barrier". They concluded about earlier numerical studies that:

> "one study did just consider the upper fine layer in which breakthrough would be found, only, if the pressure potential in the soil above the interface is positive (Frind et al. 1977), while Johnson et al. (1983) found that breakthrough can occur even when the water pressure is negative; and Billiotte et al. (1988) just worked on a laboratory scale"

Therefore, Oldenburg and Pruess (1993) simulated the steady state performance of a capillary barrier system in a two-dimensional domain with a length of 750 m and a depth of 60 m. The upper fine layer (50 m thick) was taken to have a permeability of $1 * 10^{-13}$ m^2 ($K_{s1} = 1 * 10^{-4}$ cm/sec) and an α-value of 0.001 cm^{-1} , while the lower coarse materials (10 m thick) were set with a permeability of $2 * 10^{-13}$ m^2 ($K_{s2} = 2 * 10^{-4}$ cm/sec) and a range of 0.02 - 0.08 cm^{-1} for the sorptive number (depending on which material was used in the simulation). The interface was adjusted with an angle of 5 degree and the water table was fixed at a depth of 59 m, so that it intersects with the interface at a horizontal down-dip distance of 103 m.

The ratio of leakage to infiltration for different values of α^* (α^* stands for the sorptive number of the coarse material) and Ross solution (equation 24) versus the horizontal length of the capillary barrier are depicted in Fig. 7. Grid size was found to be non-influencing the results, but since "grid orientation affects any gravity - driven problem" (Oldenburg and Pruess 1993; p.1052), a five- and a nine-point difference scheme were used by the authors to determine the magnitude of these effects.[14]

Citing Fig. 7 and other figures not shown in this report, Oldenburg and Pruess (1993) concluded that the oscillatory behavior of the simulation with $\alpha = 0.07\ cm^{-1}$, as shown in Fig. 7, "delineates the tendency to small-scale instabilities" found by Steenhuis et al. (1991). However, while Ross' solution allows no leakage in the region smaller than the diversion length, the simulations depicted in Fig.7 show an increasing ratio between leakage and infiltration.

Except for $\alpha = 2\ m^{-1}$, the diversion length, L, of Ross' solution and the one simulated do coincide with a drop in the leakage/infiltration ratio can be seen near the breakthrough point of Ross' solution. This refers to the large amount of water conducted into the coarse layer at the area of largest breakthrough, which decreases the pressure potential in down-dip distance.

Two issues in Oldenburg and Pruess paper must be critically considered. First, the water table in the domain at a depth of 59 m and intersecting the interface might influence the results of the simulation even if the sorptive number of the coarse material is not

[14] The nine-point difference scheme exhibited a better accuracy and is therefore shown in Fig.7.

smaller than 2 m^{-1}. This concern is supported by the grid size used in the simulations with 2*2 m elements; thus the region between interface and water table in down-dip distance equal to the diversion length is just represented by two elements.

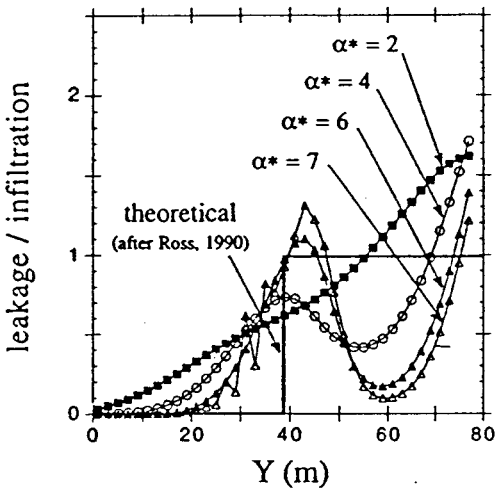

Fig. 7 Leakage/infiltration for the nine-point differencing scheme for four different values of α^*. Note the curve for $\alpha^* = 7\ m^{-1}$ shows an oscillatory behavior that might indicate the smaller-scaled instabilities found by Steenhuis et al (1991). (from Oldenburg and Pruess 1993; p.1053)

Second. and more important, the authors used relatively similar values of saturated hydraulic conductivity, K_s, with $K_s = 1 * 10^{-4}$ cm/sec for the fine and $K_s = 2 * 10^{-4}$ cm/sec for the coarse media, but the α-values differing by two to three orders of magnitude (0.01 m^{-1} for the fine and 2 m^{-1} - 8 m^{-1} for the coarse material)! Using Gardner's quasi-linear approximation for hydraulic conductivity from (32) with a pressure potential of -19 cm, the values of K_s as given above and with α - values of 0.01 cm^{-1}, 2 m^{-1} and 8 m^{-1} would lead to values of K to be about $0.998 * 10^{-4}$ cm/sec,

$1.37 * 10^{-4}$ cm/sec and $0.437 * 10^{-4}$ cm/sec, respectively. Thus, we can clearly see that K of the fine material lies in-between the K's of the two coarse media! Since the sorptive number are highly contrasting, capillary theory (e.g. Miller & Miller, 1956) would suggest even greater contrast in saturated hydraulic conductivities due to the dependency of α - value on pore sizes and that of K_s on the square of pore size.

3.6 Comparison of analytical solutions

In this chapter, the diversion length will be determined using equation: (24), (25), (28), (30), (31a, 31b), (35) and (38a, 38b); the features and properties of the capillary barrier systems used for the analytical solution coincide with those applied in the numerical simulation component of this thesis.

The values of the material properties are taken from Tab.1; referring to Fig.4 in chapter 2.2, for most of the simulations (except when the interface angle is changed) the value of angle ξ equals 79.2 ($\cos\xi = 0.19$), the value of angle ϕ is 5.71 ($\tan\phi = 0.1$), the thickness b of the fine upper layer is 64 cm and the ratio of $K_{s1,xx}$ to $K_{s1,zz}$ is 4. The latter is employed for anisotropic simulations, only.

Tab.2 to Tab.5 give the diversion lengths calculated with above mentioned equations for capillary barrier systems in which some properties are altered; those modification include changes in media combination (Tab.2), infiltration rate for an isotropic fine media (Tab.3) and an anisotropic fine media (Tab.5), and interface angle ϕ

(Tab.4). In all tables, calculation of diversion lengths with distinct analytical solutions exhibit vast differences for the same conditions.

In Tab.2 all the media combination show widespread ranges of the diversion lengths; e.g. for the 20/30 - 30/40 sand, the least contrasting materials, values of L lie between 7 cm and 983 cm (factor of 140!), while for the highest contrasting media combination, 12/20 - 40/50 sand, L ranges from 68 cm to 918 cm (factor of 13.5). Note that equation (25) does not consider the properties of the coarse media while in all other equations the diversion length is a function of fine and coarse media.

Tab. 2 Calculation of diversion length, L [cm], with tan $\phi = 0.1$, $q = 0.8$ cm/hr, under isotropic conditions for four different media combinations.

Media combination fine/coarse	**(24) Ross**	**(25) Ross - simplified**	**(28) Steenhuis**	**(30) Ross - Steenhuis simplified**	**(31a) Ross - Steenhuis $h_{a1} > h_{w2}$**	**(31b) Ross - Steenhuis $h_{a1} < h_{w2}$**
12/20 - 40/50	68	712	206	918	912	(-)
12/20 - 30/40	29	983	40	1023	1017	(-)
20/30 - 40/50	27	712	134	846	840	(-)
20/30 - 30/40	7	983	(-)[15]	875	(-)	879

The diversion lengths for a capillary barrier system, consisting of 12/20-40/50 sand with a straight interface (interface angle of tan $\phi = 0.1$) under isotropic conditions for different infiltration rates, are outlined in Tab.3. In this table we find only equation (24) to be not linear with infiltration rate q. For the same condition, different analytical

[15] Note: Since the diversion length is, after Steenhuis et al. (1990, 1991), dependent upon the values of h_{a1} and h_{w2}, some of the equations are not adequate to be used and, hence, no values are given in the tables.

solutions give again a wide range of predicted diversion lengths. For increasing infiltration rates the factor between lowest and highest prediction of L decreases from about 24 to 8.

Tab. 3 Calculation of diversion length, L [cm], with 12/20-40/50 sand, tan $\phi = 0.1$, under isotropic conditions for different infiltration rates q.

infiltration rate [cm/hr]	**(24) Ross**	**(25) Ross - simplified**	**(28) Steenhuis**	**(30) Ross - Steenhuis simplified**	**(31a) Ross - Steenhuis $h_{a1} > h_{w2}$**
0.1	298	5695	1646	7341	7310
0.2	183	2848	823	3670	3654
0.4	112	1424	411	1835	1826
0.5	95	1139	329	1468	1460
0.8	68	712	206	918	912
1.0	58	570	165	734	729
1.2	51	475	137	612	607
1.6	41	356	103	459	455
2.0	35	285	82	367	363
3.2	24	178	51	229	226
6.4	14	89	26	115	112

Contrary to changes in media combination and infiltration rate for isotropic condition, modification of interface angle ϕ gives a linear change in predicted diversion length for all equations (Doubling the interface angle or halving the infiltration rate q (except for equation 24) leads to an increase in diversion length of factor 2) (see Tab.4). The highest factor found between different analytical solution for the same condition is about 12.6. Equation (24) generally produces the lowest values of diversion length in all three tables above, followed by (28), (25), (30) and (31a)/(31b).

Tab. 4 Calculation of diversion length, L [cm], with 12/20 - 40/50 sand, under isotropic conditions for different dip angles and infiltration rates q [cm/hr].

Dip angle (interface angle) tan ϕ / q	(24) Ross	(25) Ross - simplified	(28) Steenhuis	(30) Ross - Steenhuis simplified	(31a) Ross - Steenhuis $h_{a1} > h_{w2}$
0.05 / 1.0	29	285	83	367	366
0.10 / 1.0	58	570	165	734	729
0.15 / 1.0	87	854	245	1100	1087
0.10 / 2.0	35	285	82	367	363
0.15 / 3.0	38	285	82	367	360

Tab.5 gives the prediction of diversion length for an anisotropic fine layer with a ratio of 4 between K_{xx} and K_{zz} using Ross - Stormont (35) and Steenhuis - Stormont (38b) equation for different infiltration length. The anisotropy ratio of 4 increases L by a factor of 4 when predicted with (35) (in comparison to equation 24), and a factor of >17 bigger than under isotropic condition is predicted with (38b) (in comparison to eq. 28).

Tab. 5 Calculation of diversion length, L [cm], with 12/20 - 40/50 sand, tan ϕ = 0.1, for different infiltration rates q, with an anisotropic fine layer (K_{xx} / K_{zz} = 4)

Infiltration rate [cm/hr]	(35) Ross - Stormont	(38b) Steenhuis - Stormont
1.6	175	1839
3.2	108	921
6.4	67	461
8.0	58	369
12.4	42	232

4. SIMULATION MODEL - SWMS-2D / HYDRUS-2D[16]

4.1 General aspects

HYDRUS-2D is a program that can be used to solve water flow and solute transport problems in two-dimensional variably saturated media; the code, written in ANSI FORTRAN 77 uses the Galerkin type linear finite element schemes to numerically solve the governing flow and transport equations[17] (Šimunek 1994; p.2). The program allows to incorporate irregular domain boundaries, local anisotropy, vertical and horizontal plane flow and a wide variety of boundary conditions (e.g. constant head and flux boundary, atmospheric boundary and free drainage boundary condition)[18].

Since the result of a simulation are affected by the code used, some knowledge of the program's features and limitations is a basic prerequisite for a correct interpretation of the output as well as a help for the reader to get an idea of how this program works. Thus, some important aspects of the program (see topics 4.2 and 4.3) will be discussed shortly in this chapter; a more detailed description is given in Šimunek et al. (1994).

---

[16] As mentioned in chapter 1, SWMS-2D is the former version of HYDRUS-2D; for convenience in this report the name HYDRUS-2D is used, only, to represent both versions (SWMS-2D and HYDRUS-2D).

[17] Due to their size, all simulations described in this project incorporating a conjugate gradient method to solve the symmetric matrix equation resulting from the discretization of the governing flow equation.

[18] Any further considerations about HYDRUS-2D will be directly related to the simulation performed.

4.2 Variably saturated water flow

4.2.1 Governing flow equation

The HYDRUS-2D program numerically solves the following governing equation (modified form of the Richard's equation) using the Galerkin-type linear finite element method:

$$\frac{\partial \theta}{\partial t} = \frac{\partial}{\partial x_i}\left[K\left(K_{ij}^{A} \frac{\partial h}{\partial x_j} - K_{iz}^{A} \right) \right] - S \qquad (39)$$

with

$$K(h,x,z) = K_S(x,z) * K_r(h,x,z) \qquad (40)$$

where θ is the volumetric water content [$L^3\ L^{-3}$], t is the time [T], x_i is the horizontal and z_i is the vertical spatial coordinate [L], K is the unsaturated hydraulic conductivity [LT^{-1}], K_{ij}^{A} and K_{iz}^{A} are components of the anisotropy tensor K^A [ ], h is the pressure head [L], S is a sink term and K_S is the saturated hydraulic conductivity [LT^{-1}].

The equation above does not consider effects of air captured in the soil, hysteresis as well as thermal gradients that might influence the behavior of water movement in capillary barrier systems. The program also does not consider any transport of water in form of vapour, which could be of importance for a capillary barrier system.

4.2.2 Implementation of local anisotropy

The HYDRUS-2D code permits the implementation of hydraulic conductivity anisotropy by varying the orientation of the local principal directions K_{ij}^{A} and K_{iz}^{A} from element to element (Šimunek et al. 1994; p. 33). The local coordinate axis of an element is rotated by a pre-set angle ω in a way that it matches with the principle direction of the tensor K^{A} in the governing flow equation (39). Thus, for an anisotropic material the values of the principle directions K_{ij}^{A} and K_{iz}^{A} and the angle ω have to be input for each element.

4.2.3 Unsaturated hydraulic properties

To solve the governing flow equation for each time step, the unsaturated soil hydraulic properties - soil water retention $\theta(h)$ and hydraulic conductivity $K(h)$ - in dependence of the pressure head must be known. Before starting the numerical simulations, the code computes a table in which these soil hydraulic properties for discrete pressure heads are listed; for values of pressure head in-between two entries, the code linearly interpolate the values of $\theta(h)$ and $K(h)$ from the closest tabulated values. Šimunek et al. (1994;p.33) found this technique to be computationally much faster than direct calculation of hydraulic properties from the Van Genuchten equation.

The soil water retention θ(h) and hydraulic conductivity K(h) are obtained, using a modified form of the Van Genuchten (-Mualem) equation[19], stated as

$$\theta(h) = \begin{cases} \theta_a + \dfrac{\theta_m - \theta_a}{\left(1 + |\alpha_f h|^n\right)^m} & h < h_a \\ \theta_s & h \geq h_a \end{cases} \qquad (41)$$

and

$$K(h) = \begin{cases} K_s K_r(h) & h \leq h_k \\ K_k + \dfrac{(h - h_k)(K_s - K_k)}{h_a - h_k} & h_k < h < h_a \\ K_s & h \geq h_a \end{cases} \qquad (42)$$

whereas θ_s is the saturated soil water content [L^3 L^{-3}], α_f is a coefficient in the soil water retention function [ ], n and m are parameter given by Mualem's model as m = 1 - 1/n, h is the pressure head [L], h_a is the air entry value [L], K_s and K_r are the saturated and residual hydraulic conductivity [LT^{-1}], and the parameters θ_a,θ_m, h_k and K_k are fictitious, extrapolated parameter. Those fictitious parameter are used to "increase the flexibility of the analytical solution and to allow non-zero air entry values" (Šimunek et al. 1994; p.9).

A schematic delineation of both the hydraulic conductivity and the water content in dependency of pressure head are graphed in Fig. 8 and 9. If $\theta_a = \theta_r$, $\theta_m = \theta_k = \theta_s$, and $h_k = h_k$, then (41) and (42) reduce to the original Van Genuchten equations (3a, 3b).

---

[19] This modified form of the Van Genuchten equation is used in the standard and the modified version of HYDRUS-2D; another modification uses the Brooks-Corey equation as given by means of equations (2a) and (2b).

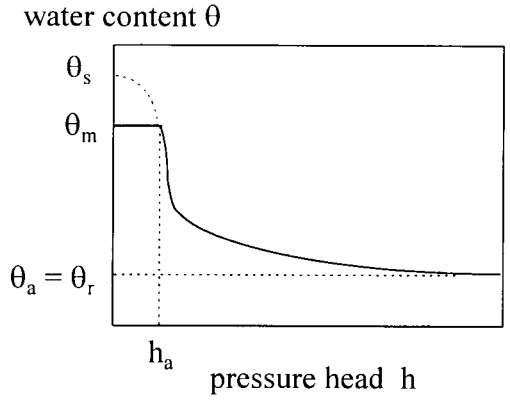

Fig. 8 Schematics of the soil water retention function in HYDRUS-2D as given by equation (41). (From Šimunek et al. 1994; p.10; modified)

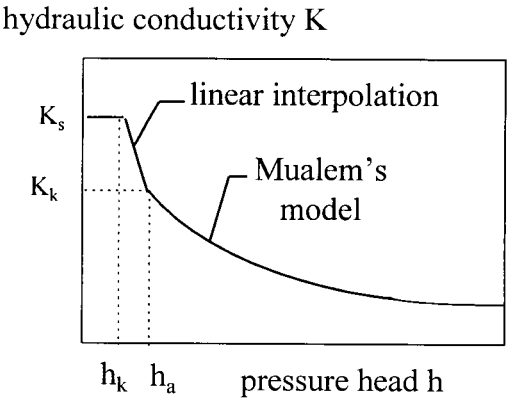

Fig. 9 Schematics of the hydraulic conductivity function in HYDRUS-2D as given by equation (42). (From Šimunek et al. 1994; p.10; modified)

4.3 Numerical solution

4.3.1 Initial and boundary condition

To solve the governing flow equation (39), initial and boundary condition must be specified. The initial condition is prescribed as the initial pressure distribution in the flow domain at time t = 0, whereas the pressure head h is a function of the coordinates x and z. For steady state, which will be reached when the simulation time is sufficiently long, the output of the model should be independent upon the initial condition, however it will be influenced by boundary condition and material properties. A plausibility analysis was performed to delineate the independence of the outputs from the initial pressure head.

The code automatically adjusts the initial water content and the hydraulic conductivity in the problem domain to the pre-set initial pressure head.

The boundary condition used for all the simulation were specified flux (Neumann type) condition at the upper bounds, the vertical lateral limits of the problem domain were put to be non-flux boundary condition and the lower boundary is characterized by a free drainage condition (see Fig. 10 in chapter 5.1).

The free drainage boundary is a unit vertical hydraulic gradient boundary condition which can account for a variable flux. Depending upon the percolation of water, the pressure head h at the nodes along the lower bound is free to vary. Thus, the discharge of water per node (out of the problem domain) is a function of K(h) and the width between the nodes. For an engineering application, the free drainage boundary condition is reasonable since (a) the design of a capillary barrier system should allow free lateral drainage and removal of percolating water at the down-dip end of the barrier and since (b) the construction site should be chosen to have no or a sufficiently deep water table and, thus, having no influence on the efficacy of the capillary barrier. To test the influence of the free drainage boundary condition, for one simulation, the lower bound was taken as a constant pressure head (Dirichlet type) boundary condition. The result of this simulation showed no difference of water movement in the vicinity of the capillary barrier system.

4.3.2 Time and space discretization - Iteration process

In order to numerically solve the governing flow equation "the spatial derivatives have to be approximated with the Galerkin method, while the time derivatives are discretized by means of finite differences" (Šimunek et al. 1994; p.37).

Due to the size of the problem domain and the fine grid size that had to be used to obtain reasonable results in the vicinity of the capillary barrier system, the code covered the problem domain with a network of triangular finite elements with the three corners of the elements set to be the nodal points. At each nodal point, the dependent variable (the pressure head h) was calculated at each iteration step and the values of all three nodal points building an element were linearly interpolated to receive the values of h within the elements. Since the water content and the hydraulic conductivity is a function of pressure head h, for each element, values of both water content and hydraulic conductivity were taken out of the tables put up in the beginning of the simulation describing the water retention and water characteristic curve (see also chapter 4.2.3.).

As mentioned above, time is discretized by means of finite differences and an implicit (backward) finite difference scheme is used to solve the governing flow equation. Maximum, minimum and first time step in HYDRUS-2D have to be pre-set before running the simulation, whereas the first time step should be kept small in order to obtain a solution in the iteration process of the first time step.

The non-linear global matrix a system of linear algebraic equations is derived, and after implementing the boundary conditions, those equations are solved for each iteration step using a conjugate gradient method (Šimunek et al. 1994; p.23). The iteration process for one time step proceeds until a pre-set value of water content and pressure head difference at all nodes between two successive time steps is reached ("until a satisfactory degree of convergence is obtained" - Šimunek et al. 1994; p.24).

The code includes a procedure by which the following time step is fixed by the number of iteration steps necessary to solve the global matrix in the former time step. In general, if those numbers were smaller than or equal to 3, the next time step was multiplied by a pre-determined value (e.g. 1.1 - 1.5); if the value was bigger or equal to 7, then the following time step was reduced by a pre-set value between 0.3 - 0.9. Due to this selection procedure of optimal time step, the program optimized the simulation process and, hence, reduced the time consumption. If a pre-established maximum iteration number was not sufficient to achieve the convergence, then, the time step was reduced by one third and the iterative process repeated.

4.3.3 Water balance computation

At prescribed time steps, the code exhibits a water balance computation and stores the relative error (e_r) of the water balance for the whole problem domain or for pre-selected sub-region in an output file. Due to the iteration process needed to solve the global matrix, at each time step - dependent upon the pre-set convergence criteria (water

content and pressure head difference) - some water is numerically lost in the problem domain. By decreasing the iteration criteria values the amount of numerically lost water can be minimized.

The relative error (e_r) for all nodes is obtained by relating the absolute value of water loss to two terms: (a) the sum of the absolute change in water content over all elements and (b) the sum of the absolute values of all fluxes in and out of the problem domain (Šimunek et al. 1994; p.31). The relative error in water balance will decrease when approaching steady state condition and is therefore a measure of numerical accuracy and a determinant of steady state condition.

5. SIMULATION OF A CAPILLARY BARRIER

5.1 Data input (material, domain and mesh properties ...)

Besides the values to be input in HYDRUS-2D described in former chapters, as like as the material properties (Tab.1 in chapter 3.1), and maximum, minimum and initial time step (chapter 4.3.2), the dimension of the problem domain, the mesh properties and the material distribution must be precised in order for the program to generate the mesh and to finally run the simulation. To view the results, print times have to be pre-set for which the program automatically creates output files in which all properties (hydraulic conductivity and velocity direction, pressure head, and water content for each element, as well as water balance error) are listed; since a steady state analysis was performed, print times were put at 10 hr, 20 hr, 30 hr, 40 hr and 50 hr, generally.

The HYDRUS-2D code includes an automatic mesh generation procedure that, after inputting the dimension of the problem domain and number of fixed nodes, creates a mesh consisting of finite triangular elements. Depending on the number and location of fixed nodes and the degree of refinement and smoothing of the mesh pre-set, the program user is able to form a mesh appropriate to the problem to be solved; The refinement of the mesh is managed by reducing the triangular element sizes, e.g., in direction of large hydraulic conductivity gradients and depending on soil hydraulic properties.
In Fig.10 the mesh and boundary condition are shown for the single straight interface simulation with a refinement above the interface. For this simulation, the node number

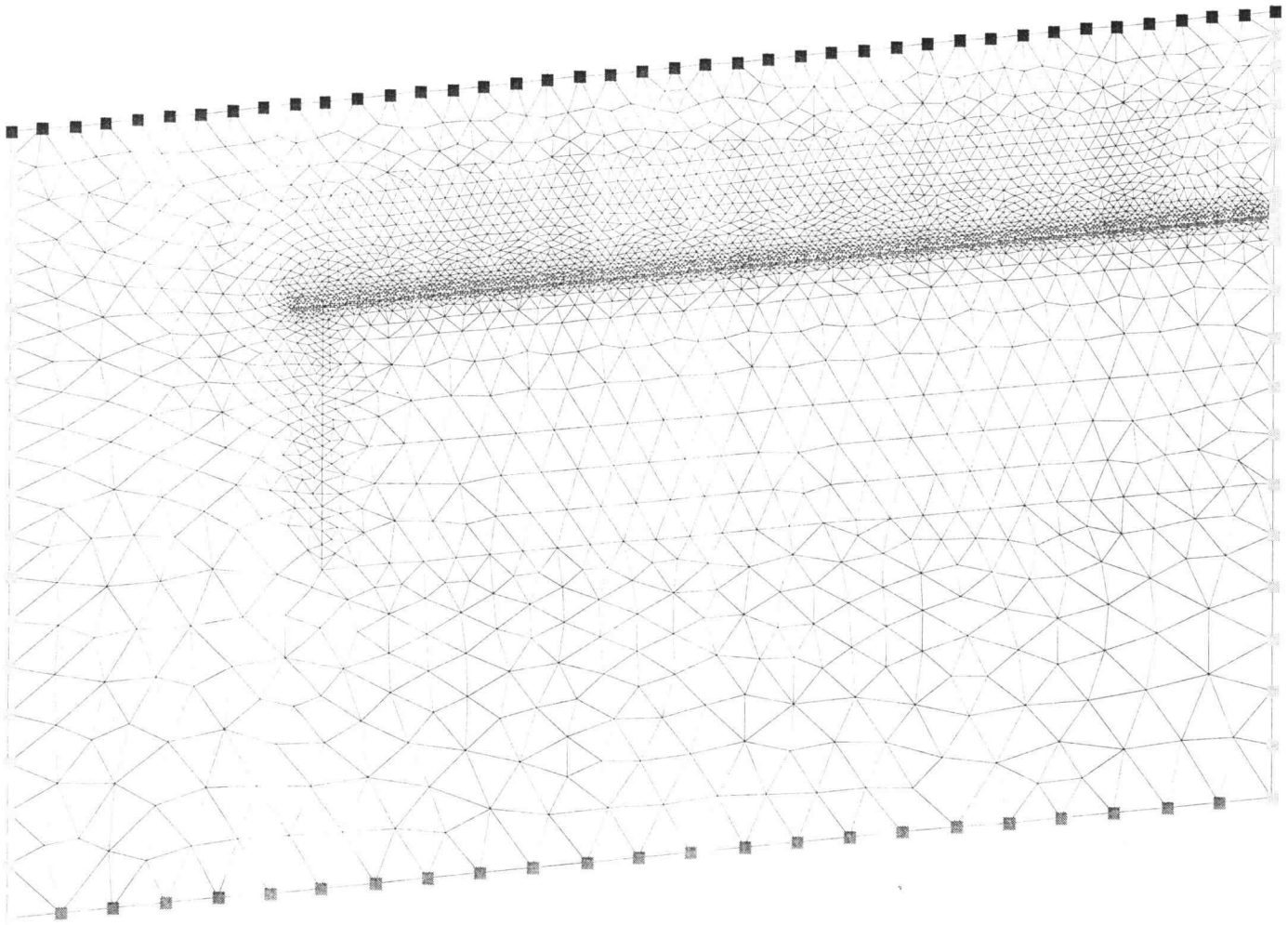

Fig.10 Typical finite element mesh used for the straight interface simulations. Ilustrations includes the boundary conditions; dark grey: constant flux boundary; medium grey: free drainage boundary; light grey: non-flux boundary.

obtained using the automatic mesh generator is about 4700 and the number of triangular elements is 9200. The upper boundary nodes, the steady flux boundary, is graphed in dark gray; the lower bound, the free drainage condition, is depicted as a medium gray, while the lateral boundaries are delineated in a light gray, representing the non-flux boundary condition.

The material distribution and the dimension of the problem domain for the (single and double) straight and curved interfaces are shown in Fig.11 and Fig.12, respectively. Note that for the single straight and curved interface simulations, the lower coarse

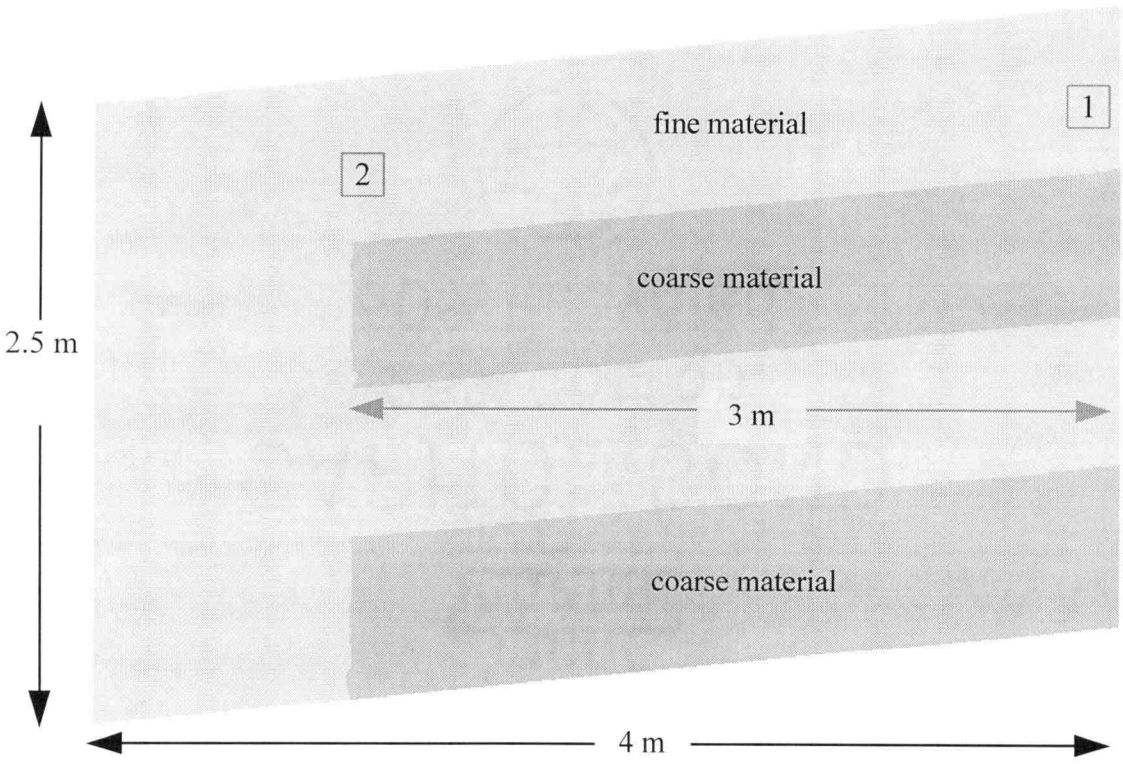

Fig.11 Problem domain and material distribution for simulations with two straight interfaces. Note: For the single straight interface simulations, the lower coarse layer was set to be fine material.

material was set to be fine material. The dimension of the problem domain were chosen in a way that (a) the horizontal length of the interface is 3 meter and (b) the thickness of the fine soil is at least 65 cm.

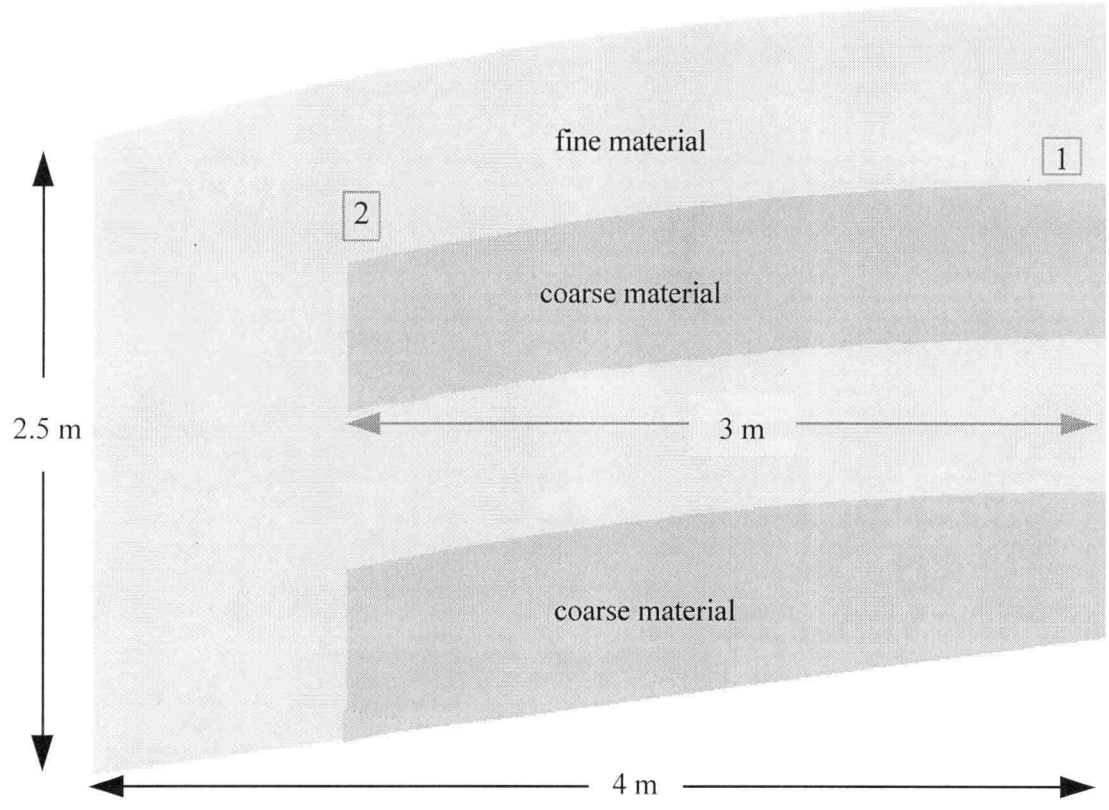

Fig.12 Problem domain and material distribution for simulations with two curved interfaces. Note: For the curved straight interface simulations, the lower coarse layer was set to be fine material.

The drop in height from the up-dip end (point 1) to the down-dip end (point 2) of the interface is equal for both the straight and the curved interface.

5.2 Sensitivity and plausibility analysis

One aspect of a steady state sensitivity analysis is to put the naturally occurring range of media properties into the model and then determine the behavior of the model upon this range (e.g. sensitivity to physical variables). A second set of issues is the sensitivity and plausibility of the steady-state solution provided by the model for a given problem to changes in initial condition, mesh geometry and iteration criteria (water content and pressure head). The analysis performed in this chapter focus on the second issue only, since the material properties are well established. Model performance is assessed by comparing critical flux values with changes in model parameters, as well as by checking the overall water balance computed by HYDRUS-2D over the entire domain, indicating the amount of water lost per iteration step[20].

A simulation was considered to be at steady state when the water pressure[21] distribution in the domain did not visually change in the vicinity of the barrier system for the last two predetermined time plots. (Those two time plots were mostly at 40 and 50 hours; if steady state condition was not reached the simulation was repeated with a longer time period). For all the simulations, the flux from the upper fine layer into the lower coarse layer was measured about 1 cm below the interface.

---

[20] Some more details about the water balance calculation are given in Chapter 6.1.

[21] Water pressure was found to be the most sensitive indicator for steady state.

5.2.1 Mesh size

The result of a simulation strongly depends upon the mesh size used; in a coarser mesh the computational error will generally be larger than it is in a finer mesh (if the iteration criteria are sufficiently small). However, precision is not a linear function of the mesh, (e.g. doubling the mesh elements, will not decrease the computational error by half); of course a finer mesh also increases the amount of computational time per simulation. This leads to a process in which is tried to optimize the relation between needed accuracy and computational capabilities.

To test the effects of mesh size upon the effectiveness of a capillary barrier, four simulations were performed in which the mesh size was changed with all conditions held constant. This was executed for the "standard" and the "modified" version of HYDRUS-2D.

The standard version[22] does not allow to implement a sharp interface between two materials, since the material properties in HYDRUS-2D are attached to the nodal points and not to the elements. As shown in Fig.13, where two materials are adjacent to each other, the code averages the material properties of the three nodes that built the corners of an element and guides these averaged properties to the element. Thus an intermediate layer with an alternating pattern is generated between two materials.

---

[22] The standard code is the version offered by the US Salinity Laboratory

This intermediate layer shows up immediately above the interface, wherefore it is most critical for the water movement in the vicinity of the capillary barrier due to a decrease in contrast of material properties; Thus, the height of this intermediate layer h_{il} will have an effect on the breakthrough velocity. The expectation is thereupon that a

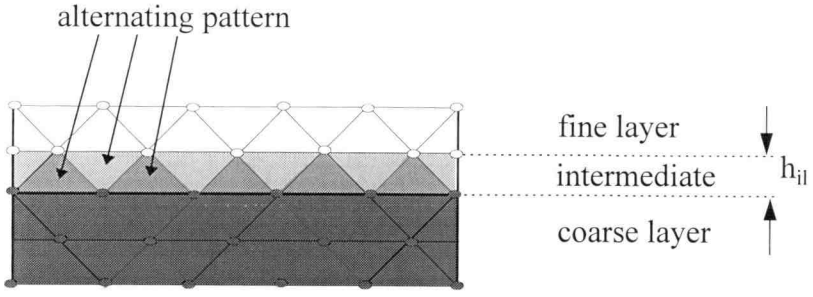

Fig.13 Material distribution at the interface of two media as given by standard HYDRUS-2D.
Material at the nodal points: • coarse ○ fine

decreasing intermediate layer will lower the breakthrough velocity, as displayed in Fig.14, where the percentage of breakthrough velocity to infiltration rate along the interface is graphed. But from this figure, we also see that the artifacts at a down-dip distance of about 220 cm are not (even with a very small h_{il}) appropriately diminished.

The modified version of HYDRUS-2D allows abrupt changes in material properties, since in this code sub-regions can be defined. In these sub-regions materials are associated with elements rather than nodal points. The results of the four simulations with the modified version are also shown in Fig.14. In contrast to the standard version,

the coarser mesh has a lower percentage of breakthrough, but with refinement of the mesh above the interface the graphs approach the same asymptote obtained in using the very fine mesh in the standard version. Also the artifacts, found in the standard version, are diminished for the fine and very fine mesh.

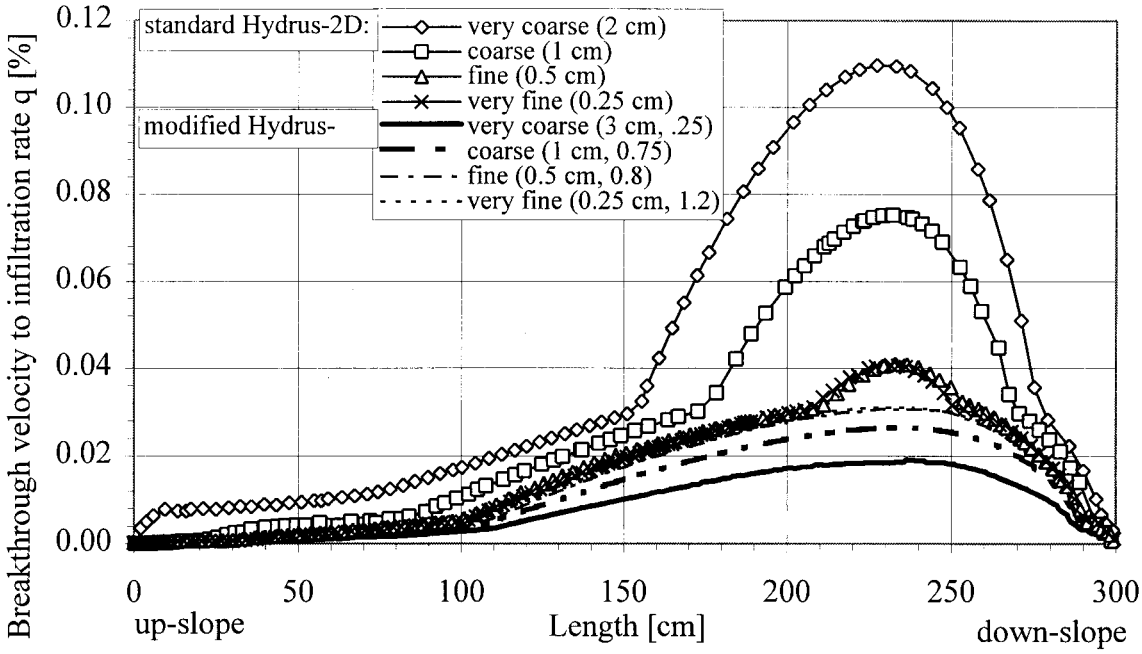

Fig.14 Sensitivity analysis: Breakthrough velocity in percentage of infiltration rate q below the interface for different mesh sizes. Results obtained with both versions: standard Hydrus-2d (gradual interface) and modified Hydrus-2d (abrupt interface). Note: both version uses the look-up table to obtain the hydraulic properties. Number given in parenthesis is the average element height h_{il} above the interface. (q = 0.4 cm/hr, tan(phi) = 0.1, straight interface, (12/20 - 40/50)

This artifact (artificial arch) is considered to be a result of the tabulation of the hydraulic properties, since for any value of pressure head in-between two entries, a linear

interpolation is used to obtain the values of water content and hydraulic conductivity; this means that for a small change in pressure head the program might jump into the next pressure head interval between two entries to get a different water content and hydraulic conductivity value, respectively. In App.B-Fig.2, the pressure head versus the hydraulic conductivity for the same nodes below the interface is depicted. The graph indicates the step function (tabulated values with linear interpolation of values in-between two entries) used to determine the hydraulic conductivity.

Concluding from above, the very fine mesh simulation with the modified version does not significantly improve the result, and since computational time is also of interest (Fig.14), the fine mesh with abrupt material changes will be used in all subsequent simulations (This mesh is shown in Fig.10). In the next two chapter, this mesh is used to perform a sensitivity and plausibility analysis of the model (modified version of HYDRUS-2D) on changes in iteration criteria, maximum time step and initial pressure. This will be executed in two ways: Using the modified HYDRUS-2D version with (a) the tabulation procedure of the hydraulic properties (look-up tables) and (b) with direct calculation of the properties from the Van Genuchten equation.

5.2.2 Iteration criteria

To solve the non-linear global matrix equation for each discretized new time step, an iterative process must be performed. HYDRUS-2D utilizes a conjugate gradient method, with an implicit (backward) finite difference scheme to discretize the time

domain. As mentioned in chapter 4, the iteration procedure is repeated until a specific degree of convergence is achieved; In this program this is satisfied when all nodes exhibit a change of water content (in the unsaturated zone) or of pressure head (in the saturated zone) between two consecutive iteration steps as specified by the operator.

The magnitude of the iteration criteria regulates the accuracy of the numerical solution. Therefore, a stricter iteration criteria leads to less computational (iterational) water losses in the problem domain and, hence, the relative computational mass balance error (e_r) decreases. However, a stricter (smaller) iteration criteria means that the number of iterations to reach the pre-set criteria enlarges and, thus, the computational time increases; If the selection of an iteration criteria is not strict enough, then the accuracy of the computation diminishes which leads to poor results.

The dependency of the results on the choice of iteration criteria for the modified version is borne out in Fig.15 with both hydraulic properties obtained from look-up tables and calculated directly from the Van Genuchten equation. The ratio of breakthrough in percentage of infiltration rate q below the interface is used to determine the sensitivity of the model. All simulations made with the modified version using the look-up tables to obtain the hydraulic properties showed, depending on the iteration criteria, more or less developed artifacts. Two of those simulations are depicted in Fig.15, whereas the pressure head difference (pr) was set to be non-restrictive while the water content criteria was refined from $5*10^{-4}$ cm^3/cm^3 to $5*10^{-5}$ cm^3/cm^3. The graphs show a decrease in leakage with this refinement. A similar result is found when changing the pressure head iteration

criteria from $1*10^{-2}$ cm to $1*10^{-7}$ cm and keeping the water content criteria non-restrictive ($1*10^{-2}$ cm^3/cm^3) (Note: Those results are not shown in Fig.15). From Fig.15, we can clearly see that the tabulation issue is responsible for changing the breakthrough velocity

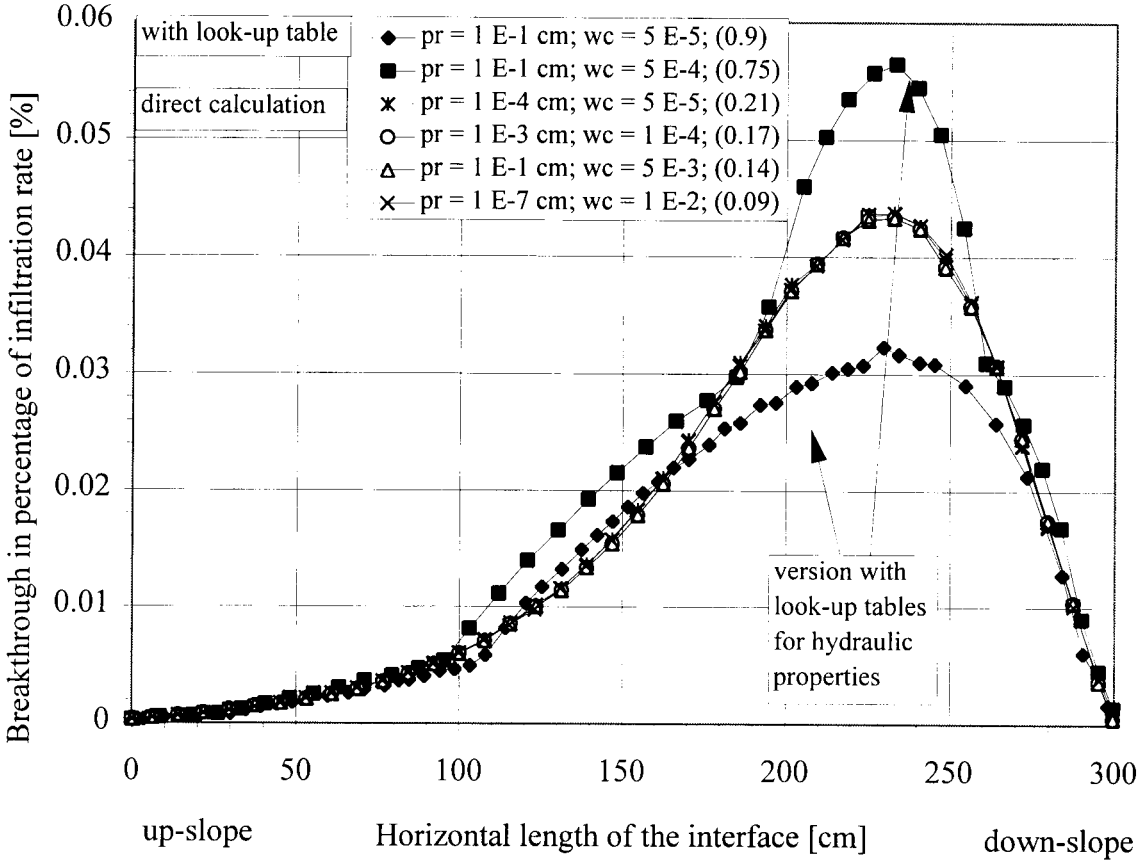

Fig.15 Sensitivity analysis: Breakthrough velocity in percentage of infiltration rate below the interface when changing the iteration criteria (absolute change in water content (wc) and pressure head (pr) between two successive iterations) in the modified Hydrus-2D version with look-up tables and with calculation of hydraulic properties directly from the Van Genuchten equation. Note: Computational time in Pentium days is given in parenthesis. (q = 0.4 cm/hr, tan(phi) = 0.1, 12/20-40/50 sand)

approximately by a factor of two. The relative water balance error (e_r) at time t = 50 hr for the second simulation is relatively high (circa 5 %) due to the non-restrictive water content criteria, while for the first one it is 0.2 %, only. The increase in computational time (in Pentium days) from 0.75 to 0.9 Pentium days indicates the dependence on the choice of the iteration criteria.

The results obtained with the modified version of HYDRUS-2D with direct calculation of the hydraulic properties from the Van Genuchten equation (Fig.15; graph 3 to 6) are not as sensitive to changes in iteration criteria as found with the look-up table version. Despite vast differences in water content criteria, ranging from $1*10^{-2}$ cm^3/cm^3 to $5*10^{-5}$ cm^3/cm^3, and pressure head criteria ($1*10^{-1}$ cm to $1*10^{-7}$ cm), all the graphs exhibit a very nice fit, independent of which iteration criteria was set to be more restrictive. The graphs also do not show any artifacts, but are rather follow a smooth line. The simulation time is, as found with the look-up table version of HYDRUS-2D, strongly dependent on the magnitude of iteration criteria; however, all results with direct calculation of hydraulic properties are obtained in a shorter time (0.09 - 0.21 Pentium days) when compared to the version with look-up tables (0.75 - 0.9 Pentium days).

5.2.3 Maximum time step and initial pressure

As mentioned in chapter 4.3.1, in the beginning of a simulation, HYDRUS-2D adjusts water content and hydraulic conductivity for each element in the flow domain due to the pre-set initial pressure distribution. It then uses the predetermined initial time step

to start the iteration process. If all nodes in the problem domain do not exceed a prescribed water content and pressure head criteria, the code determines the next time step, Δt, to again, for time $t = t + \Delta t$, achieve convergence in the iterative process. The optimization procedure of selecting the upcoming time step (see chapter 4.3.2) will continue and depending on the convergence criteria and the properties and features of the problem to be solved, the pre-set maximum time step might be reached. If the iteration criteria are set to be sufficiently restrictive, the magnitude of the maximum time step should not significantly influence the result at steady state. The initial pressure head distribution should have no effects on the outputs at steady state as well, since HYDRUS-2D does not account for any effects of hysteresis.

In a plausibility analysis, initial pressure and maximum time step were varied and again the leakage pattern into the coarse material was used to compare the effects of those changes. As in chapter 5.2.2, simulations were performed with both direct calculation of hydraulic properties from the Van Genuchten equation and with the look-up table version.

The first two simulations, graphed in Fig.16, are obtained using the look-up table version, whereas the initial pressure head in the problem domain was set to be -35 cm and -25 cm. The leakage into the coarse media for these two simulations differ approximately by a factor of two; thus, these results do not support the expectation that the steady state result are independent of initial pressure head in the look-up table version.

However, applying the same initial pressure heads in the flow domain when using the modified HYDRUS-2D version with direct calculation of hydraulic properties, then the graphs do not exhibit vast differences in breakthrough velocity (graphs 3 and 4 in Fig.16). A nice fit is also found with an initial pressure head of -20 cm in the domain. As in Fig.15, the graphs in Fig.16 obtained with the look-up table version show artifacts,

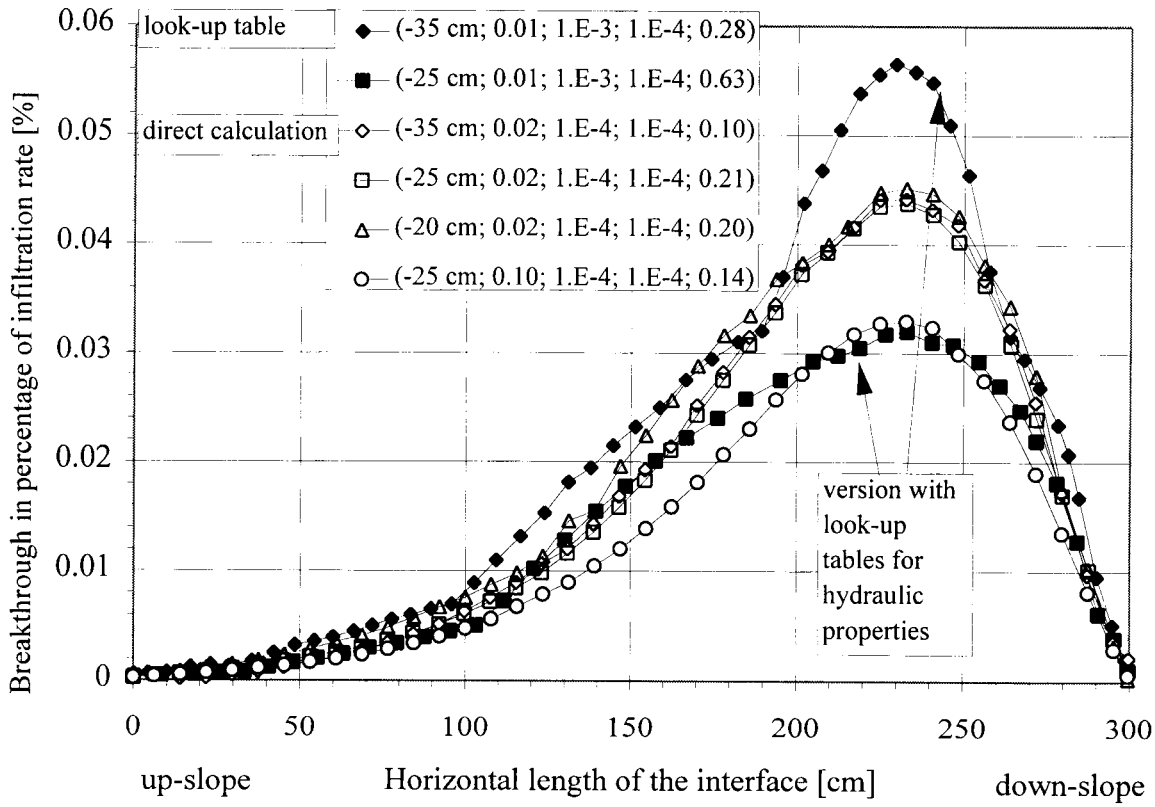

Fig.16 Plausibility analysis: Breakthrough in percentage of infiltration rate q below the interface when changing initial pressure and maximum time step in the modified HYDRUS-2D version (abrupt interface) with (a) look-up tables and with (b) calculation of hydraulic properties directly from the Van Genuchten equation. The values in parenthesis are: initial pressure; maximum time step; pressure head and water content criteria; computational time in Pentium days). (q = 0.4 cm/hr, tan(phi) = 0.1, straight interface, 12/20-40/50 sand).

while the method of direct calculation of hydraulic properties leads to smooth variation. However, the maximum time step seems to play a role even in this version; this is indicated by enlarging the maximum time step from 0.02 hr to 0.1 hr and plotting the results in Fig.16 (graph 4 and 6); the breakthrough into the coarse media decreases with this alteration in maximum time step. Decreasing the maximum time step to 0.02 hr was found to be sufficient in avoiding effects of maximum time step on the results.

As found in the former chapter, the time consumption with the look-up table version was generally higher than when applying the version with direct calculation of hydraulic properties.

5.2.4 Summary of sensitivity/plausibility analysis

The standard version of HYDRUS-2D (gradual interface) was found to be relatively sensitive to mesh size due to the effects of the intermediate layer. The modified version (abrupt interface) with the fine mesh significantly improved the results, and was therefore used in all further simulations. However, all of the graphs showed more or less developed artifacts (artificial arches), which are concluded to be a result of the tabulation of hydraulic properties (look-up tables). Furthermore it can be concluded that the results in Fig.14 would be less sensitive on changes in mesh size when using the direct calculation of hydraulic properties from the Van Genuchten equation

Comparison between simulations using the modified look-up table version of HYDRUS-2D and the version in which the hydraulic properties are calculated directly from the Van Genuchten equation, showed that the latter version is far less sensitive to changes in iteration criteria and preset initial pressure head in the flow domain. The artifacts found in the look-up table version were not discovered in the version with direct calculation of hydraulic properties.

In contrast to Šimunek's statement (1994; p.33), the look-up table version did not reduce the computational time. On the contrary, the modified HYDRUS-2D version with direct calculation of hydraulic properties performed equivalent simulations in a much shorter time (see Fig.15 and Fig.16). The reduction is up to ten times. An explanation for that might be that with the tabulated version the chance is relatively high that some of the nodes have a pressure head that is close to an entry value in the table, and slight changes in pressure head between two time steps put the value of those nodes in another interval with a different interpolation slope. Due to the different slope a change in pressure head and, hence, of water content between two consecutive time steps for those nodes might be higher than allowed by the water content iteration criteria and thus more iteration steps are needed to converge.

A maximum time step chosen too large (Fig.16; graph 6 with 0.1 hr) seems to influence the result, since for larger time steps and depending on the iteration criteria, the computational error increases. The procedure for selecting the next time step, Δt, at time

$t = t + \Delta t$, depends on the number of iteration at time t; this procedure in interaction with the iteration criteria might play a role in the difference of breakthrough velocity found in graph four and six of Fig.16. Therefore, the maximum time step is set to be 0.02 hr, and for most of the simulations, the iteration criteria are put to $1*10^{-4}$ cm and $1*10^{-4}$ cm^3 cm^{-3} for pressure head and water content criteria, respectively.

6. RESULTS OF THE SIMULATION - DISCUSSION OF THE RESULTS

6.1 General effects of a capillary barrier in the simulations

Before going into more details on the effects of water movement in the vicinity of capillary barrier systems, in this chapter, the water content and pressure head distribution pattern in the problem domain is briefly outlined using a capillary barrier system with a single straight interface.

Setting the initial pressure head in the problem domain to -25 cm and applying a steady infiltration rate of 1.6 cm/hr at the upper bound, water will infiltrate into the fine media (App.B-Fig.3)[23]. Then, an infiltration front will hit the interface and built up a fringe of higher water content above the contact of fine and coarse media (App.B-Fig.4). With increasing water content, the barrier starts to divert water, laterally (App.B-Fig.4 and App.B-Fig.5), and pressure head and hydraulic conductivity in the coarse sand will adjust to the changing properties in the upper fine material. With further increase in water content in the capillary fringe, water begins to leak into the coarse media (App.B-Fig.6).

After 60 hours of steady infiltration, the system reached quasi-steady-state condition (the water content distribution is shown in Fig.17). A typical characteristic of a straight interface, as indicated in Fig.17, is the almost linear increase in water content in

[23] A sequence of figures illustrates the development of a typical flow pattern in a capillary barrier system (See App.B-Fig.3 through App.B-Fig.6 and Fig.17 and Fig.18)

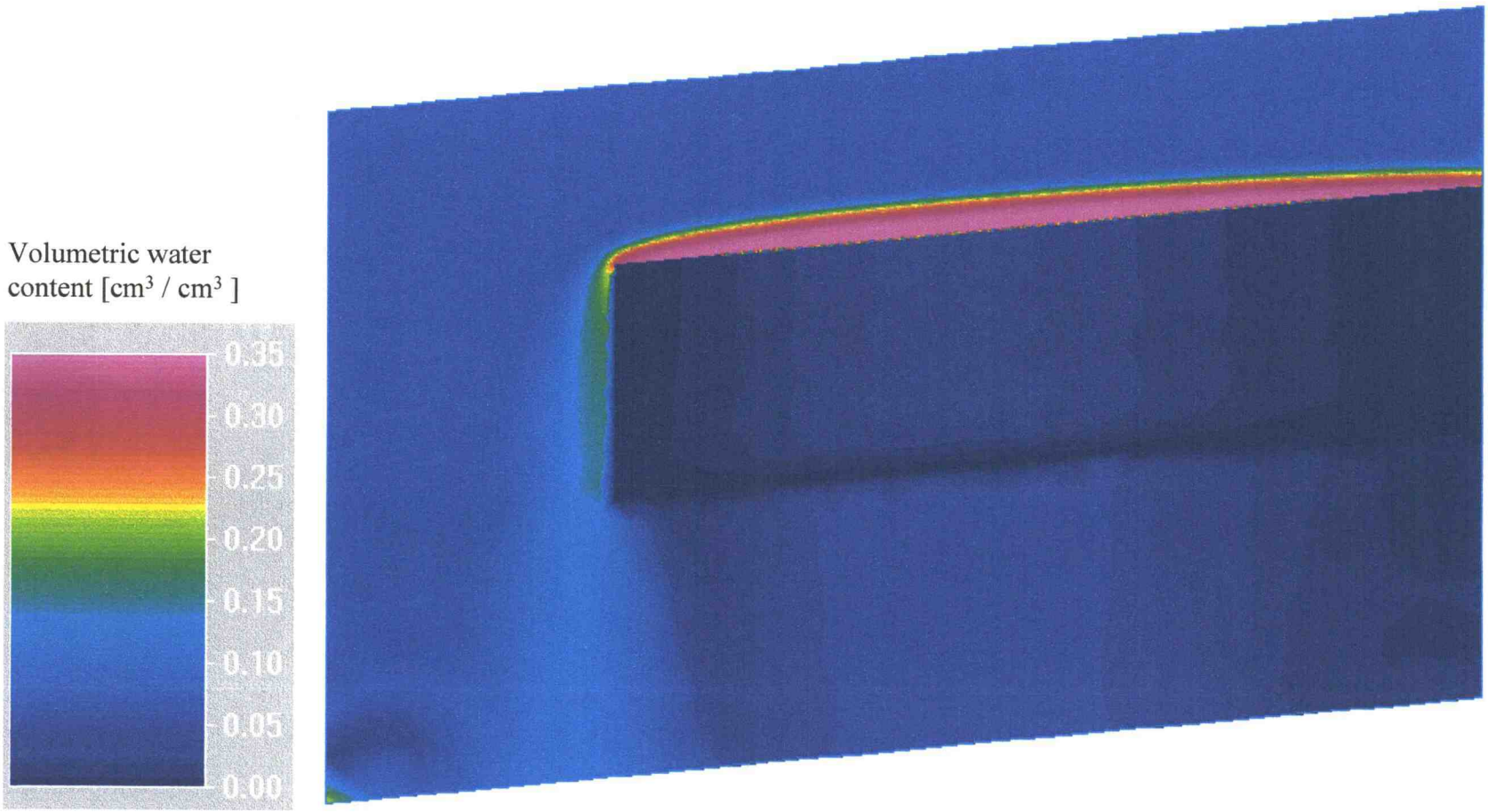

Fig.17 Volumetric water content [cm³ / cm³] in the flow domain of a capillary barrier system at steady state after 60.0 hr of steady infiltration q. (3 m long straight interface, q = 1.6 cm/hr, tan(phi) = 0.1, 12/20 - 40/50 sand)

down-dip direction and the decrease close to the down-dip end due to water being accelerated and spilled over the down-dip edge (down-dip effect). Hence, the highest leakage into the coarse layer is not at the furthest down-dip position but rather about two third in down-dip direction (190 cm). At this point, the volumetric water content is close to full saturation and the capillary fringe height is about 25 cm; this corresponds to the α^{-1}-value for the fine material (40/50 sand).

The highest leakage into the coarse soil is found to be 45 % of the infiltration rate and, hence, the asymptotic down-dip limit is not reached yet. While the water content in the fine soil above the interface reaches a value close to saturation, the highest value of water content in the coarse material is about 5 %, only.

The pressure head distribution in the problem domain after 60 hr is shown in Fig.18, where the coarse material is bordered by a black line. Corresponding to the high water content in the fine material above the interface and at the down-dip end of the interface, the pressure head is increased as well, with the highest value to be at the region of largest leakage.

Appropriate to the different hydraulic properties of fine and coarse media, in comparison to the fine soil, the coarse material exhibits a lower water pressure for most of its area with lowest value being -10 cm. Only at the interface, the fine soil shows equally low pressure heads.

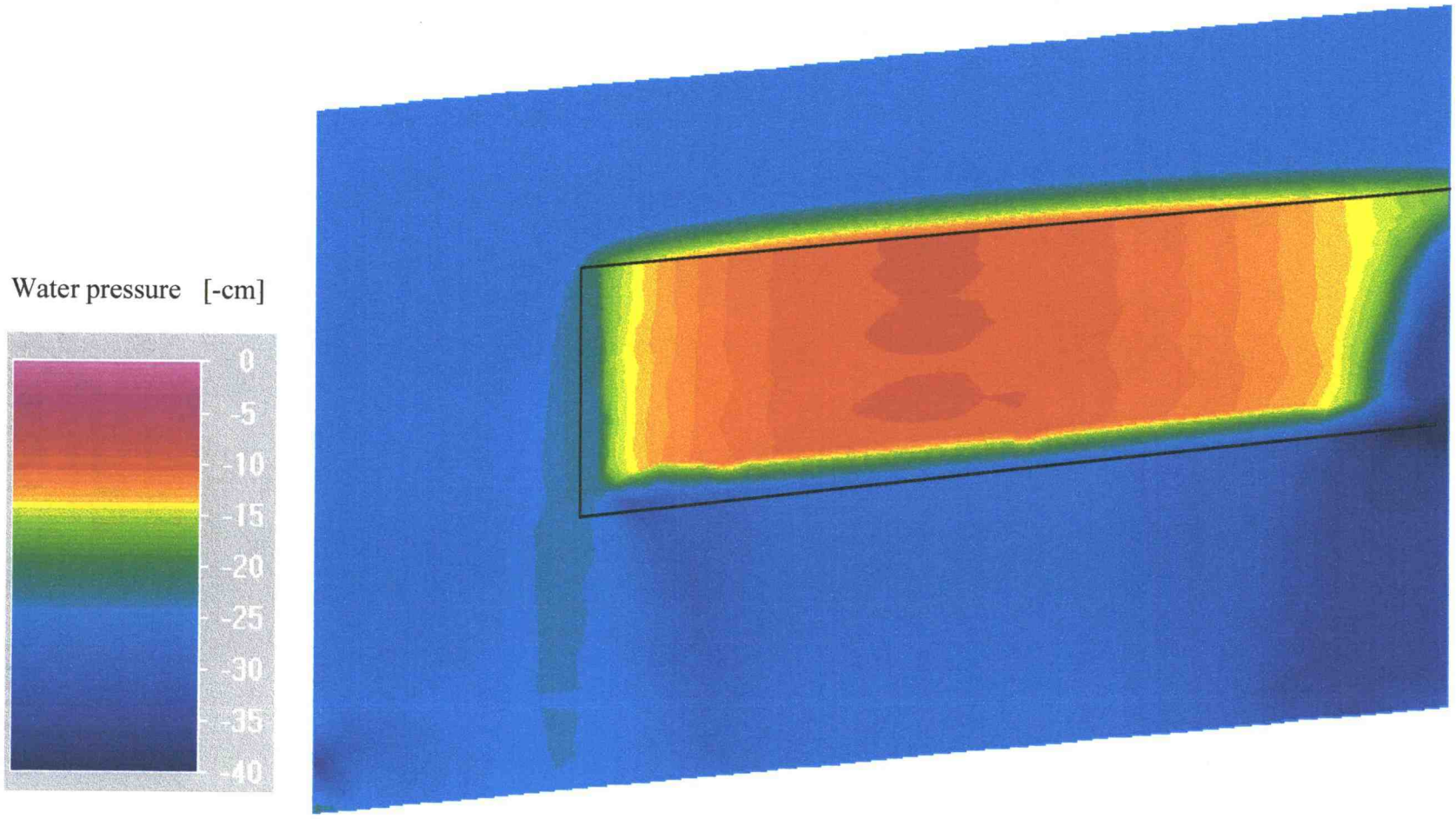

Fig.18 Water pressure distribution [-cm] in the flow domain of a capillary barrier system at steady state after 60.0 hr of steady infiltration q. (3 m long straight interface, q = 1.6 cm/hr, tan(phi) = 0.1, 12/20 - 40/50 sand)

6.2. Effects of a three meter and a nine meter long straight interface - Discussion of the results

This chapter describes the results of simulations in which some of the properties of a three meter and a nine meter long capillary barrier system were altered. Those modifications include changes in infiltration rate q, interface angle θ, anisotropy, material properties and defects along the interface. The numerical results will then be compared to the analytical results given in chapter 3.

6.2.1 Distinct infiltration rates

As discussed in chapter 2, infiltrating water and water diverted laterally along the interface increase the water content in the capillary fringe in down-dip direction and, thus, reduce the pressure potential above the interface. Since the hydraulic conductivity is a function of pressure head (Fig.5), a decreasing pressure potential in down-dip direction enlarges the hydraulic conductivity down-dip.

At the contact of fine and coarse media, due to continuity, the pressure potential and the flux across the interface must be equal for both fine and coarse sand. This means that with a decreasing pressure potential in down-dip direction and depending on the hydraulic properties of fine and coarse media (Fig.5 and Fig.6), more and more water will flow into the coarse media.

If we now consider a point at a certain down-dip distance in Fig. 4 and applying two different infiltration rates on the upper bound of the flow domain, we can expect from above thought model that more water is collected in the capillary fringe for the higher infiltration rate; this means that the pressure potential at the interface is smaller and thus from Fig.5 that the leakage into the coarse layer is bigger. Therefore, it can be stated that the water movement in the vicinity of a capillary barrier directly depends on the magnitude of infiltration rate q.

Based on a capillary barrier system built up by 12/20 - 40/50 sand and an interface angle of $\tan(\theta) = 0.1$, the leakage pattern into the coarse layer with different infiltration rates q, ranging from 0.4 cm/hr to 6.4 cm/hr for a three meter long barrier, and 0.2 cm/hr to 2.0 cm/hr for a nine meter long barrier is depicted in Fig.19 and Fig.20, respectively. The water balance error (e_r) at time t = 50 hr is smaller than 0.6 % for all simulations.

Since the hydraulic conductivity in the coarse material depends on the pressure potential at the interface and, thus, on the non-linear relationship between pressure potential and water content (Fig.6), the leakage at a certain point on the interface will not linearly increase with higher infiltration rates. The graphs in Fig.19 and Fig.20 support this non-linear correlation of leakage and infiltration rate. For example, doubling the infiltration rate q from 0.4 cm/hr to 0.8 cm/hr in Fig.19 increases the maximum leakage by a factor of about 12. For very high infiltration rates, a doubling will give a smaller factor; e.g. changes from 1.6 cm/hr to 3.2 cm/hr leads to a factor of about 2, only.

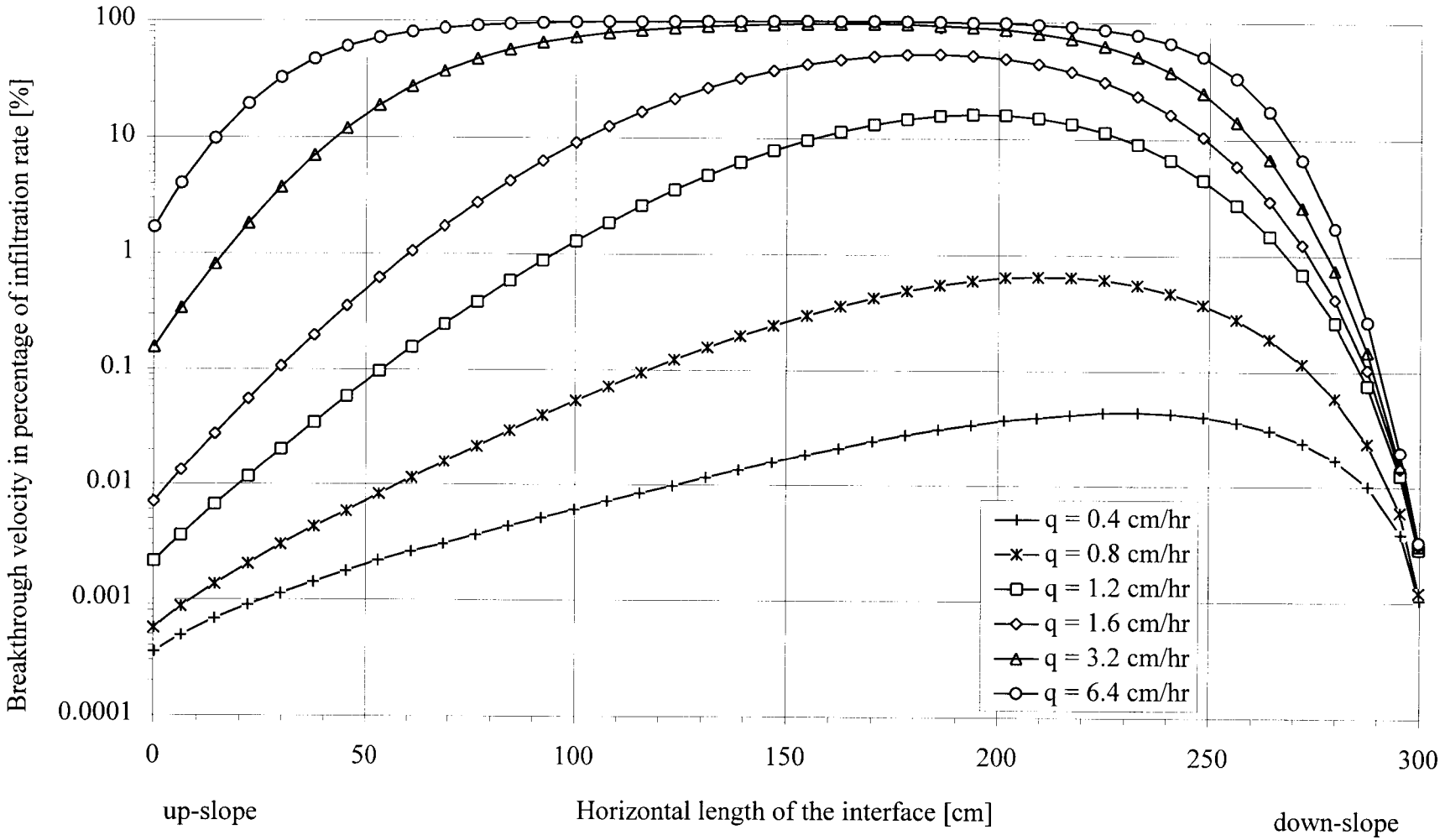

Fig. 19 Breakthrough velocity in percentage of infiltration rate below the straight interface of a three meter long capillary barrier at steady state for different infiltration rates q. (t = 50 hr, 12/20 - 40/50 sand)

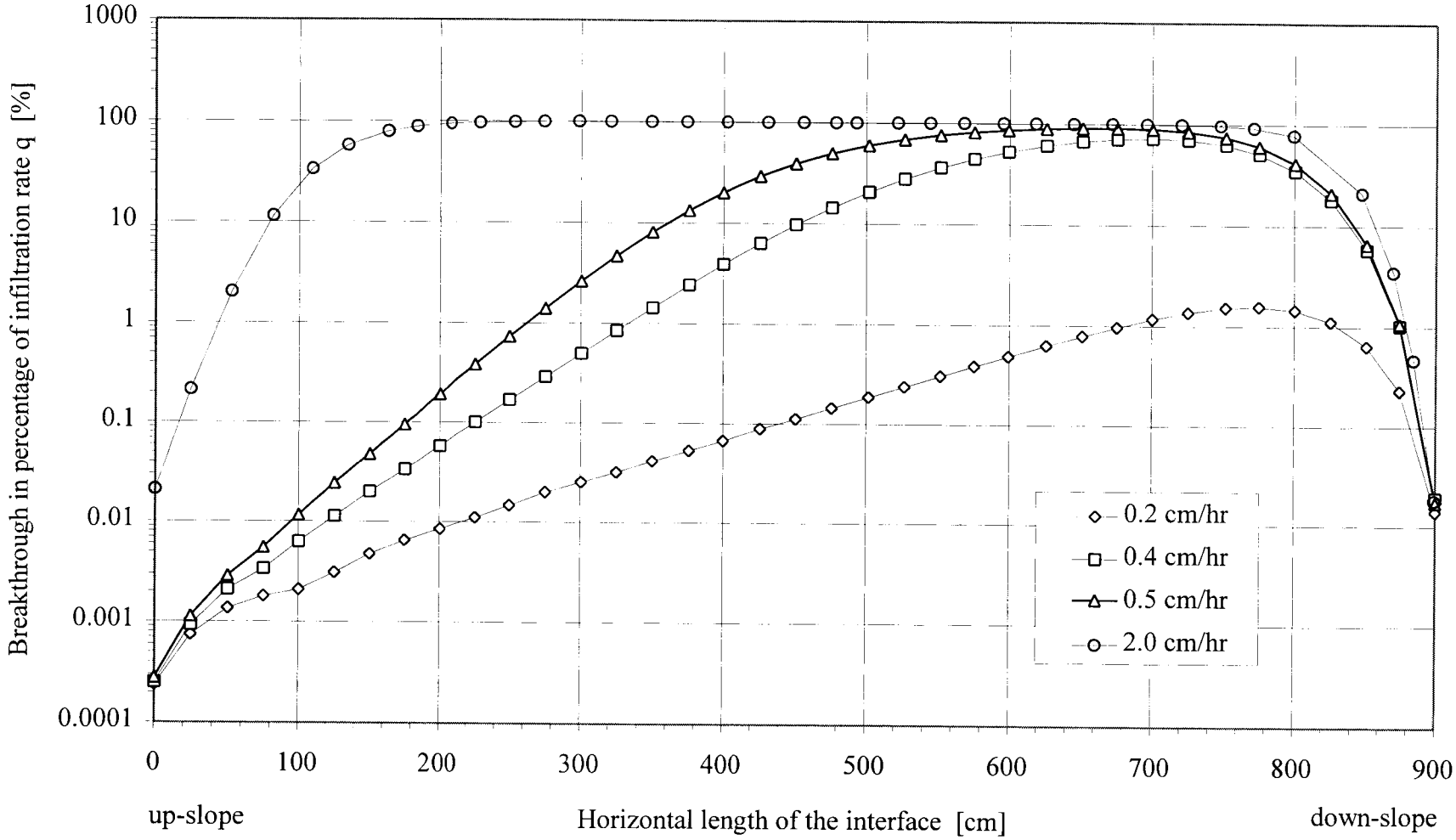

Fig. 20 Breakthrough in percentage of infiltration rate q at steady state below a 9 meter long straight interface for different infiltration rates. (t = 50 hr, 12/20 - 40/50 sand, tan(phi) = 0.1)

Ross stated that for highly contrasting media, the transitional zone between the point of first leakage and the asymptotic down-dip limit is rather short. The results presented do not support this assertion. Fig.19 and Fig.20 show a gradual breakthrough along the interface rather than the pattern predicted by Ross with no leakage in the up-slope area followed by this short transitional zone. For example, if we define the first breakthrough as 1 % and the asymptotic down-dip limit as 100 % breakthrough, in Fig.19, the down-dip distances for the graph with q = 3.2 cm/hr are given as 18 cm and 160 cm, respectively. Hence, we see a factor of about 9 in down-dip slope position. In Fig.20 this factor is about 5 for the simulation with q = 2.0 cm/hr and for q = 0.5 cm/hr about 2.5. Given the very narrow particle size distribution for these sands, we would expect natural media to be even more gradual in its breakthrough transition.

From (25), (28), (30), (31a) and from the appropriate values of diversion length (Tab.3) obtained with these equations (with the exception of (24)), the upper limits of the diversion length are found to be linearly related to the infiltration rate q. Depending on the applied equation the values of L in Tab.3 denote vast differences in predicted diversion length for equal infiltration rates. Those values and the appropriate magnitude of leakage in percentage of infiltration rate q [% of q] from the graphs in Fig.19 and Fig.20 for different infiltration rates are summarized in Tab.6.[24] From this table, we can gather that (24) and (28) are rather conservative when compared to (25), (30) and (31a). The latter three extremely overestimate the capability of a barrier to divert water laterally.

[24] Note: No percentage values are given for some values of L in Tab.6 due to the down-dip effect or due to the length of the capillary barrier.

Tab.6 Diversion length, L [cm], and the appropriate leakage in percentage of q [% of q] from Fig.19 and Fig.20 for different infiltration rates q. (12/20-40/50 sand, $\tan \phi = 0.1$, isotropic conditions). Note: No percentage values are given for some values of L due to the down-dip effect or due to the length of the capillary barrier. Values smaller than 0.1 are denoted as < 0.1.

infiltration rate [cm/hr]	**(24) Ross** **L / [% of q]**	**(25) Ross - simplified** **L / [% of q]**	**(28) Steenhuis** **L / [% of q]**	**(30) Ross - Steenhuis simplified** **L / [% of q]**	**(31a) Ross - Steenhuis $h_{a1} > h_{w2}$** **L / [% of q]**
0.2	183 / < 0.1	2848 / -	823 / -	3670 / -	3654 / -
0.4	112 / < 0.1	1424 / -	411 / 4.9	1835 / -	1826 / -
0.5	95 / < 0.1	1139 / -	329 / 5.0	1468 / -	1460 / -
1.2	51 / < 0.1	475 / -	137 / 5.1	612 / -	607 / -
1.6	41 / 0.25	356 / -	103 / 9.5	459 / -	455 / -
2.0	35 / 0.3	285 / 100	82 / 12	367 / 100	363 / 100
3.2	24 / 2.2	178 / 92	51 / 17	229 / -	226 / -
6.4	14 / 9.5	89 / 95	26 / 23	115 / 100	112 / 100

6.2.2 Distinct interface slopes

Another capillary barrier property that impacts the water movement in the flow domain is the angle of the inclined contact between fine and coarse media (ϕ in Fig.4). For a non-sloped interface, infiltrating water builds up a capillary fringe; with progression of water input, water will more and more percolate into the coarse layer due to the increased water content above the interface. However, sloping the interface will allow water to move laterally, whereas for small angles this diversion is rather small. With a bigger slope this diversion capability increases and less water infiltrates into the coarse layer; This relationship is outlined in Fig.21, with distinct interface angles ranging from $\tan(\phi) = 0.05$ to $\tan(\phi) = 0.15$.

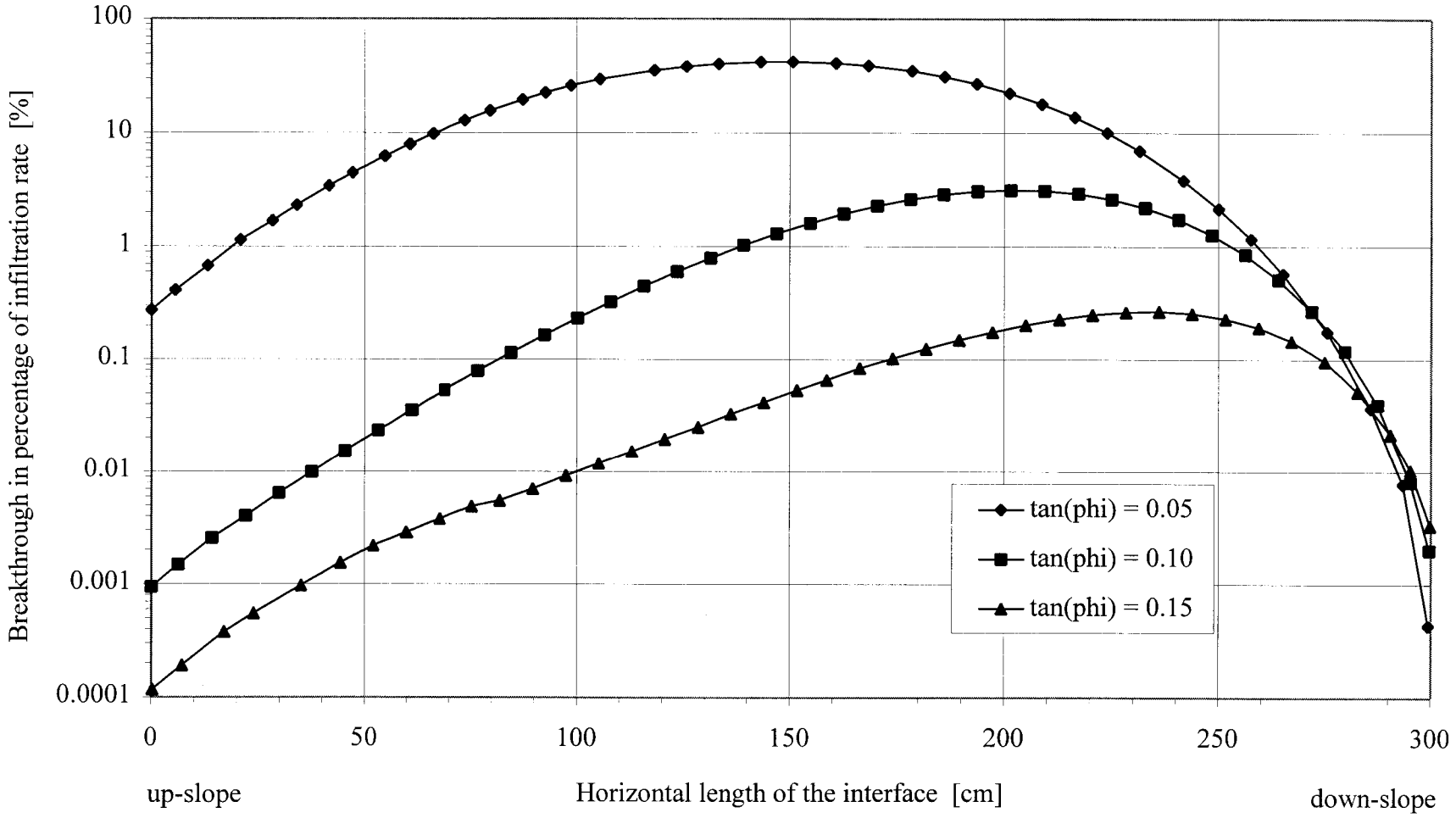

Fig. 21 Breakthrough in percentage of infiltration rate q at steady state below the straight interface of a three meter long capillary barrier for different interface angles. (q = 1.0 cm/hr, t = 50 hr, 12/20 - 40/50 sand).

The figure indicates that doubling the interface angle from $\tan(\phi) = 0.05$ to $\tan(\phi) = 0.10$ reduces the highest maximum breakthrough from 42 % to about 3.1 percent; enlarging the angle by a factor of three diminishes the breakthrough from 42 % to 0.26 % of q. Capillary barrier applied with smaller infiltration rates show less of a down-dip effect if the magnitude of highest breakthrough did not reach the magnitude of q (Fig.19); similar to that, the down-dip effect is less developed for bigger interface angles (Fig.21).

In all equations denoted in chapter 3 and from Tab.4, the diversion length, L, is linearly related to the interface angle ϕ; or in other words, $L \sim \tan(\phi) / q$. Thus, doubling the interface angle while halving the infiltration rate should result in the same leakage pattern (diversion length). However, this could not be proven with the numerical solution (App.B-Fig.7); A reason for that discrepancy between analytical and numerical solution could be the down-dip effect.

While (24) and (28) give diversion length smaller than 245 cm for all angles (Tab.4), (25) predicts values of L not to be less than 285 cm and for (30) and (31a) those values are far beyond the length of the barrier (367 cm - 1100 cm). If we compare the values of breakthrough given by Fig.21 that are appropriate to the values of L in Tab.4, we find again equation (24) to be relatively conservative; breakthrough values appropriate to the given diversion length L for (24) and (28) are 1.8 % and 18,5 % for $\tan(\phi) = 0.05$, 0.03 % and 20.5 % of q for $\tan(\phi) = 0.1$, and 0.006 % and < 1 % of q for $\tan(\phi) = 0.15$, only. The breakthrough value of (28) for $\tan(\phi) = 0.15$ is influenced by the down-dip effect.

6.2.3 Distinct material combinations

As outlined in chapter 2 and 3, the material building up the capillary barrier should have highly contrasting hydraulic properties. As outlined in Fig.5 and Fig.6, where hydraulic conductivity and water content, respectively, are graphed versus pressure potential, a combination of 12/20 sand for the coarse and 40/50 sand for the fine media would indicate such a big contrast. On the other side an alliance of 20/30 sand and 30/40 sand stands for the least disparity.

Four different material combinations building a three meter long capillary barrier system (12/20 - 40/50; 12/20 - 30/40; 20/30 - 40/50; 20/30 - 30/40) were implemented into HYDRUS-2D and the leakage pattern along the interface for all four simulations determined; the results are delineated in Fig.22.

In Fig.22 the least contrasting material combination, 20/30 - 40/50 sand, exhibits an almost entirely ineffective barrier system. The lowest leakage is located at the up-slope crest with about 6 %. Maximum leakage decreases from 100 % for the 20/30 - 40/50 sand combination over 48.4 % with 12/20 - 30/40 sand and 25.6 % with 20/30-40/50 sand to 0.65 % of q with 12/20 - 40/50 sand. The results confirm the statement that the highest contrasting media combination produce the lowest leakage.

From Tab.2 we find once more that (24) predicts the shortest diversion length and with this equation the appropriate breakthrough values for the calculated L are found in Fig.22 to be less than 1 % for all media combination except for 20/30 - 30/40.

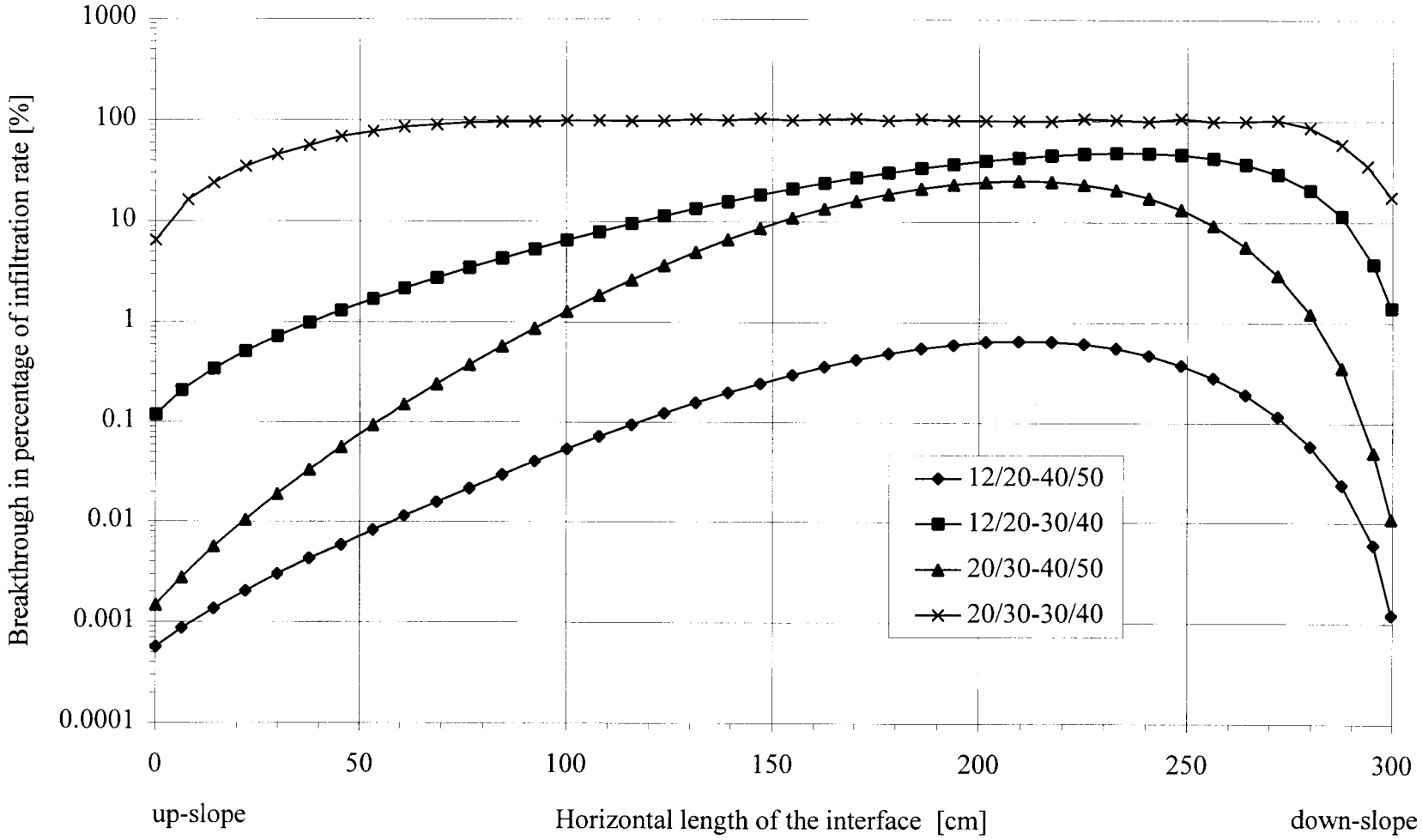

Fig. 22 Breakthrough in percentage of infiltration rate q at steady state below the straight interface of a three meter long capillary barrier for different material combination. (q = 0.8 cm/hr, tan(phi) = 0.1, t = 50 hr)

For all media combinations, equations (25), (30), (31a) and (31b) seem to overestimate the efficacy of the capillary barriers systems. The breakthrough values given in Fig.22 that are appropriate to the denoted diversion lengths obtained with (28) (see Tab.2) range from 0.65 % for 12/20 - 40/50 sand to 5.8 % with 20/30 - 40/50 sand[25].

6.2.4 Anisotropy of the fine layer

Stormont (1995: p.783) stated that in a homogenous layer, anisotropy is due to particle orientation which could be engineered purposefully; the limit of anisotropy in natural homogenous media is about 4. Stormont reported furthermore that an anisotropic fine layer with $K_{xx} = 4 * K_{zz}$ can increase the diversion length four times.

Above statements were tested performing simulations in HYDRUS-2D with a capillary barrier system built by 12/20-4050 sand and an interface angle of $\tan(\phi) = 0.10$. Such a system with an infiltration rate of 1.6 cm/hr is depicted in Fig.23 showing the water content distribution in the problem domain. The deflection of water on the left side of Fig.23 (water flowing from the down-dip edge) is due to the anisotropic fine layer. Anisotropy of the fine media is adjusted in a way that the hydraulic conductivity parallel to the interface is four times the one perpendicular to it.

Comparing the water content distribution at steady state of the same capillary barrier system for two cases, with (a) an isotropic fine layer (Fig.17) and (b) an anisotropic fine layer (Fig.23), put out vast differences. The capillary fringe of the

[25] Note: The value of diversion length for 20/30 - 30/40 sand can not be calculated with (28)

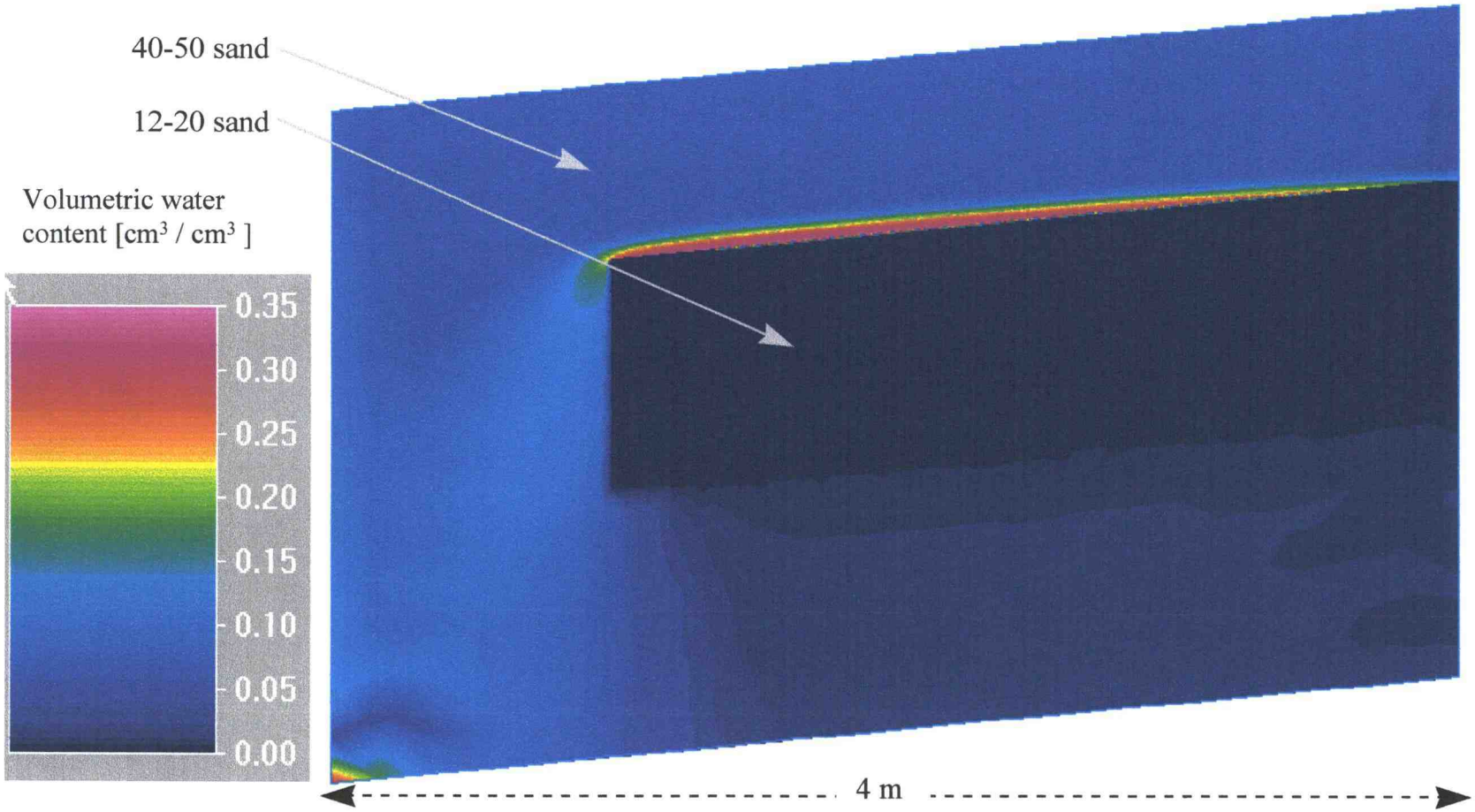

Fig. 23 Volumetric water content in the flow domain of a capillary barrier system at steady state consisting of an isotropic 12-20 and an anisotropic 40-50 sand with a straight 3 meter-long interface. (t = 50 hr, q = 1.6 cm/hr, tan phi = 0.1)

isotropic fine media in Fig.17 is much higher than it is for the anisotropic fine layer in Fig.23. This means that the volumetric water content, and thus, the pressure potential in the capillary fringe differ. The lower pressure head at the contact of fine and coarse material found in the anisotropy case gives a smaller hydraulic conductivity value for the coarse media and, hence, less water percolates into the lower layer. This is reflected in Fig.23 by the very low water content of the coarse material.

The leakage pattern into the coarse layer for both cases anisotropic and isotropic fine sand is outlined in Fig.24. For q = 1.6 cm/hr the maximum leakage in percentage of infiltration rate q is obtained from this figure to be 0.009 % for anisotropic conditions and 52.8 % for the isotropic state.

Besides the two simulations described above with q = 1.6 cm/hr, different infiltration rates were applied on the anisotropic system. The results of those simulations are depicted in Fig.24, as well. As found in chapter 6.2.1 the values of maximum leakage do not increase linearly with higher infiltration rates, due to the non-linear dependency of hydraulic conductivity and water content from pressure potential. Doubling the input from 3.2 cm/hr to 6.4 cm/hr enlarges the maximum leakage from 0.14 % to 27.5 %, and a quadruple leads to 88.8 %.

Stormont stated that an anisotropy ratio of four extends the diversion lengths by a factor of four. Taking the 0.1 percent breakthrough value of a simulation with isotropic conditions and infiltration rate of q =1.2 cm/hr (Fig.19), we obtain a diversion length of about 55 cm. For the anisotropic case with q = 6.4 cm/hr a similar diversion length for

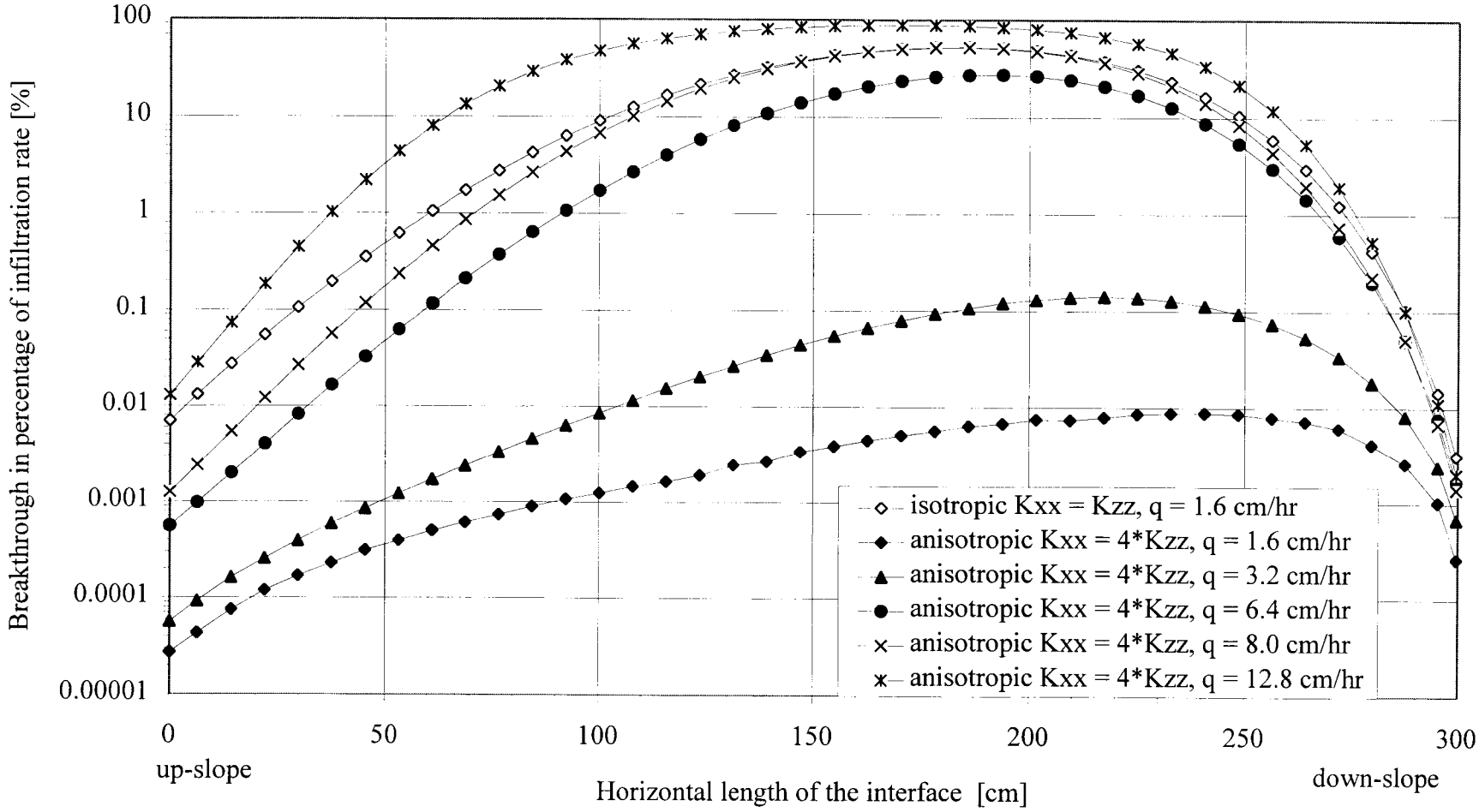

Fig. 24 Breakthrough in percentage of infiltration rate q at steady state below the straight interface of a three meter long capillary barrier with an isotropic fine media in comparison to simulations with an ansiotropic fine media with different infiltration rates. (3 meter long straight interface, t = 50 hr, tan(phi) = 0.1, 12/20 - 40/50 sand)

the 0.1 % breakthrough value (Fig.24) is given with 58 cm. Similar to that the diversion length for q = 3.2cm/hr under anisotropic condition is found to be 178 cm/hr, while for isotropic condition with q = 0.8 cm/hr and q = 0.4 cm/hr, L is given with 117 cm and >250 cm, respectively. From shape and location of those two graphs (0.4 cm/hr and 0.8 cm/hr in Fig.19) we can assume the result with q equals 0.6 cm/hr might give a similar value of L as found with the anisotropic barrier with q = 3.2 cm/hr. Thus, the diversion length improves by a factor of about five for an anisotropic fine layer with $K_{xx} = 4 * K_{zz}$.

From the predicted L - values in Tab.5 and the appropriate diversion lengths in Fig.24 we find equation (35) to be rather conservative with breakthrough values below 2 % for all infiltration rates. Contrary to (35), (38b) over-predicts the diversion lengths, e.g. graph for q = 12.4 cm/hr reaches 100 % breakthrough for predicted value in Tab.5.

6.2.5 Interface defects

Defects along the interface either produced during the construction of the capillary barrier or due to settling of soil and deposits, are able to diminish the capability of capillary barrier systems to divert water laterally and, thus, reduce the degree of deposit protection. Since the failure of a capillary barrier system is very critical to the underlying deposits, one should have some knowledge about the change in leakage pattern due to a certain sized defect.

To get some ideas about the influence of interface defects on the water movement, a small (1.5 cm high) and a large (3 cm high) triangular shaped upward defect and a small

(1.5 cm deep) triangular shaped downward defect were implemented in a three meter long capillary barrier. The defects are located at a location 1.5 m in down-dip direction and the infiltration rate was set to be q = 0.8 cm/hr. The computational error (e_r) at time t = 50 hr was found to be smaller than 0.35 % for all simulations.

In Fig.25 the leakage pattern into the coarse media is depicted for simulations with upward defects in comparison to one simulation without any defect. The figure illustrates that the small defect has hardly any effect on the water movement, except in the region exactly below the defect. In this area a lower breakthrough is found while the up-slope area shows a slightly higher leakage.

With the extension of defect height to 3 cm more lateral flowing water is dammed above the interface, which enlarges the pressure head in the up-slope region and, hence, increases the leakage up-dip (maximum breakthrough increases by a factor of 2). The leakage into the coarse layer down-dip of the defect is higher as well. It can be assumed that for the given capillary barrier system a further increase in defect height will enlarge the leakage into the coarse media in a non-linear fashion, since more water will be retained in the area up-dip of the defect.

Fig.26 shows the water content distribution in the flow domain of a three meter long capillary barrier with a down-dip interface defect (1.5 cm deep) located 1.5 meter in down-dip direction. The defect increases the height of the capillary fringe and, thus, reduces the pressure potential above the contact of fine and coarse soil at this point. Since the hydraulic properties of the lower coarse soil is regulated by the increased pressure

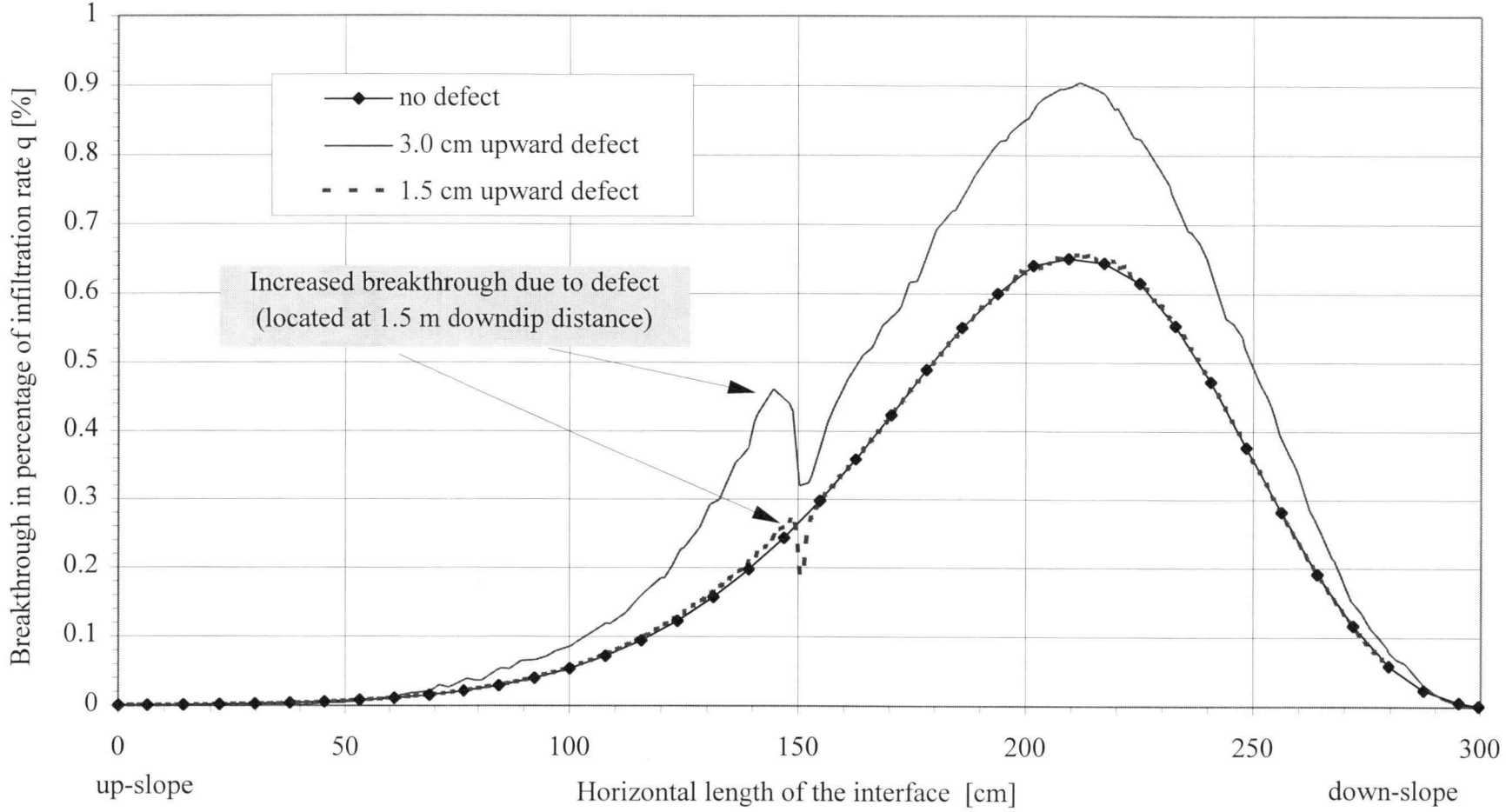

Fig. 25 Breakthrough in percentage of infiltration rate q at steady state below the straight interface of a three meter long capillary barrier for a simulation with no defects in comparison to simulations with upward defects. Note: Height of defects in parenthesis.(q = 0.8 cm/hr, t = 50 hr, tan(phi) = 0.1, 12/20 - 40/50 sand)

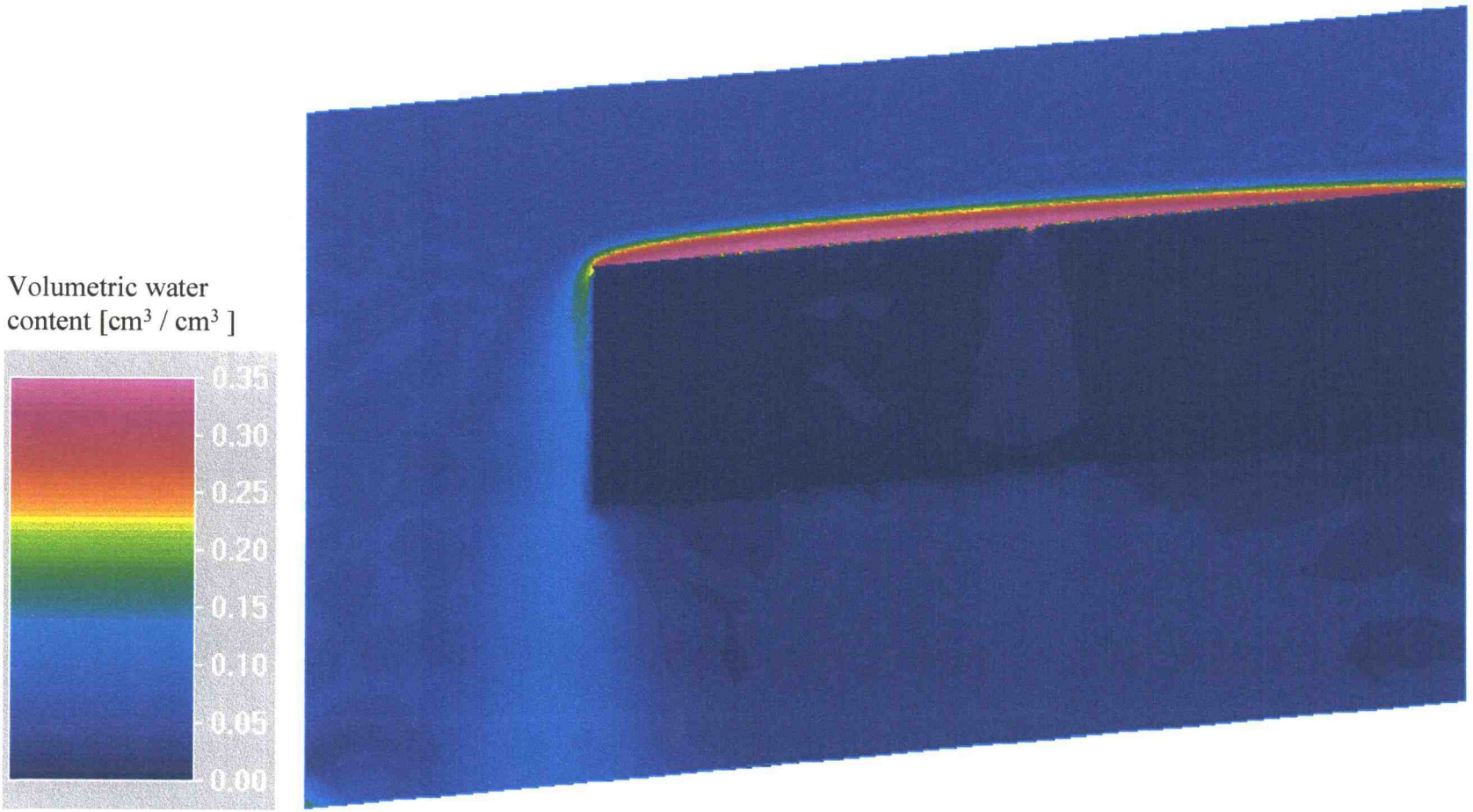

Fig. 26 Volumetric water content [cm³ / cm³] in the flow domain of a capillary barrier system with a downward interface defect (1.5 cm deep) after 50 hr of steady infiltration q. (3 m long straight interface, q = 0.8 cm/hr, tan(phi) = 0.1, 12/20 - 40/50 sand)

potential at the contact of fine and coarse media, and due to the conservation laws, more water percolates into the coarse material below the defect. The leakage in the vicinity of the defect increased from 0.3 % to 8 % (Fig.27). The defect has only an insignificant influence on the down-dip portion of the barrier but decreases the breakthrough in the upper part of the barrier system.

We can assume, similar to the upward defect that a deeper downward defect enlarges the flux into the coarse layer strongly; a very deep defect will be able to divert all water flowing laterally from the up-dip portion of the barrier system. A sequence of such large downward defects would give a similar "fingering" flow pattern as found by Steenhuis et al. (1991) (see App.B-Fig.1).

The downward defect in comparison to an equally sized upward defect has a much higher influence on the flow pattern in the vicinity of a capillary barrier system. This is depicted in Fig.25 and Fig.27 with the upward defect (1.5 cm high) showing no significantly different flux pattern into the coarse media while the downward defect increases the leakage by more than an order of magnitude.

In Fig.28 both an one meter long and 3 cm deep downward defect at a down-dip distance of 4 m and a 3 cm high upward interface defect starting at a down-dip distance of 7 m was implemented in a nine meter long capillary barrier system. Such defects extending over a certain area might be due to settling of soil or deposits. For this simulation the applied infiltration rate q equaled 0.2 cm/hr and the computational error (e_r) is found as 0.5 %.

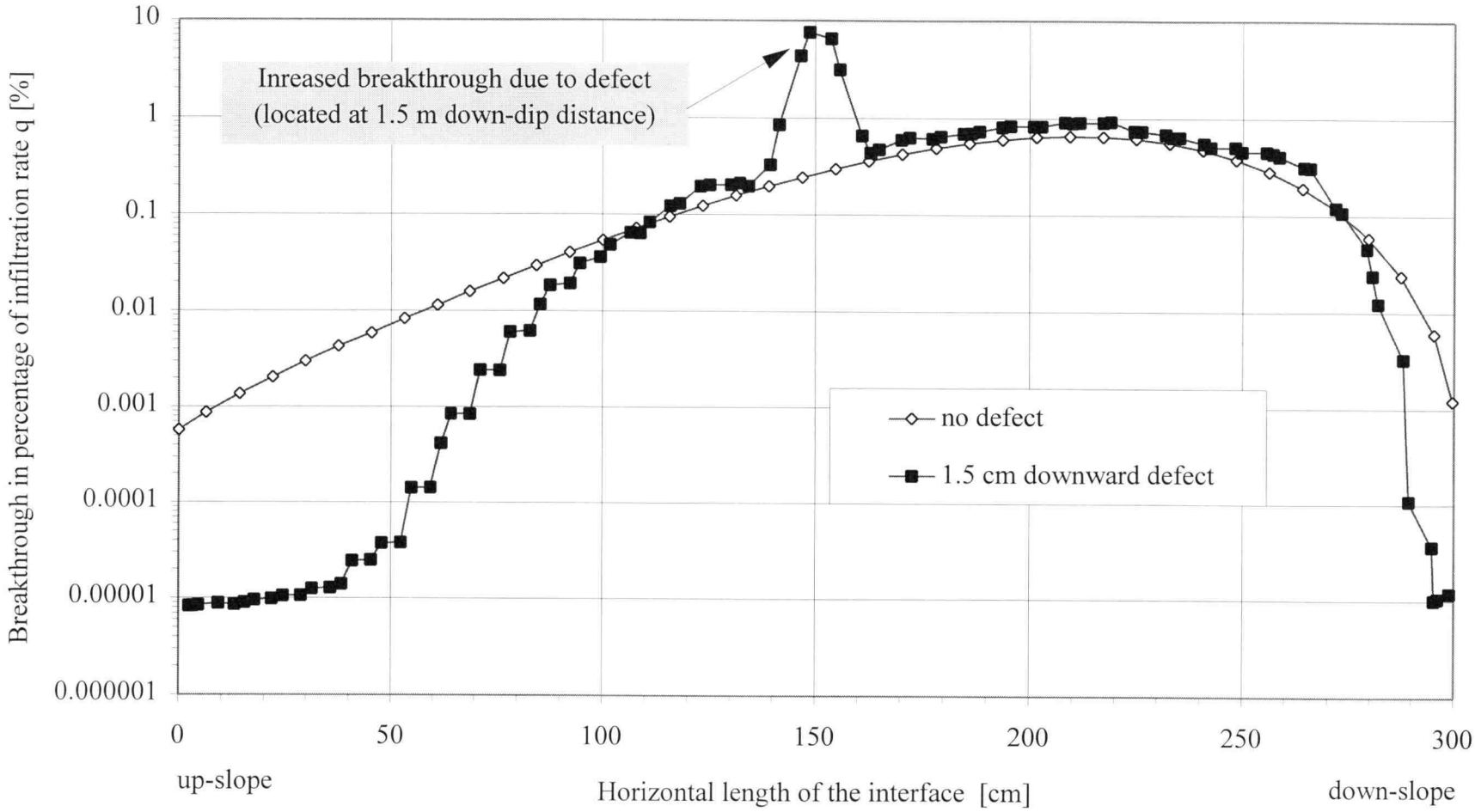

Fig. 27 Breakthrough velocity in percentage of infiltration rate q at steady state below the straight interface of a three meter long capillary barrier for a simulation with no defects in comparison to a simulation with a downward defect (1.5 cm deep). Note: Breakthrough is measured 10 cm below the interface. (q = 0.8 cm/hr, t = 50 hr, 12/20 - 40/50 sand)

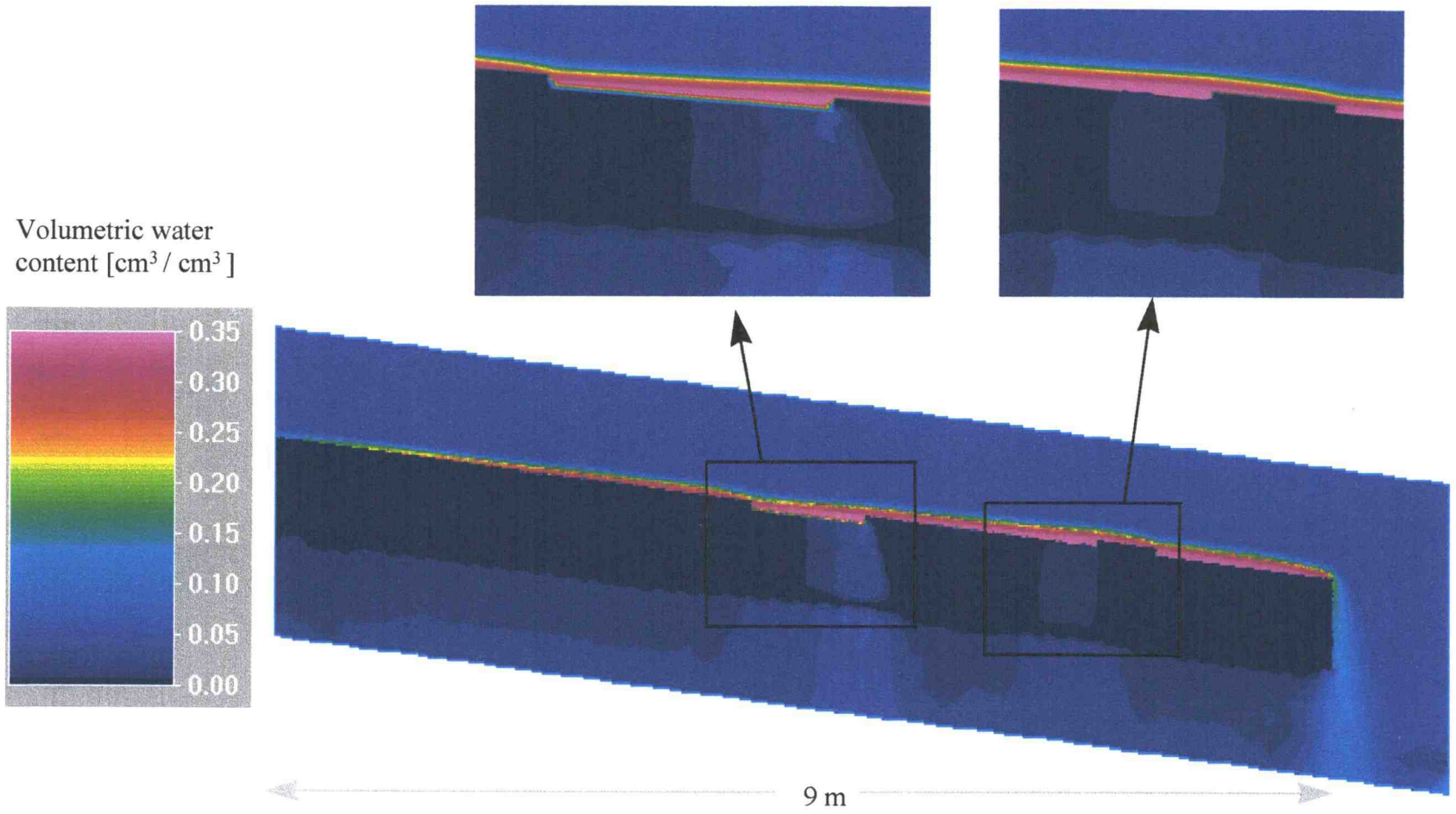

Fig.28 Volumetric water content [cm³ / cm³] in the flow domain of a capillary barrier system with a one meter long and 3 cm deep downward interface defect beginning at a down-dip distance of 4 m, and a 50 cm long, 3 cm high upward interface defect starting at a down-dip distance of 7 m. (9 m long straight interface, q = 0.2 cm/hr, tan(phi) = 0.1, 12/20 - 40/50 sand)

The maximum leakage in the vicinity of the down-dip defect exceeded four times the infiltration rate q, while the maximum values for the up-dip defect did not exceed 30 % of q. In comparison to that for the same capillary barrier system but without any defects the highest breakthrough value is below 2 % of q.

6.3 Alteration of capillary barrier systems: Curved, straight segmented and double-layered systems

In the former chapters consideration of capillary barrier systems primarily focused on single inclined straight interfaces; in the simulations performed and discussed in chapter 6.2, the straight interface system was modified by changing the material properties, the interface angle and by applying an anisotropic fine soil layer.

In this chapter two new ideas will be introduced that are able to improve the capability of a capillary barrier system to protect underlying deposits: The first idea is the use of double-layered interface systems which allow to divert water that percolated through the first upper coarse layer along a second lower interface. The second idea, introduced by Selker (1996), is to engineer a curved interface with an increasing slope in down-dip direction.

Let us first consider the second idea, the curved interface, in some more details. Referring to Fig.17 the volumetric water content in the capillary fringe above a single straight interface enlarges in down-dip direction. Similar to that we also find a linear

increase in diversion capacity, Q_{max}, down-dip ($Q_{max} = q\ x'$ with x' as the horizontal distance of the interface). In Fig.19 the maximum leakage in this system is found (due to the influence of the down-dip effect) 190 cm in down-dip direction with a value of 52 % of q while at the up-dip end the leakage is below 0.1 % of q, only.

Selker (1996) stated that the optimal use of the total fall in elevation has been achieved when the breakthrough flux through the interface is constant along the entire interface. This means for the case depicted in Fig.17 that the local slope in the upper portion of the barrier must decrease to allow a higher breakthrough while in down-dip direction the local slope must increase to lessen the leakage. Selker (1996) found furthermore that a parabolic shaped interface provides an optimal diversion, since the capillary fringe at each location above such an interface is equally developed.

In Fig.29 the volumetric water content in the flow domain of such a parabolic-shaped capillary barrier system is depicted.[26] As mentioned above, contrary to the water content of a straight capillary barrier system as shown in Fig.17, the parabolic shape leads to an equally developed capillary fringe above the interface. In this figure and in Fig.30, where the leakage pattern of both straight and curved double-layered barrier systems with equal drop height and layer thickness (see Fig.11 and Fig.12) as well as infiltration rate q is exhibited, the advantage of a curved interface system is clearly shown. The value of breakthrough is corresponding to the equally evolved capillary fringe constant along the interface except for the lower portion where the down-dip effect lessens the leakage.

[26] Note: In this figure the second idea, the double layered system, is also applied. The material distribution for this double-layered curved interface system is shown in Fig.12.

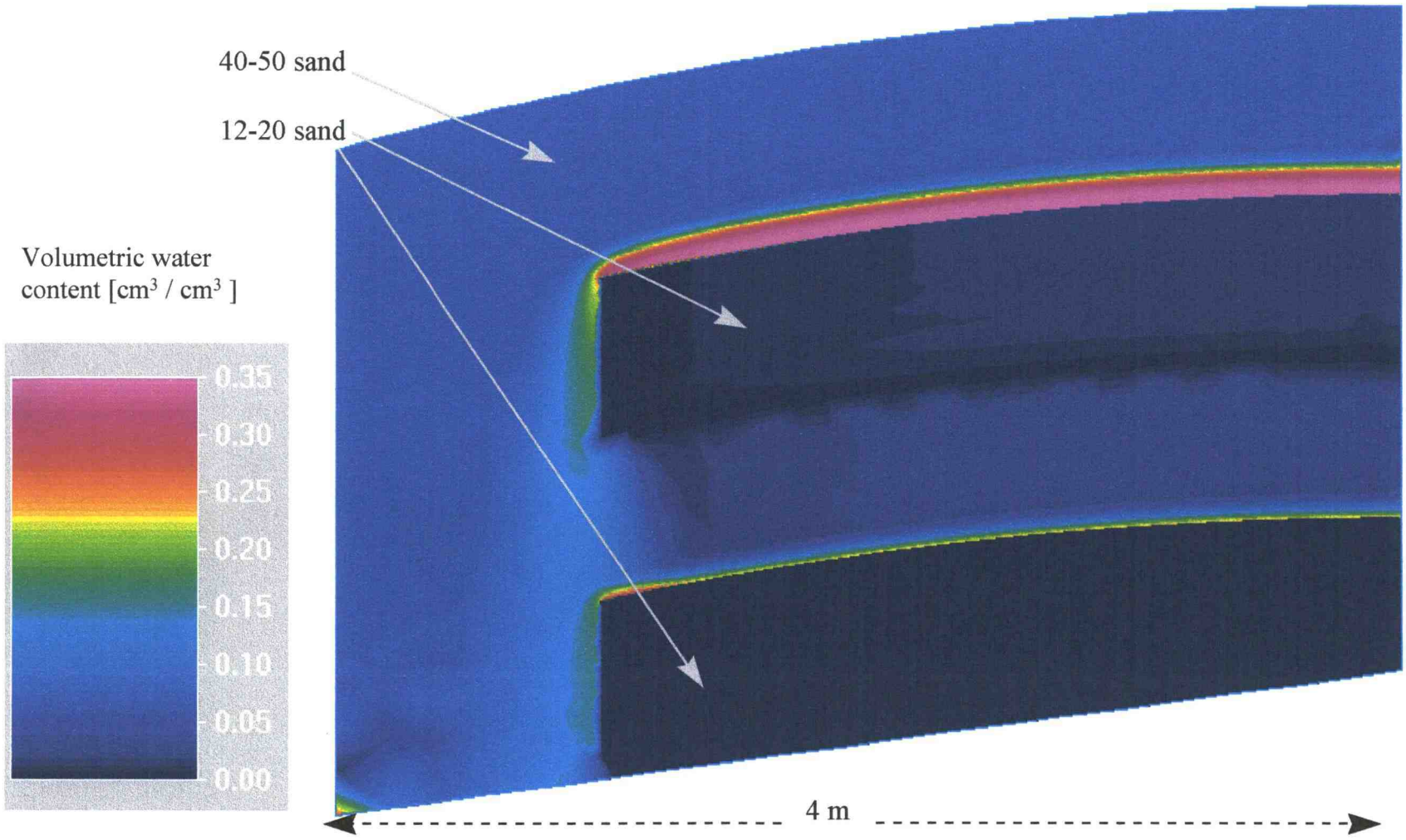

Fig. 29 Volumetric water content in the flow domain of a capillary barrier system at steady state consisting of 12-20 and 40-50 sand with two 3 meter-long, overlaying, curved interfaces (q = 1.6 cm/hr, t = 50 hr)

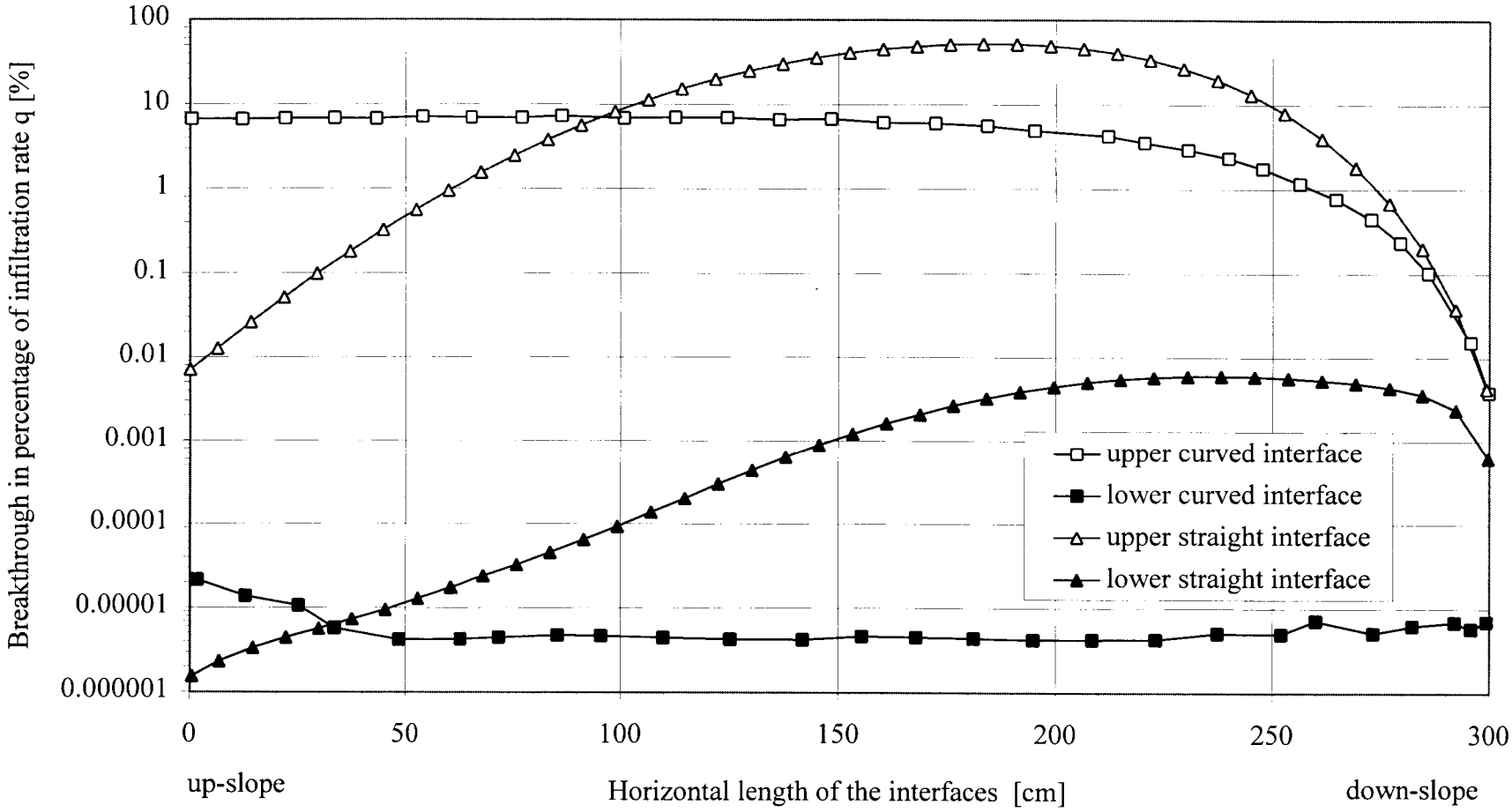

Fig. 30 Breakthrough in percentage of infiltration rate q at steady state for double-layered capillary barrier interfaces: curved versus straight interfaces. Note: The curved and the straight interfaces have the same drop in height from up- to down-dip end. (3 meter long interfaces, q = 1.6 cm/hr, t = 50 hr, 12/20 - 40/50 sand)

The maximum breakthrough flux for the upper curved interface does not exceed 7 % of q while the value for the upper straight interface reaches 52 %. The second layer of both straight and curved interfaces does diminish the breakthrough flux below 0.01 %; Note that on a log-normal plot the straight interface exhibits a typical curved-shaped and the curved interface a quasi-straight-shaped graph for both upper and lower interface.

From chapter 6.2.1 we know that the breakthrough pattern for a straight interface is not linearly dependent on the magnitude of infiltration rate q. Since the same physical properties also apply for the curved interface we can expect to obtain an equivalent behavior for curved capillary barrier systems. The relationship of breakthrough flux to distinct infiltration rates q below a double-layered curved interface system is delineated in Fig.31. As expected doubling the infiltration rate q from q = 1.6 cm/hr to 3.2 cm/hr increases the maximum leakage through the upper interface from 7 % of q to 48 %, while the lower coarse media is percolated by a leakage flux of practically zero percent and 1.6 % of q, respectively. However, quadrupling the infiltration rate q leads to maximum breakthrough values of 74 % for the upper and 46 % for the lower interface.

Selker (1996) stated that the construction of a smoothly changing slope might present some logistical difficulties. However, the parabolic shaped interface could be approached using n straight segments instead, whereas the total drop in elevation from up-dip to down-dip end of the barrier would equal to the one given with the parabolic shaped interface[27].

[27] The parabolic-shaped barrier can be considered as a straight interface with an infinitesimal number of straight segments with distinct local slopes.

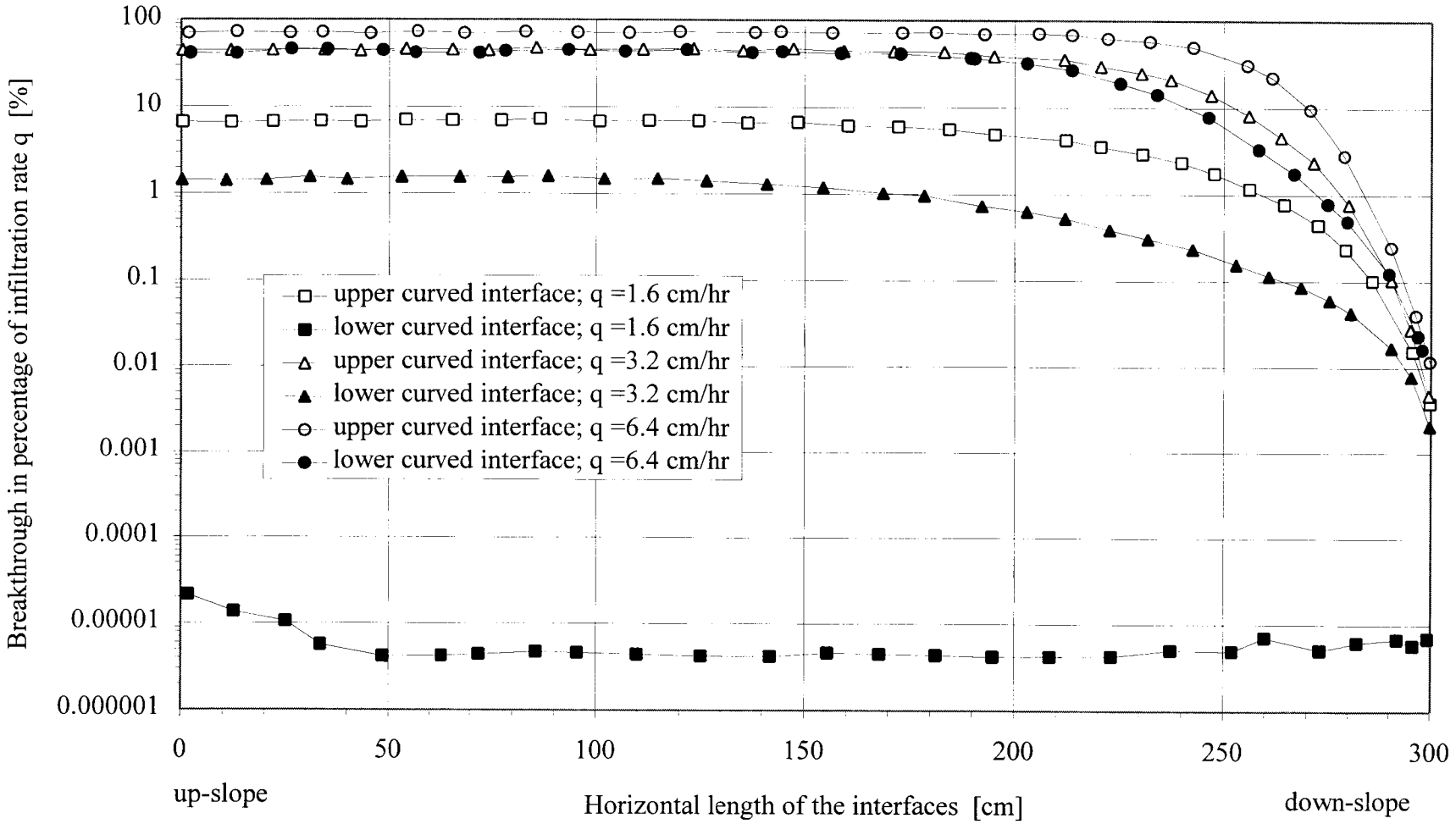

Fig. 31 Breakthrough in percentage of infiltration rate q at steady state for double-layered curved capillary barrier interfaces with different infiltration rates q. (t = 50 hr, 12/20 - 40/50 sand, 3 m long interfaces)

Such a segmented interface system is tested with HYDRUS-2D by setting up two double-layered capillary barrier systems whereas one utilizes five straight interface segments and the other three segments to approach the parabolic shape. On these systems, two distinct infiltration rates (q= 3.2 cm/hr and q = 6.4 cm/hr) are applied and the leakage pattern into the coarse media for both the upper and the lower interface is depicted in Fig.32 and Fig.33, respectively[28]. By means of comparison the leakage pattern, the results for the parabolic-shaped interface system is shown in these figures as well.

From the knowledge of straight interfaces we would expect the highest breakthrough values to occur not at the lowest end of the straight segments due to the down-dip effect between two segments but rather in somewhat up-dip distance of the segment's end. This flow pattern is indeed given in Fig.32 and Fig.33 for both the upper and the lower interface of the three-segmented and five-segmented interface system. The lowest breakthrough generally occurs in the vicinity of two joining segments.

Compared to the three-segmented system, the five-segmented interface systems shows less fluctuation in maximum and minimum breakthrough flux and, hence, the five-segmented system does approach the result given with the parabolic shaped system in a better way. From this we can assume that a higher segmentation leads to a smaller range of maximum and minimum leakage values. An infinitesimal high segmentation achieves the leakage pattern of the parabolic system.

---

[28] Note: Fig.32 is on a log-linear scale while Fig.33 is a non-logarithmic plot

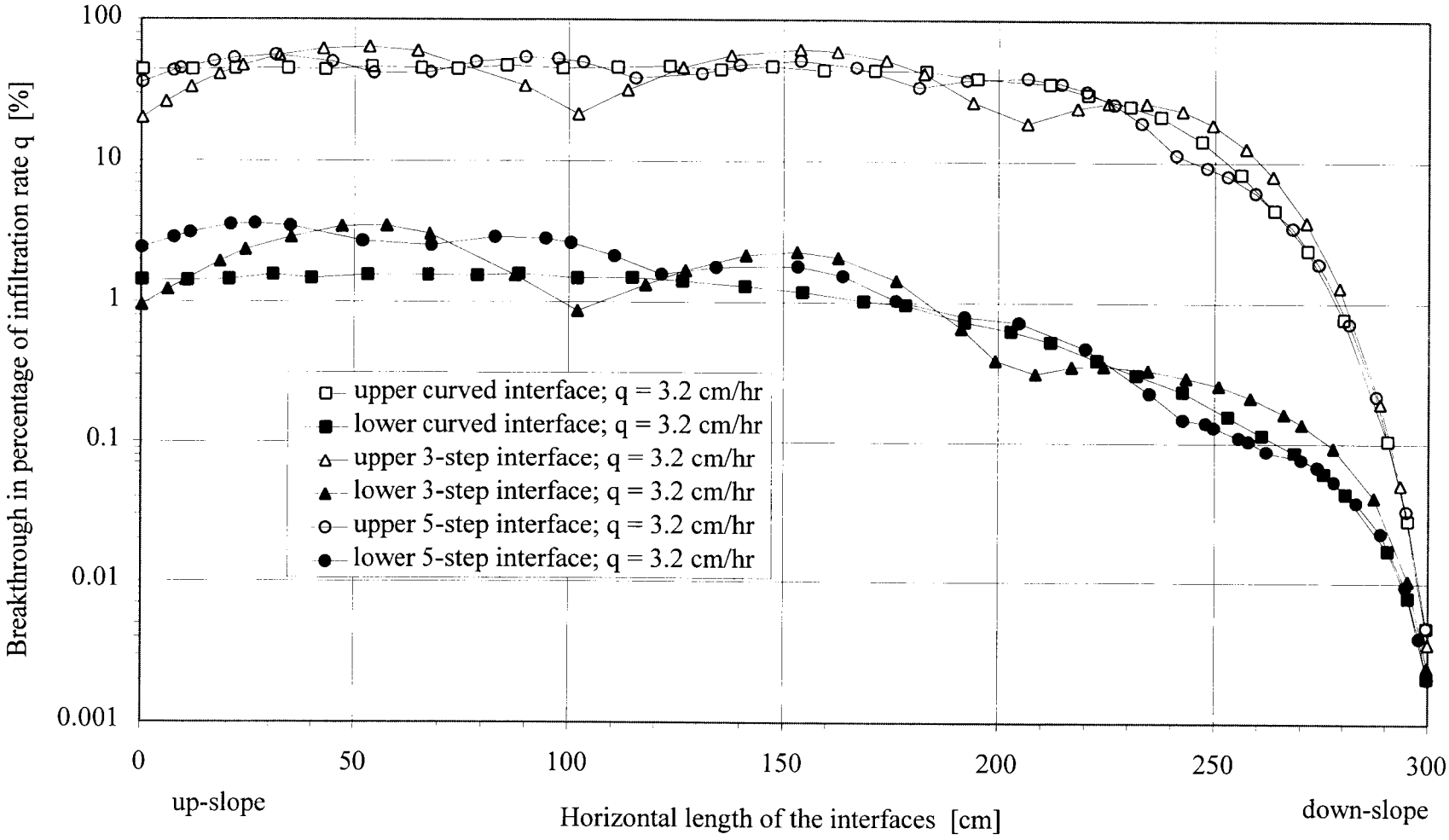

Fig. 32 Breakthrough in percentage of infiltration rate q at steady state for double-layered curved and straight segmented (3-step and 5-step) capillary barrier interfaces. (t = 50 hr, 12/20 - 40/50 sand, 3 m long interfaces, q = 3.2 cm/hr)

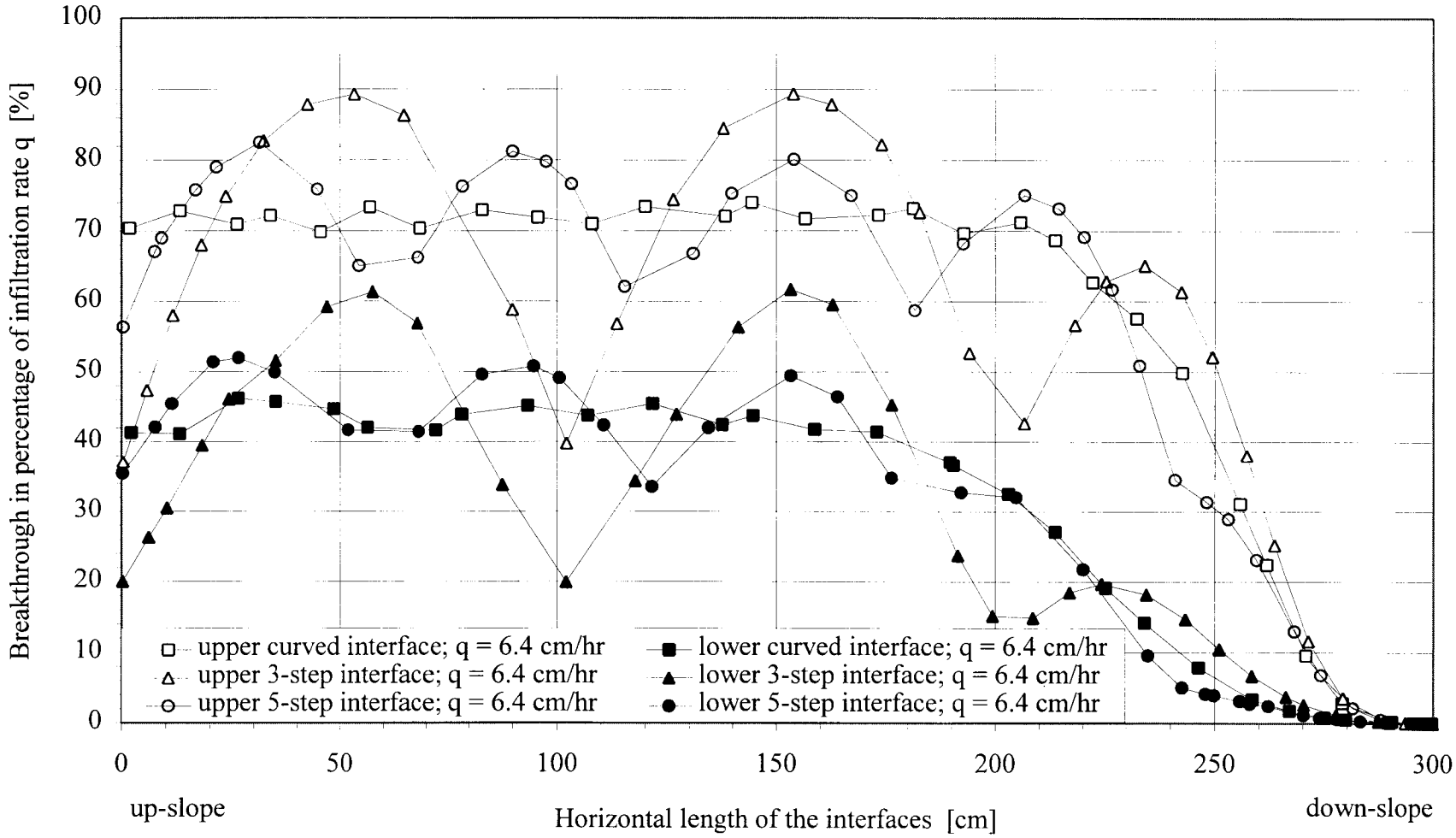

Fig. 33 Breakthrough in percentage of infiltration rate q at steady state for double-layered curved and straight segmented (3-step and 5-step) capillary barrier interfaces. (t = 50 hr, 12/20 - 40/50 sand, 3 m long interfaces, q = 6.4 cm/hr)

After Selker (1996) a three-segmented barrier system increases the diversion capacity by 50 % when compared to a straight barrier system and a five-segmented interface system exhibits 83 % of the parabolic-shaped interface system.

The total amount of water diverted laterally along the interface for different infiltration rates q and for differently shaped interfaces (straight, three- and five-segmented, and parabolic) is pointed out in Tab.7. From this figure it can be seen that only the straight interface exhibits lower amounts of deflected water while the other three interface types show practically similar values for all infiltration rates; the upper straight interface diverts about 8 % to 9 % less water than the other types of upper interfaces; except for the lowest infiltration rate (q = 1.6 cm/hr) this percentage value is found for the lower interface, too.

Tab.7 Total amount of water diverted laterally in three meter long capillary barrier systems with differently shaped interfaces. The total amount of water diverted laterally is given in percentage of water infiltrating into the fine layer above the barrier.

infiltration rate	straight system upper/lower	three-segmented system upper/lower	five-segmented system upper/lower	parabolic-shaped system upper/lower
q = 1.6 cm/hr	82.3 / 100	94.3 / 100	94.1 / 100	94.9 / 100
q = 3.2 cm/hr	51.2 / 87.1	64.4 / 98.6	64.6 / 98.4	64.9 / 99.0
q = 6.4 cm/hr	32.1 / 53.6	40.0 / 67.7	40.9 / 67.8	40.4 / 68.0

Although the maximum values for the upper and lower three- and five-segmented and curved interfaces differ by up to 17 % for equal infiltration rates (Fig.34), the total amount of water diverted laterally (Tab.7) does change minimal, only.

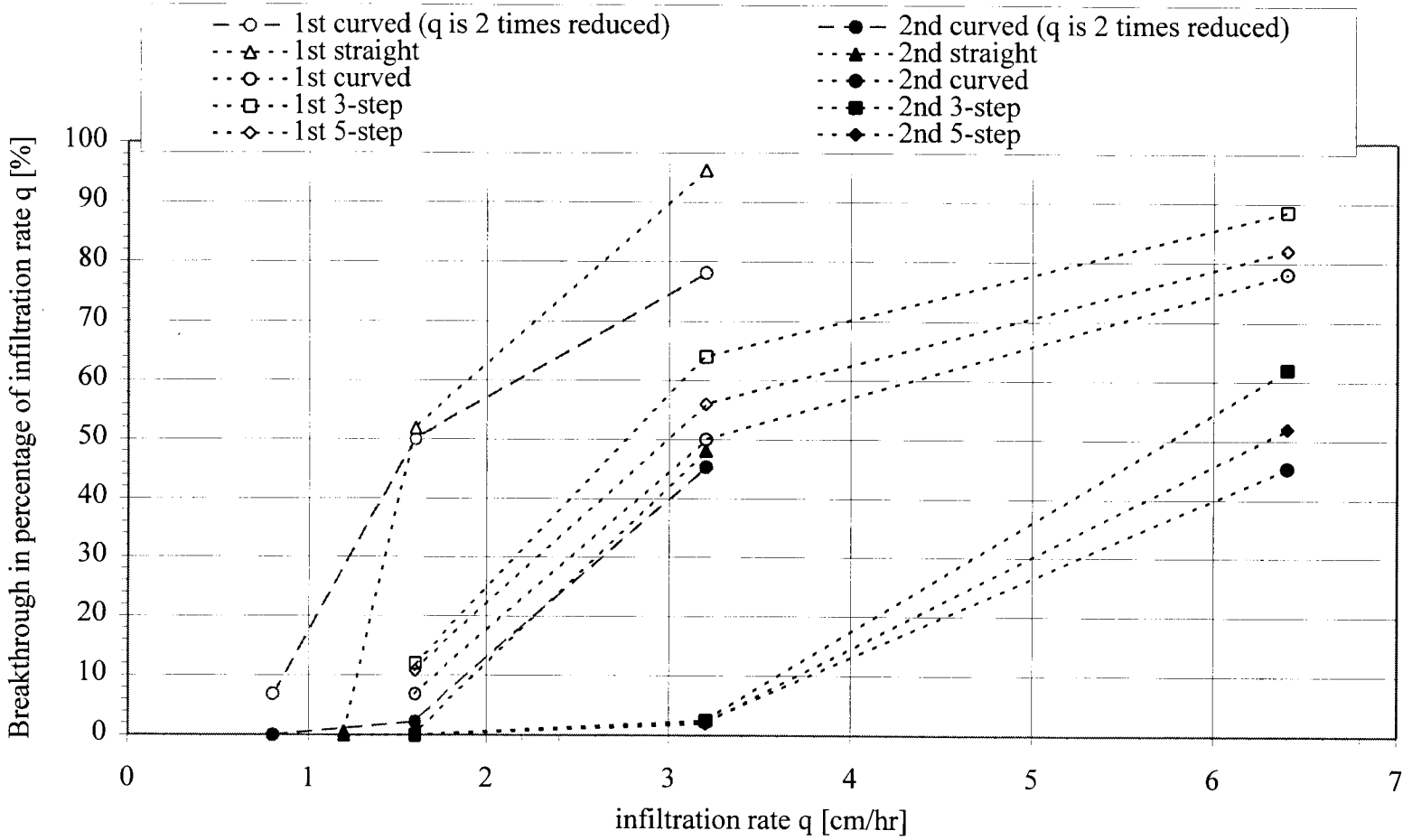

Fig.34 Maximum breakthrough fluxes into the coarse media obtained with distinct infiltration rates for capillary barrier systems with differently shaped interfaces (straight, 3-segmented and 5-segmented, and curved). Note: The drop in elevation from up- to down-dip end of the interface is equal for all systems; in the upper two graphs in the legend the infiltration rate q is reduced by a factor of two.

In Fig.34 we also see that the upper curved interface shows similar maximum leakage values with an infiltration rate of 3.2 cm/hr than the straight interface with half of that infiltration rate. For higher infiltration rates the reduction in infiltration rates from upper curved to upper straight interface to obtain similar maximum leakage value seems to be even higher than a factor of two. The reduction factor of maximum leakage for the lower interfaces between curved and straight capillary barrier to obtain the same values of leakage exhibits a factor of two as well.

As mentioned for Fig.32 and Fig.33, the less-segmented interfaces generally displays a higher maximum leakage value than the higher segmented barrier types; Note that the curved interface is considered to be an infinitesimal highly straight-segmented interface. Since the five-segmented interface in comparison to the curved interface differs by less than 6 % in maximum leakage, only, this capillary barrier system might be an acceptable alternative to the more difficult to construct curved interface system. Depending on the design criteria even the three-segmented interface system might give sufficient results.

7. DISCUSSION SUMMARY

From the statement of Montazer and Wilson (1984: p.29) and from chapter 2.2 (physical background of capillary barriers) we expect a capillary barrier with a horizontal interface to show smaller leakage into the coarse media when the barrier is built by media with higher property contrasts. In Tab.2 equations (30) and (31a) give shorter diversion lengths for a combination of 12/20-40/50 sand than for the less contrasting 12/20-30/40 sand; From this we can conclude that a capillary barrier system with an inclined interface does not necessarily perform better with highly contrasting materials, since the amount of water diverted laterally depends on the hydraulic conductivity of the fine media (K_{s1}); In this example, the values of K_{s1} for 30/40 sand is two times bigger than the one for the 40/50 sand. The numerical solution, however, does not lead to the same result; in Fig.19 the diversion length is bigger for a combination of 12/20 - 40/50 sand than it is for 12/20 - 30/40 sand. Simulations with higher infiltration rate, q, for both material combinations lead to the same result (q = 3.2 cm/hr; results are not shown in this thesis).

The determination procedure of air entry and water entry values, outlined on page 16, must be critically reviewed since those evaluations are used to determine the diversion lengths with equations (28), (30) and (31a and 31b)[29]. The method used to obtain h_a and h_w results in relatively small values of (h_{a1}-h_{w2}) and, hence, the predicted diversion length, L, from the analytical solutions are rather conservative.

---

[29] Note: (31a) is reduced to (30) if q/K_{s1} is close to zero; this is approximated for most of the simulations since $q \leq 12.8$ cm/hr and $K_{s1} \geq 258$ cm/hr. Equation (30) is a direct combination of (25) and (28); thus, only the first term in (30) depends directly on h_{a1} and h_{w2}.

Referring to Fig.6, we can use the same procedure as outlined on page 16 with the exception of taking values of 2.5 * θ_r (1.5 * θ_r) to get h_{w2} and θ_s - 1.5 * θ_r (θ_s - 0.5 * θ_r) to obtain h_{a1} for a more progressive (conservative) case; from this we calculate values of -8.0 cm (progressive) and -4.2 cm (conservative) for (h_{a1}-h_{w2}). Using these two values in (28) leads to a range of diversion length between 135 cm and 258 cm. Hence, we can conclude that the procedure to determine the values of h_a and h_w is very critical to equation (28); These estimates are less critical to (30) and (31a) since the values of L calculated with those equations are more influenced by the second term of (30) which equals equation (25).

Another point to be discussed are the vast differences in diversion length given with the analytical solutions. In Tab.2 a factor in diversion length difference of up to 140 (!) is depicted when using (24) compared to (25). In the same table the smallest factor between maximum and minimum values of L is given with >13 for 12/20-40/50 sand. Similar discrepancies are found between values of L for distinct equations in Tab.3 and Tab.4. From a design perspective these extreme differences in predicted diversion length render the choice of the "right" equation much more difficult. Another disadvantage of these analytical solutions is their uselessness when a design criteria allows, e.g., an acceptable leakage (q_a) of ten percent of the maximum expectable infiltration rate q. Those equations are not directly able to implement such an criteria. However, an acceptable leakage value could be implemented in Ross' solution scheme in equation (21) with $K_s e^{\alpha_1 \psi(0)} = K_{r1}(0) = \left(q_a / K_{s2}\right)^{(\alpha_1/\alpha_2)}$ and, hence, (24) could be written as

$$L = \frac{K_{s1} \tan\phi}{q\alpha_1}\left[\left(\frac{q_a}{K_{s2}}\right)^{\frac{\alpha_1}{\alpha_2}} - \left(\frac{q}{K_{s1}}\right)\right] \qquad (24a)$$

For a combination of 12/20 - 40/50 sand with q = 0.5 cm/hr and tan(ϕ) = 0.1, the diversion length, L, is found as 47 cm with $q_a = 0.1 * q$ while the value of L with (24) results in 95 cm (Tab.2). From the comparison of those two results and from the leakage patterns found in all numerical solutions we can conclude that Ross' statement of having a rather short transition zone for highly contrasting media between the point of first leakage and the down-dip limit is not reasonable.

All equations (24), (25), (28), (30) and (31a) show that L ~ tan (ϕ) / q (see Tab.4). This means that doubling interface angle, ϕ, while halving infiltration rate, q, should give a similar breakthrough pattern. The numerical solution, however, did not proof this expectation (App.B-Fig.7). The influence of the down-dip effect might be able to partly explain the discrepancy between analytical and numerical solution. Similar to the interface angle, all equations except (24) are linearly related to infiltration rate q (linear related to 1/q). The numerical solution leads to the same conclusion that the relationship between diversion length, L, and the inverse of infiltration rate, q, is linear (App.B-Fig.8).

In Tab.5 equations (35) and (38) predict an increase in diversion length by a factor of 4 and >17, respectively, using an anisotropic fine layer with $K_{xx} = 4 * K_{zz}$ instead of an isotropic fine layer. In the numerical solution, the diversion length increases by about a factor of five and, thus, the statement of Stormont (1995) who predicted a factor of four is

a conservative approximation. Equation (38) rather over-predicts the diversion length while (35) leads to predicted L - values that are close to the numerical observations.

In general, the movement of water in the vicinity of a capillary barrier system is significantly influenced by both upward and downward defects. Interface defects implemented in the numerical model resulted in a "fingering flow pattern" into the coarse media (Fig.26). Upward defects exhibited less of a breakthrough than similar seized downward defects. A 1.5 cm deep downward defect located half the distance in down-dip direction increased the flux into the coarse media by about 8 % (Fig.27). Big defects are found to divert large amounts of water ($q_t = 4 * q$; Fig.28) from the up-dip area; very large defects are expected to divert all water from the up-dip area. Defects might be purposefully constructed at a certain down-dip position to collect water from up-dip. This water could then be diverted away from the capillary barrier system using a half-pipe below the defect; The effect would be a reduction in total amount of water above the interface and thus (a) decrease the magnitude of leakage into the coarse media at non-constructed defects and (b) enlarge the diversion length.

Both the use of double-layered and parabolic-shaped interface systems exhibited a significant improvement in total lateral water diversion. The second lower straight interface showed an increase in laterally diverted water of up to 28 % (Tab.7) and reduced the maximum breakthrough values extremely from 52 % to 0.01 % (Fig.30). The use of a parabolic-shaped interface exhibited an equally developed capillary fringe which lead to a constant leakage into the coarse media along the entire interface (except at the down-dip

end due to the down-dip effect) (Fig.29). Thus, "the optimal use of the total fall in elevation has been achieved when the breakthrough flux through the interface is constant along the entire interface" (Selker, 1996), is accomplished by the use of a parabolic shaped interface (Fig.30). The alteration of the interface from a straight to a parabolic shape changes the leakage pattern into the coarse media from a more curved to a quasi-straight shaped graph (Fig.30). To obtain similar maximum breakthrough fluxes into the coarse media, the parabolic shaped barrier systems could be applied with about two times the infiltration rate of a straight interface (Fig.34).

Due to the logistic difficulties in constructing a curved interface (Selker, 1996), the parabolic shaped interface was approximated by the use of three and five straight segments instead. The total amount of water diverted laterally in such double-layered systems showed equal values for both the upper and lower interface as found with the parabolic shaped barrier system (Tab.7). The maximum breakthrough values increased by a factor of up to 17 % for the three-segmented and up to 10 % for the five-segmented system when compared to the parabolic shaped interfaces (Fig.34).

By means of comparison, the same parameter and properties of a 1.6 meter long capillary barrier system built by 12/20 - 40/50 sand with two distinct infiltration rates with equal boundary and initial conditions were implemented in two numerical models; in a finite element model (HYDRUS-2D) and in a finite difference model (STOMP). The results showed differences in maximum breakthrough flux of 7 % for q = 4.36 cm/hr and 4 % for 8.76 cm/hr when using the Van Genuchten equation (App.B-Fig.9). In this

figure, the shape of all graphs and the down-dip direction at which the maximum breakthrough occurs are similar. The Brooks-Corey equation in the STOMP model exhibited generally smaller breakthrough fluxes which is expected from the graphs in Fig.5 and Fig.6 (HYDRUS-2D is not able to integrate the Brooks-Corey model).

Some critical remarks have to be made about the results with regards to (a) the restriction of the HYDRUS-2D model and to (b) the validation of the results with the help of experimental results and the use of a finite difference method (STOMP-model). The HYDRUS-2D code is not able to implement any effects of hysteresis, water vapor transport (e.g. across the contact of fine and coarse media) and thermal gradients that might influence the water movement in the vicinity of a capillary barrier. Also the use of steady flow conditions does not represent of what a capillary barrier might be exposed to under field conditions. At the time this report was finished, no experimental data were available to prove or disprove the numerical results due to technical problems with the experimental device. However, the relatively small differences in breakthrough pattern between HYDRUS-2D and the STOMP model (App.B-Fig.9) might lead to the conclusion that the results shown in this report approximate what could be expected for capillary barrier systems under field conditions, since Schroth et al. (1996) found similar experimental and numerical results using the STOMP-model.

8. CONCLUSIONS

The water movement in the vicinity of a capillary barrier is strongly influenced by the media used to built a capillary barrier, the interface shape and angle, and infiltration rate q. In comparison to a straight shape a parabolic shaped interface increases the diversion capacity significantly. Three-segmented and five-segmented straight interfaces exhibit slightly higher maximum breakthrough fluxes into the coarse media than the parabolic shaped system but might be less critical to construct. In general, double-layered interfaces improve the total amount of laterally diverted water significantly.
An anisotropy factor of four for the fine layer increases the diversion length by a factor of about five.

Similar to the widely used low permeability layer as a protector of underlying deposits, the performance of capillary barrier systems is very sensitive to defects along the interface. It is not possible with the presented results, only, to make judgments which capping system might be more efficient. Therefore, future research should numerically and experimentally study the advantages of both systems.

Using distinct analytical solutions for the same capillary barrier system showed vast differences in diversion length. In general, equation (25), (30), (31a and 31b) and (38) over-estimated the diversion length when compared to the numerical results, while equation (25) and (28) gave rather conservative values of L.

Due to the restriction of HYDRUS-2D (no implementation of hysteresis, water vapor transport and thermal gradients), the code is not able to fully represent processes influencing the water movement in the vicinity of a capillary barrier. Reducing these limitations could help to broaden the applicability of the code with regards to certain field conditions. This might especially be of importance for comparison between experimental and numerical results.

The lack of experimental data to prove or disprove the results presented in this thesis reduce the value of the results; therefore, future research should be undertaken to experimentally validate these results. A more detailed comparison of the STOMP model with the HYDRUS-2D model might also be an interesting issue to be explored.

BIBLIOGRAPHY

Billiotte J., M. Bourgeois, M. Deveughele, C. Jacquard, and M. Arnould. 1988. Étude d'un systèm bicouche sol fin-sol grossier à effect de barrière capillaire. Proceedings of the International Symposium on Hydrogeology and Safety of Radioactive and Industrial Hazardous Waste Disposal, Doc. 160 (1988): p.149-161.

Brooks R. H. and A. T. Corey. 1966. Properties of porous media affecting fluid flow; Journal of the Irrigation and Drainage Division, Proceedings of the American Society of Civil Engineers no. 92, (IR 2) (June 1964); page: 61 - 88.

Fayer M. J., M. L. Rockhold and M. D. Campbell. 1992. Hydrologic modeling of protective barriers: Comparison of field data and simulation results; Soil Science Society of America Journal no. 56, (1992); page: 690 - 700.

Frind, E. O., R. W. Gillham and J. F. Pickens. 1977. Application of unsaturated flow properties in the design of geologic environments for radioactive waste storage facilities. In Finite Elements in Water Resources, edited by W. G. Gray. G. F. Pinder and C. A. Brebbia. Pentech. London (1977): p. 3.133 - 3.163.

Genuchten Van M. Th. 1980. A closed-form equation for predicting the hydraulic conductivity of unsaturated soils; Soil Science Society of American Journal no. 44 (1980); page 892 - 898.

Genuchten Van M. Th., F. J. Leij, S. R. Yates. 1991. The RETC code for quantifying the hydraulic functions of unsaturated soils. U.S. Salinity Laboratory, U.U. Department of Agriculture, Agricultural Research Service. Riverside, CA. (1991)

Miyazaki T. 1988. Water flow in unsaturated soil in layered slopes; Journal of Hydrology no. 102, (1988); page: 201 - 214.

Montazer P. and W. E. Wilson. 1984. Conceptual hydrological model of flow in the unsaturated zone, Yucca Mountain, Nevada; U.S. Geological Survey, Water Resources Investigation, Rep. 84-4345 (1990); page: 26 - 31.

Mualem Y. 1976. A new model for predicting the hydraulic conductivity of unsaturated porous media; Water Resources Research vol. 12, no. 3 (June 1976); page: 513 - 522.

Oldenburg C. M. and K. Pruess. 1993. On numerical modeling of capillary barriers; Water Resources Research, vol. 29, no. 4 (April 1993); page: 1045 - 1056.

Ross B. 1990. The diversion capacity of capillary barriers; Water Resources Research, vol. 26, no. 10 (October 1990); page: 2625 - 2629.

Ross B. 1991. Reply; Water Resources Research, vol. 27, no. 8 (Aug. 1991); page: 2157.

Schroth M. H., S. J. Ahearn, J. S. Selker and J. D. Istok. 1996. Characterization of Miller-Similar Silica Sands for laboratory subsurface hydrologic studies; Soil Science Society of America Journal (submitted Aug. 1995;1996 in press).

Selker J. S. 1996. Design of interface shape for protective capillary barriers; submitted to Water Resources Research on March 26, 1996.

Šimunek J., T. Vogel and M. Th. Van Genuchten. 1994. The SWMS-2D code for simulating water flow and solute transport in two-dimensional variably saturated media - Version 1.21; research report no. 132 of the U.S. Salinity Laboratory (USDA, ARS) Riverside , California. (February 1994).

Steenhuis T. S., K.-J. S. Kung, J.-Yves Parlange, J. S. Selker and X.-X. Chen. 1990. Flow regimes in sandy soils with inclined layers, paper presented at tenth Annual American Geophysical Union Hydrology Days, Colorado state University, Fort Collins (April 10 - 12, 1990).

Steenhuis T. S., J.-Yves Parlange and K.-J. S. King. 1991. Comment on "The diversion capacity of capillary barriers" by Benjamin Ross; Water Resources Research, vol. 27, no. 8 (August 1991); page: 2155 - 2156.

Stormont J. C. 1995. The effect of constant anisotropy on capillary barrier performance; Water Resources Research, vol. 31, no. 3 (March 1995); page: 783 - 785.

Warrick A. J., P. J. Wierenga and L. Pan. 1996. Downward water flow through sloping layers in the vadose zone: Analytical solutions for diversions; submitted to Journal of Hydrology (January 18. 1996)

APPENDICES

APPENDIX A

A.1 Derivation of Ross' solution

A.1.1 Derivation of the governing flow equation

Ross (1990) used Richard's equation stated as:

$$\frac{\partial\theta}{\partial t} = -\nabla\left[K\bar{v}(H)\right] \tag{A1}$$

to obtain the governing equation for steady unsaturated water flow, whereas H is the total potential, θ is the water content, K is the hydraulic conductivity, t is the time and ∇ is the Laplacian operator.

Setting the potential H equal to ψ - z', where ψ is the pressure potential, Richard's equation can be written as

$$\frac{\partial\theta}{\partial t} = -\nabla\left[K\bar{v}(\psi - z')\right] \tag{A2}$$

whereas z' can be defined from Fig.4 in chapter 2 as $z' = x\sin\phi + z\cos\phi$.

Therefore we can rearrange (A2)

$$\frac{\partial\theta}{\partial t} = -\nabla[K\nabla\psi] + \nabla\left[K\bar{v}(x\sin\phi + z\cos\phi)\right] \tag{A3}$$

or

$$\frac{\partial\theta}{\partial t} = -\nabla[K\nabla\psi] + K\hat{x}\sin\phi + K\hat{z}\cos\phi \qquad (A4)$$

where $\hat{x}$ and $\hat{z}$ are the unit vectors and ϕ is the interface angle.

Finally Richard's equation can be written for steady state, where $\partial\theta/\partial t$ is zero, as follows

$$0 = -\nabla[K\nabla\psi] + \frac{\partial K}{\partial x}\sin\phi + \frac{\partial K}{\partial z}\cos\phi \qquad (A5)$$

Gardner's relationship ($K = K_s e^{\alpha\psi}$) between pressure and conductivity can also be written as ($K = K_s K_r$) with K_s and K_r as saturated and relative hydraulic conductivity. Substituting $K = K_s K_r$ into (A5) and factoring out K_s gives:

$$\nabla[K_r\nabla\psi] = \frac{\partial K_r}{\partial x}\sin\phi + \frac{\partial K_r}{\partial z}\cos\phi \qquad (A6)$$

whereas on the left hand site ψ can be substituted by $\psi = (1/\alpha)\ln(K_r)$, to obtain:

$$\nabla[K_r\nabla\psi] = \nabla\left[K_r\nabla\left(\frac{1}{\alpha}\ln K_r\right)\right] \qquad (A7)$$

or

$$\nabla[K_r\nabla\psi] = \frac{1}{\alpha}(\nabla)^2 K_r \qquad (A8)$$

Putting (A8) into (A6) and multiply both sides with α gives the governing equation:

$$\nabla^2 K_r = \frac{\partial K_r}{\partial x}\alpha\sin\phi + \frac{\partial K_r}{\partial z}\alpha\cos\phi \qquad (4)$$

A.1.2 General solution for equation (4) in chapter 3.2

To find a general solution for equation below:

$$\frac{\partial^2 K_r}{\partial z^2} - \alpha \cos\phi \frac{\partial K_r}{\partial z} = 0 \qquad (7)$$

we integrate (7) to obtain

$$\frac{\partial K_r}{\partial z} - \alpha \cos\phi K_r - \alpha \cos\phi C_b = 0 \qquad (A9)$$

rearrange (A9) to

$$\int \frac{\partial K_r}{K_r - C_b} = \alpha \cos\phi \partial z \qquad (A10)$$

then integrating (A10) to

$$\ln(K_r - C_b) = \alpha \cos\phi \, z + \ln C_a \qquad (A11)$$

and finally rewrite (A11) to end up with the general solution:

$$K_r = C_a^{\alpha \cos\phi z} + C_b \qquad (7)$$

A.2 Derivation of Steenhuis' equation with Ross' solution scheme

In the reply of Ross (1991) to Steenhuis et al. (1991) derived Ross the Ross Steenhuis - equation, which includes both the α-value and h_{a1} and h_{w2}, using his solution scheme. He pointed out that Steenhuis' water entry pressure of the coarse soil, h_{w2}, is equal to his ψ_1 (0), or

$$h_{w2} = \frac{1}{\alpha_2} \ln \frac{q}{K_{s2}} \tag{A12}$$

Solving (A12) for q and substitute this into the first term within the parenthesis of Ross' equation (24), depicted as

$$L = \frac{K_{s1} \tan\phi}{q\alpha_1} \left[\left(\frac{q}{K_{s2}} \right)^{\frac{\alpha_1}{\alpha_2}} - \left(\frac{q}{K_{s1}} \right) \right] \tag{24}$$

gives for $h_a = 0$

$$L = \frac{K_{s1} \tan\phi}{q\alpha_1} \left[\left(\frac{K_{s2} e^{h_{w2}\alpha_2}}{K_{s2}} \right)^{\frac{\alpha_1}{\alpha_2}} - \left(\frac{q}{K_{s1}} \right) \right] \tag{A13}$$

or

$$L = \frac{K_{s1} \tan\phi}{q\alpha_1} \left[e^{-h_{w2}\alpha_2} - \left(\frac{q}{K_{s1}} \right) \right] \tag{A14}$$

Since the divergence capacity for all $h_{a1} \neq 0$ is dependent on the relative magnitude of h_{a1} and h_{w2}, Q_{max} and L must be calculated for two cases, when (a) $h_{a1} \leq h_{w2}$ and (b) $h_{a1} > h_{w2}$.

For the first case, Ross (1991; p.2157) reports that the values of K_{s1} in (A14) can be substituted with

$$K_{s1} = K_{s1} e^{\alpha_1 h_{a1}} \tag{A15}$$

to obtain

$$L = \frac{K_{s1} \tan\phi}{q\alpha_1}\left[e^{(h_{a1}-h_{w2})\alpha_2} - \left(\frac{q}{K_{s1}}\right)\right] \qquad h_{a1} \leq h_{w2} \tag{31b}$$

Note: Setting $h_{a1} = 0$ in (31b) leads to (A13).

APPENDIX B

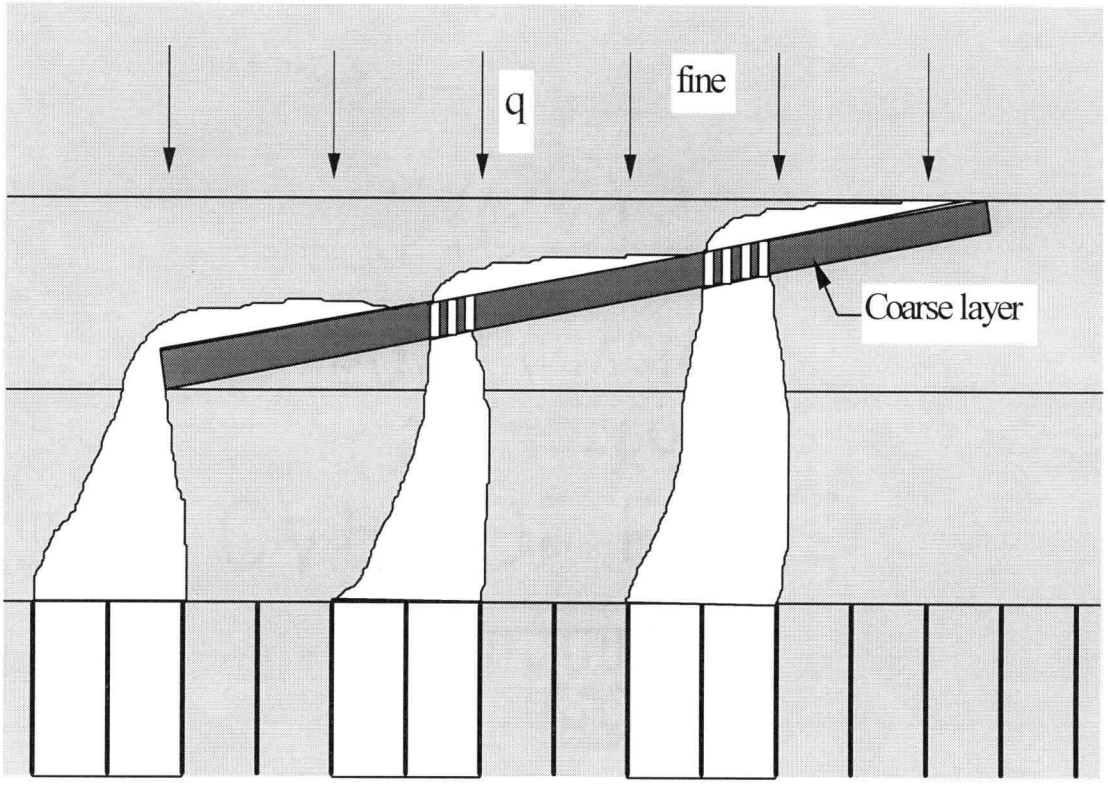

App.B - Fig.1 Fingering in a coarse soil lense (Steenhuis et al. 1991; p.11, modified)

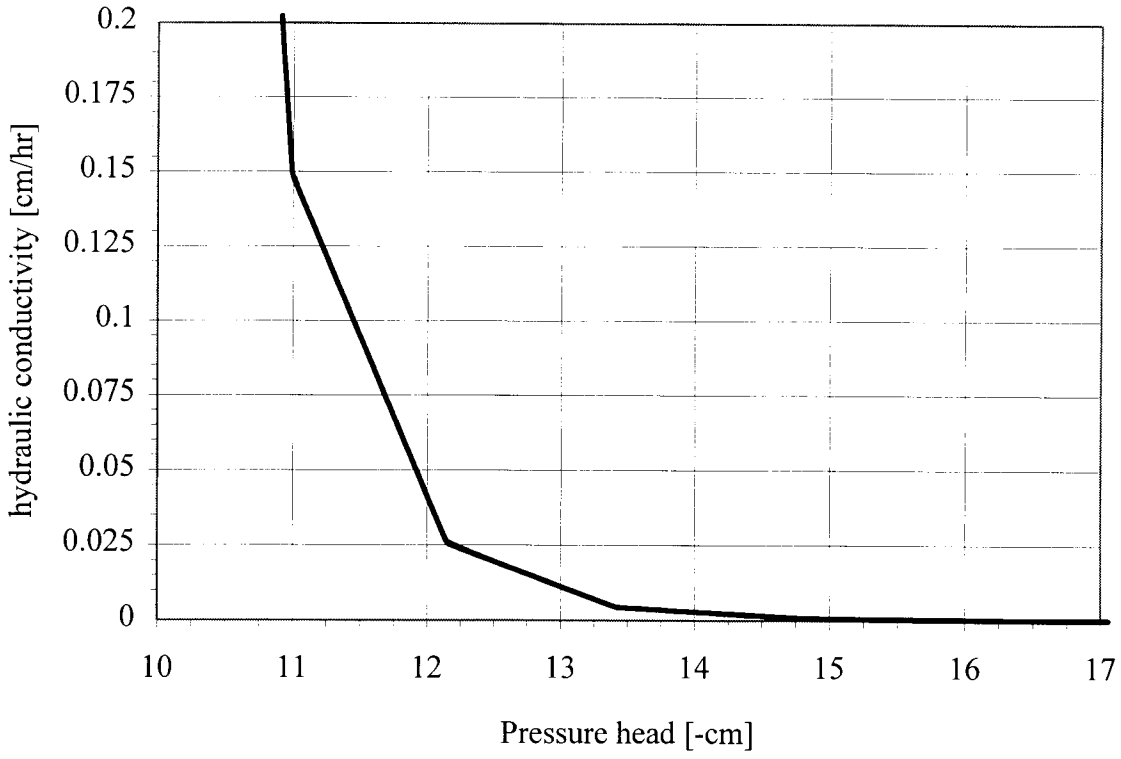

App.B - Fig.2 Hydraulic conductivity versus pressure head. Step function with linear interpolation of values in-between pressure head entries due to the tabulation procedure of the hydraulic properties in HYDRUS-2D.

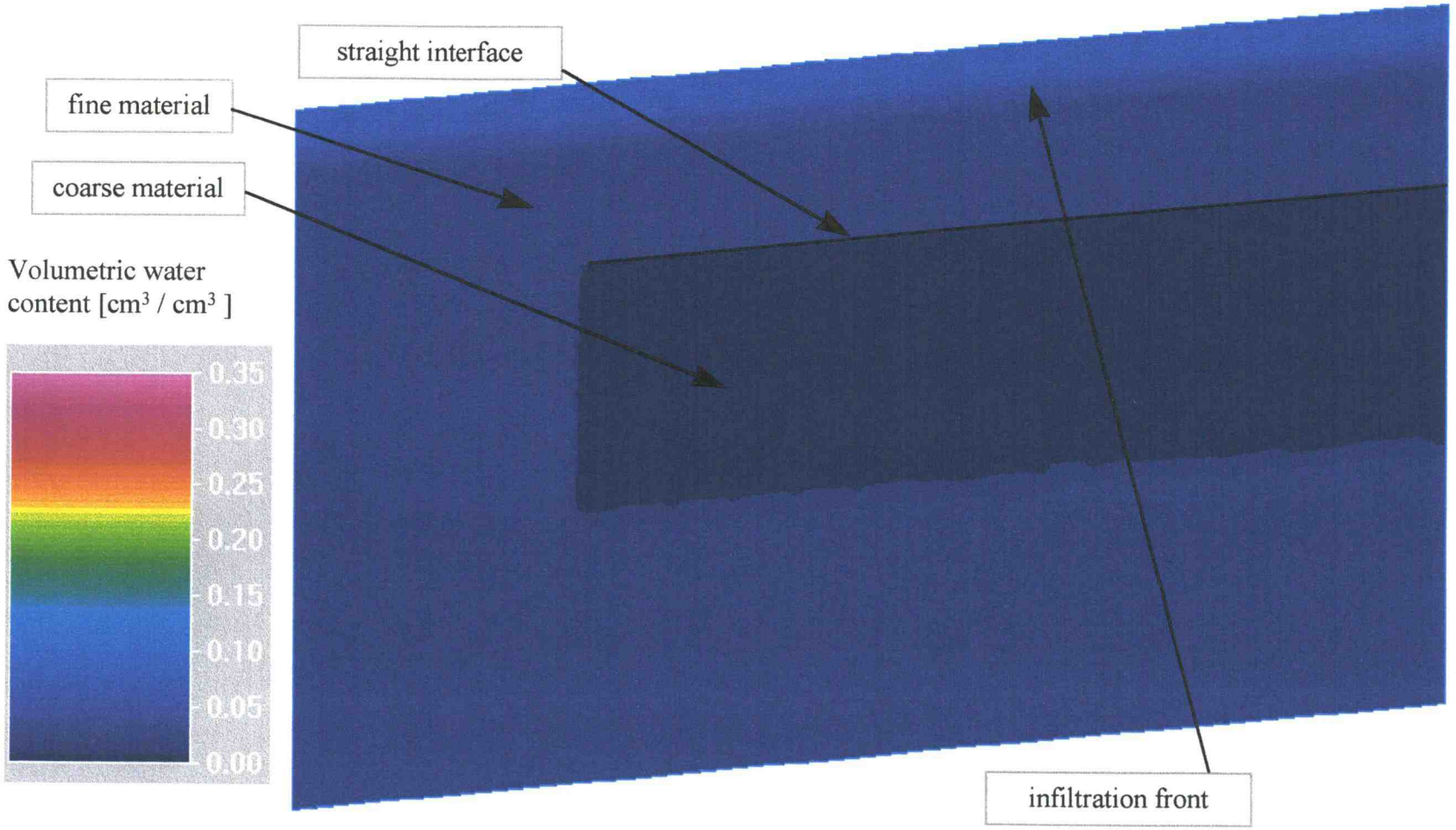

App.B - Fig.3 Volumetric water content [cm³ / cm³] in the flow domain of a capillary barrier system after 0.5 hr of steady infiltration q. (3 m long, straight interface, q = 1.6 cm/hr, tan(phi) = 0.1, 12/20 - 40/50 sand)

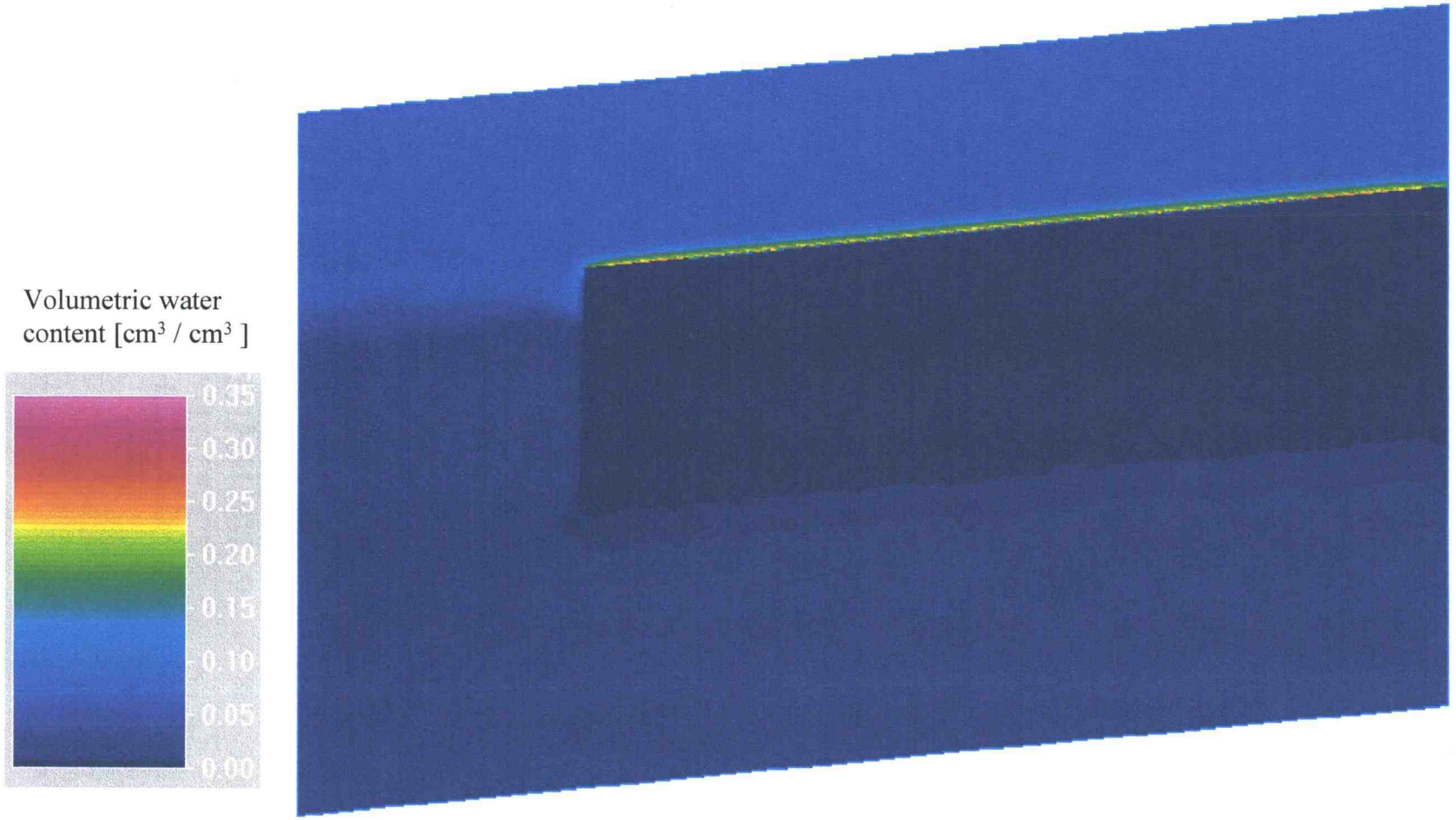

App.B - Fig.4 Volumetric water content [cm³ / cm³] in the flow domain of a capillary barrier system after 2.0 hr of steady infiltration q. (3 m long straight interface, q = 1.6 cm/hr, tan(phi) = 0.1, 12/20 - 40/50 sand)

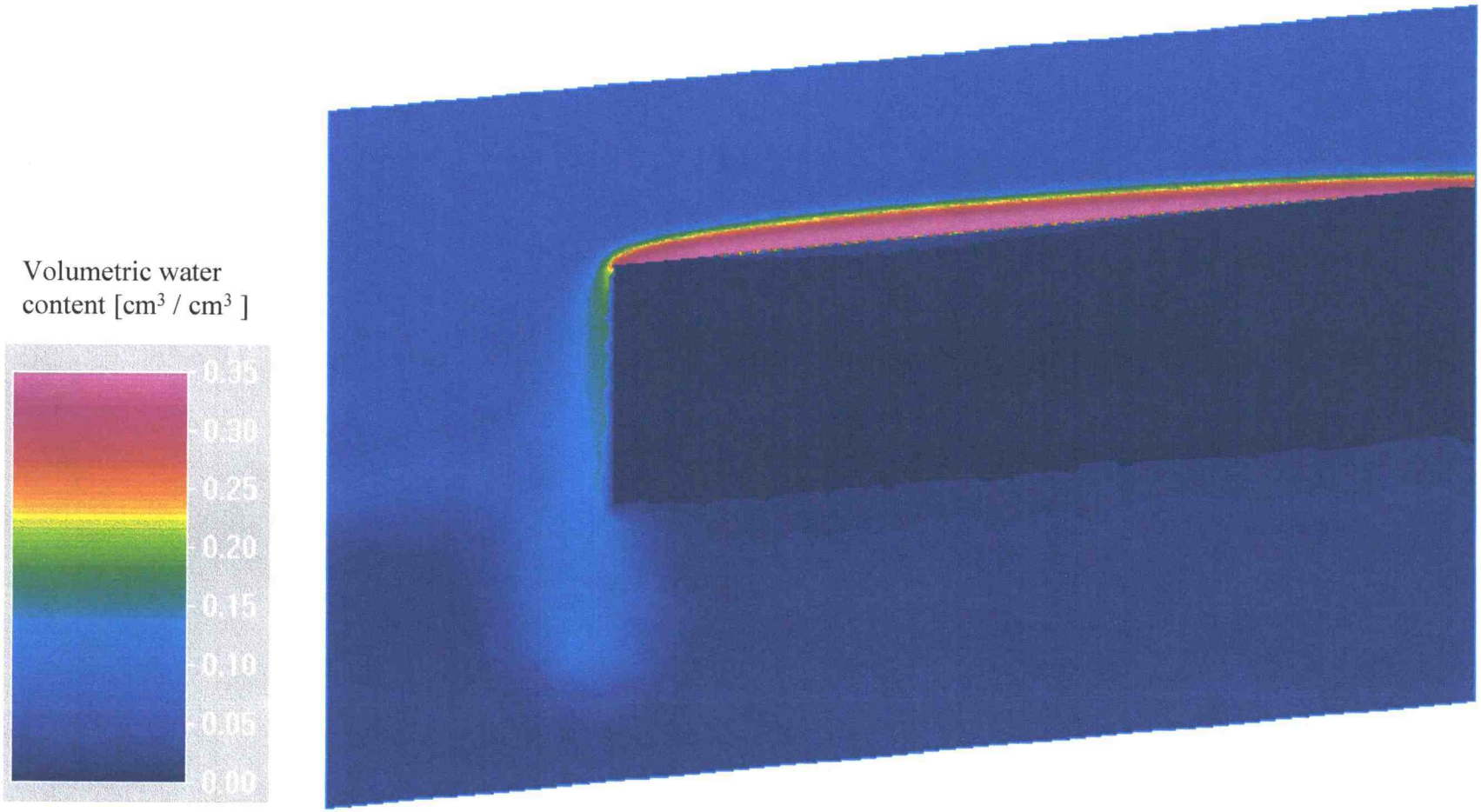

App.B - Fig.5 Volumetric water content [cm³ / cm³] in the flow domain of a capillary barrier system after 4.0 hr of steady infiltration q. (3 m long straight interface, q = 1.6 cm/hr, tan(phi) = 0.1, 12/20 - 40/50 sand)

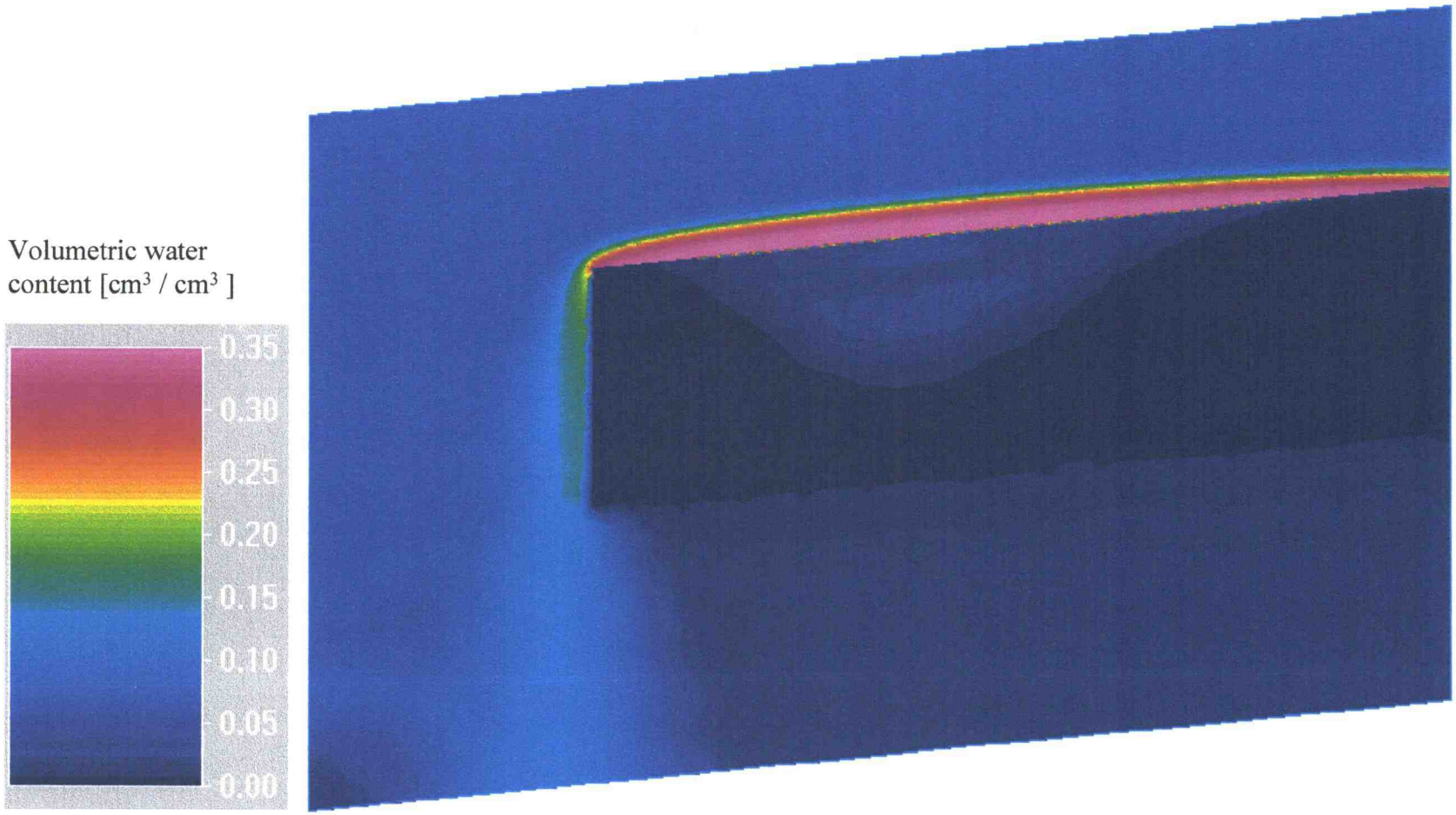

App.B - Fig.6 Volumetric water content [cm³ / cm³] in the flow domain of a capillary barrier system after 6.0 hr of steady infiltration q. (3 m long straight interface, q = 1.6 cm/hr, tan(phi) = 0.1, 12/20 - 40/50 sand)

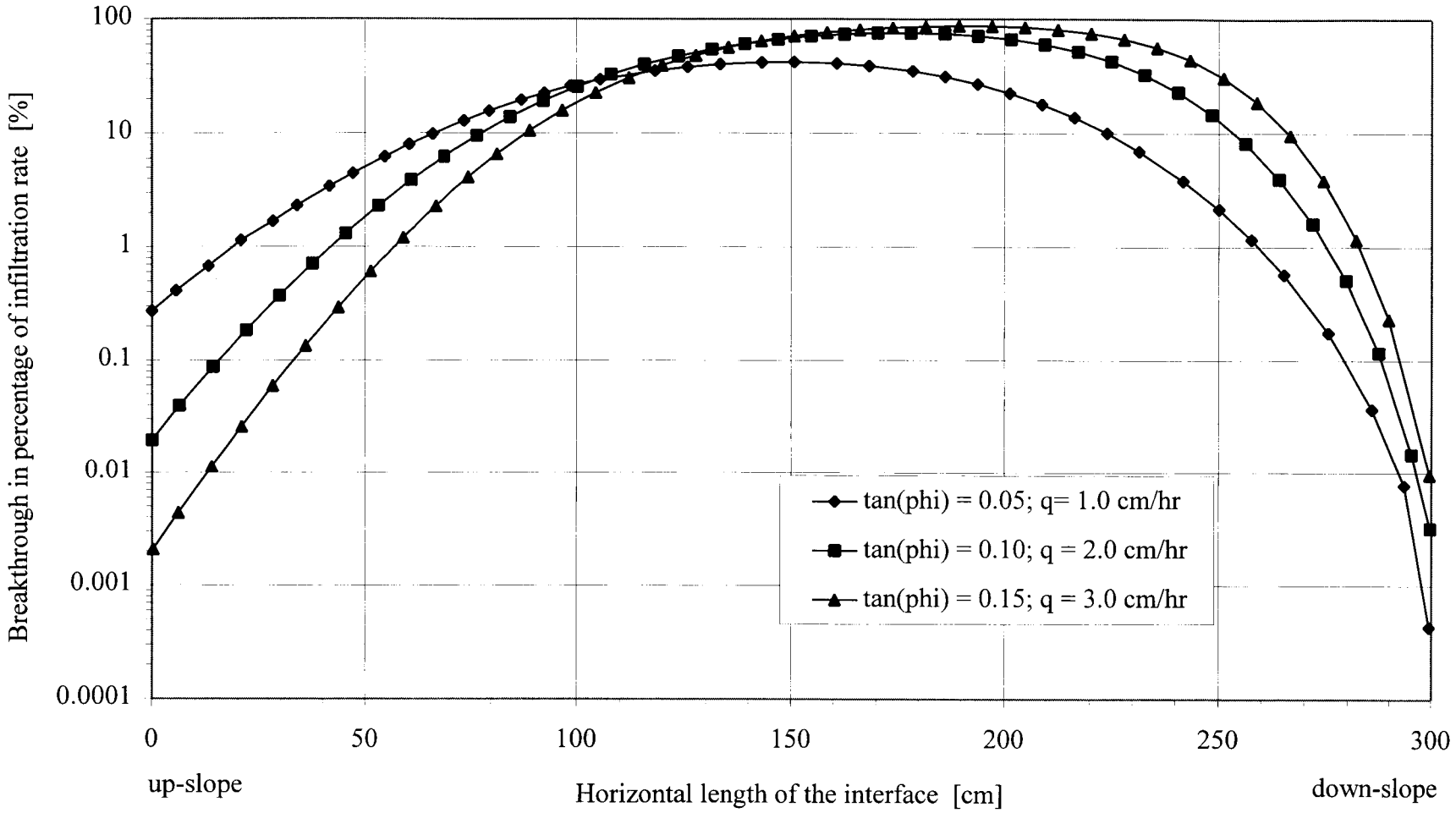

App.B - Fig.7 Breakthrough in percentage of infiltration rate q at steady state below the straight interface of a three meter long capillary barrier for different interface angles and infiltration rates. (t = 50 hr, 12/20 - 40/50 sand).

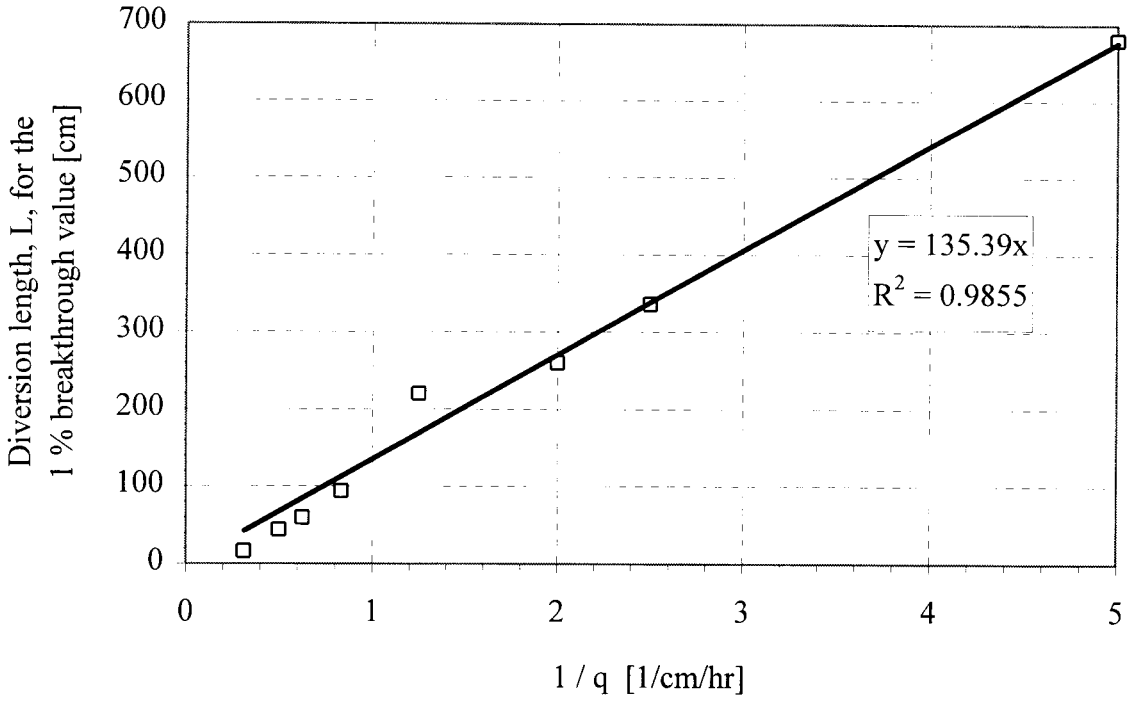

App.B - Fig.8 Numerical results of diversion length, L, for the 1 % breakthrough value [cm] with different infiltration rates, q, for a capillary barrier system with a straight interface. (12/20 - 40/50 sand, tan(phi) = 0.1).

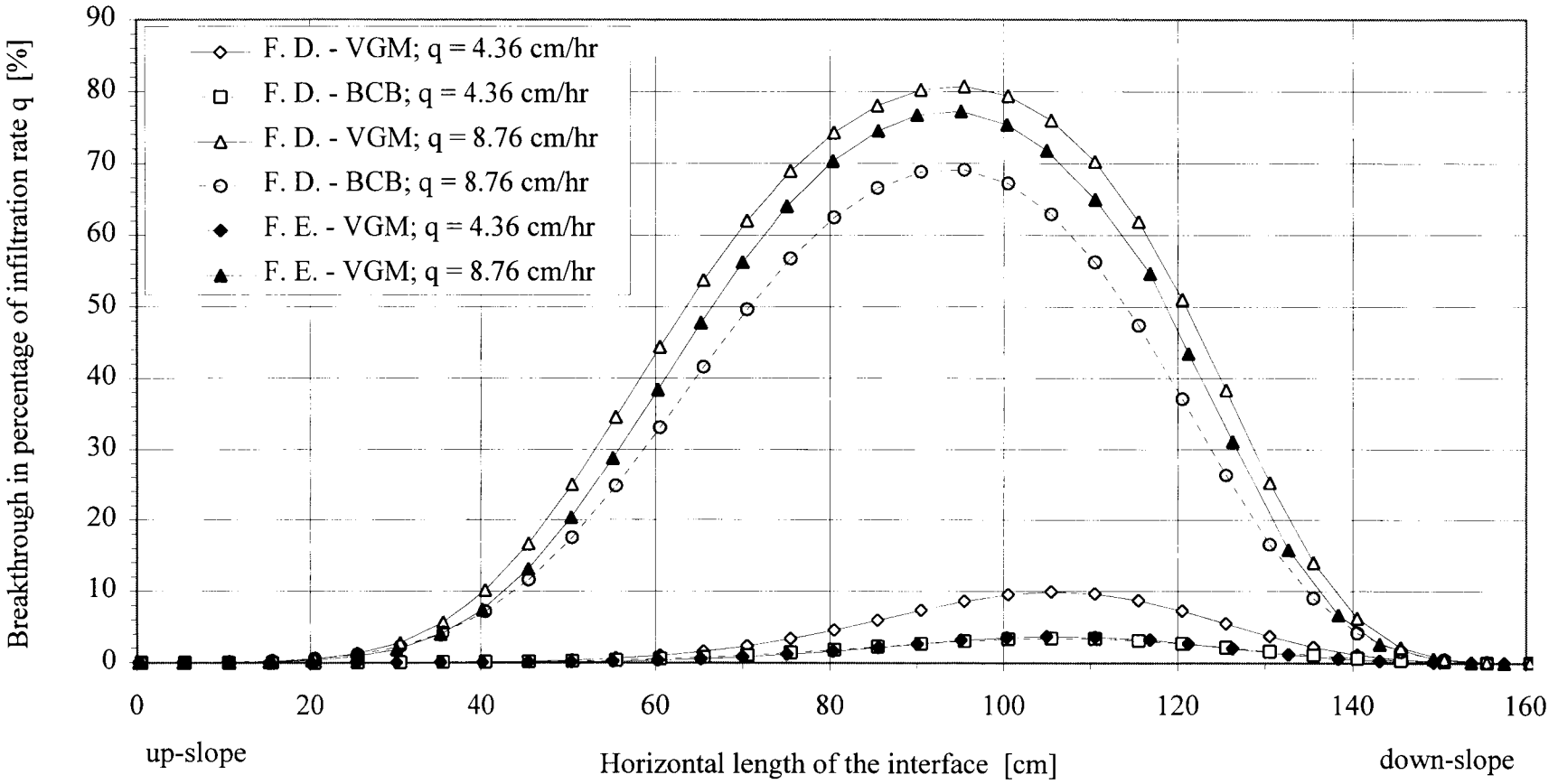

App.B - Fig.9 Comparison of breakthrough pattern into the coarse media of a 1.6 meter long capillary barrier system obtained with a finite element method (F. E. - HYDRUS-2D) and a finite difference method (F. D. - STOMP-model) for two different infiltration rates q. VGM: Van Genuchten-(Mualem) model; BCB: Brooks-Corey-(Burdine) model. (1.6 m long straight interface, 12/20 - 40/50 sand, phi = 10 degree)